Novel Synthesis and Characterization of Few-Layered Graphene (FLG), Doped FLG and Metal (Mg, Zn, Ni) Oxides Decked FLG

A thesis

Submitted by

Naresh Kumar Rotte

in partial fulfilment of the requirement for the award of the degree of

Doctor of Philosophy

in

Materials Engineering

Under the supervision of

Dr.-Ing. V. V. S. S. Srikanth

School of Engineering Sciences and Technology

March 2016

With all gratitude, I dedicate this thesis firstly to Lord and Saviour JESUS for all his grace and favour in life, and secondly to my family

Because in much wisdom is much grief, and increase of knowledge is increase of sorrow

Ecclesiastes 1:18

DECLARATION

I, **Naresh Kumar Rotte**, declare that this thesis work entitled "**Novel Synthesis and Characterization of Few-Layered Graphene (FLG), Doped FLG and Metal (Mg, Zn, Ni) Oxides Decked FLG**", submitted in partial fulfilment of the requirements for the award of **Doctor of Philosophy** (Materials Engineering) in the School of Engineering Sciences and Technology (SEST), University of Hyderabad is completely my work except for those referenced. This work was done under the supervision of **Dr.-Ing. V. V. S. S. Srikanth**. This report is a record of the bonafide research work carried out by me and the results incorporated in it have not been reproduced/copied from any source. This work has not been submitted to any other University or Institute for the award of any other degree or equivalent.

Naresh Kumar Rotte
Reg. No.: 10ETPM04
School of Engineering Sciences and Technology
University of Hyderabad

CERTIFICATE

This is to certify that the thesis work entitled "**Novel Synthesis and Characterization of Few-Layered Graphene (FLG), Doped FLG and Metal (Mg, Zn, Ni) Oxides Decked FLG**" submitted by **Naresh Kumar Rotte** (bearing Reg. No. **10ETPM04**) in partial fulfilment of the requirements for the award of the degree of **Doctor of Philosophy** in **Materials Engineering** is a bonafide research work carried out by him under my guidance. The thesis work has not been submitted previously in part or in full to this or any other University or Institute for the award of any degree or equivalent.

Thesis supervisor

Dr.-Ing. Vadali V. S. S. Srikanth
Assistant Professor
School of Engineering Sciences and Technology
University of Hyderabad

M. Ghanashyam Krishna
Dean
School of Engineering Sciences and Technology
University of Hyderabad

ACKNOWLEDGEMENTS

First and foremost, I would like to thank my research advisor Dr.-Ing. V. V. S. S. Srikanth for his continual support and guidance throughout my Ph.D. work. I am thankful to former dean Prof. K. Bhanu Sankara Rao who guided me upto his retirement. I am also grateful to my doctoral review committee members, Dr. Koteswara Rao V Rajulapati from School of Engineering Sciences and Technology (SEST), University of Hyderabad (UoH), Dr. P. K. Jain from International Advanced Research Center for Powder Metallurgy and New Materials (ARCI), Hyderabad and Prof. R. Singh for their helpful suggestions during the DRC meetings. My sincere thanks to former dean of SEST, Prof. Sundararaman Mahadevan and the current dean, Prof. M. Ghanashyam Krishna for their support.

I wish to thank, Mr. Balaji Padya and Mr. S. B. Chandrasekhar, Scientists, ARCI, Hyderabad for their helpful research discussions.

I express my gratitude to my spiritual father Dr. P. Satish Kumar (Calvary temple, Hyderabad) who has been a source of encouragement through the God messages since 2007.

I wish like to thank Dr. Md. Ahamad Mohiddon, Center for Nanotechnology (CFN), UoH, for his support in carrying out Raman scattering measurements. I wish to thank Mr. M. Durga Prasad, Mr. S. Pankaj and Ms. Sandhya, CFN for assisting me in TEM experiments. I express my gratitude to Mr. Lakshmi Narayana, Ms. Arundhati, Mr. Sunil, Ms. Sunita, UoH, for assisting me in FESEM experiments. My special thanks to Mr. P. Ramana Babu, Mr. Mallesh and Mrs. Padma, technical staff, SEST, UoH, who helped me in carrying out XRD measurements. My sincere thanks to the other technical staff of SEST namely Mr. Venkat, Mrs. Kranthi, Mr. Dinakar and Mrs. Malathi, SEST for their technical support. My special thanks to Mr. Venu, SEST, UoH, for helping me in administrative matters. My sincere thanks to technical staff of various Schools in UoH for their technical support.

I am thankful to Dr. Hari Prasad, Dr. G. Venkata Ramana, Dr. Archana, Dr. Mokthar, Dr. Rajesh, Dr. Suresh Pittala, Dr. Antaiah and Dr. Pavan Kumar Naik for their continuous encouragement throughout the period of my PhD work. My sincere thanks to research scholars E. Nagesewararao, Omar Pasha, Anil Kumar, Ramakanth, Santhanam, Narasimha, Narasihmappa, Varma and Siva Nagireddy, School of Physics, UoH, for the invaluable time they spent with me in discussing scientific matters. My sincere thanks to Obaiah, Narayana, Krishna, Ganesh, Naidu, School of Chemistry, UoH for helping with chemicals when needed.

My sincere thanks to my friends Paul Praveen, Balaji, Kolla Vijay, Pandu Sunil, Ramya, Swathi Manivana, Kamal Mankari and Ram Naik, from SEST, UoH and Chandrasekhar (IISc

Bangalore), Sommaih (IISc, Bangalore), Sateesh Prathapaneni (IIT Bombay), Mohan Dasari and Thirummala Rao (IIT Madras) for their support and friendship.

My sincere thanks to Dr. Rajendra, Satish and Chaintanya from JNTU Hyderabad for helping me in carrying out FTIR experiments. My sincere thanks to Dr. Venu Reddy, Dr. Govind and Satish Kasthuri and Mullamuri Banu for helping me at the end of my Ph.D. dissertation work.

I thank my colleagues in Surface and Interface Engineering Laboratory (SIEL), UoH, Mohan Kumar, Harish Ojha, Srinivasulu, Sravani, Aneela, Varalakshmi, Koya Applaraju and Charan for their support. I am thankful to project students Manikanta, Shayam, Nagalakshmi, Pavan Kumar, Suman, Sandhya, Jaya, and Rekha who helped me in my thesis work. I am very thank to all my friends who are working in different laboratories of SEST.

I thank to Dr. Joy and my ETC colleagues who helped me in improving my communication skills and personality. My sincere thanks to Dean, School of Humanities, UoH for allowing me to learn foreign languages namely German, Japanese and Korean.

My special thanks to Mr. Subbareddy Yerramala, Dr. Jeyaraj Boniface, Dr. M. V. Reddy and Prof. B. V. R. Chowdary for their kind support and collaboration.

I am thankful to Dr. Ravindra Kumar, Chief Medical Officer and Santosh (Medical Staff), University hospital for their hospitality, whenever I was unhealthy.

My gratitude to University Grants Commission for providing financial support through Rajiv Gandhi National Fellowship (Letter No: F.14-2(SC)/2010 (SA-III)) to pursue my PhD at UoH.

My special thanks to my brother Sampath Reddy Puttapati, SEST, UoH, for his continuous help and support during the entire time my Ph.D. work.

Finally, I am thankful to my parents and siblings (Bhargavi and Sashi Kumar) for their love and for supporting me at all times.

Naresh Kumar Rotte

List of Publications

1. **N. K. Rotte**, S. Petnikota, V. V. S. S. Srikanth, B. S. R. Kota, "Reducing agent free synthesis of graphene from graphene oxide", **AIP Conference Proceedings** 1538, 262 (2013).

2. S. Petnikota, **N. K. Rotte**, V. V. S. S. Srikanth, B. S. R. Kota, M. V. Reddy, K. P. Loh, B. V. R. Chowdari, "Electrochemical studies of few-layered graphene as an anode material for Li ion batteries", **Journal of Solid State Electrochemistry**, 18(4), 941 (2014).

3. **N. K. Rotte**, S. Yerramala, J. Boniface, V. V. S. S. Srikanth, "Equilibrium and kinetics of Safranin O adsorption on MgO decked multi-layered graphene", **Chemical Engineering Journal**, 258, 412 (2014).

4. S. Petnikota, **N. K. Rotte**, M. V. Reddy, V. V. S. S. Srikanth, B. V. R. Chowdari, "MgO decorated few-layered graphene as an anode for Li ion batteries", **ACS Applied Materials and Interfaces** 7, 2301 (2015).

5. **N. K. Rotte**, A. Koyya, N. Remalli, V. V. S. S. Srikanth, "Simple combustion synthesis of MgO and NiO decorated graphenaceous nanotubes", to be submitted to **Materials Letters** (2016).

6. K. V. Sreenivasulu, **N. K. Rotte**, V. V. S. S. Srikanth, and S. N. Kaul, "Non-Collinear ferromagnetic short range order in MgO decked multi-layered graphene", to be submitted (2016).

7. S. Yerramala, **N. K. Rotte**, J. Boniface, V. V. S. S. Srikanth, "Equilibrium and kinetics of the adsorption of Acid Blue 9 and Safranin O from aqueous solutions by MgO decoraged FLG coated Fuller's Earth", to be submitted (2016).

8. **N. K. Rotte**, D. P. Muvva, Md. Ahamad Mohiddon, V. V. S. S. Srikanth, "Synthesis, characterization and photoluminescence of ZnO decorated S, N doped few-layered graphene", to be submitted (2016).

9. **N. K. Rotte**, B. Govindh, Venu Reddy, V. V. S. S. Srikanth, "Synthesis of 6-aryl-5-cyano-2-oxo uracil using S, N doped few-layered graphene as a catalyst", to be submitted (2016).

Contents

Abstract

The use of graphene and related materials in diverse applications has been established beyond doubt. However, the greatest challenge is to synthesize the graphenaceous materials using processes that are industrially viable, environmental friendly, inexpensive and time-effective. In this context, through this PhD thesis work, different novel synthesis methods to obtain variety of graphenaceous materials have been experimentally demonstrated. In this work, i) graphene oxide (GO) was converted into few-layered graphene (FLG) without using any reducing agent, ii) heteroatom doped FLG and ZnO decorated heteroatom doped FLG are synthesized using novel methods, and iii) MgO decorated FLG and MgO and NiO decorated FLG are synthesized using a simple combustion method. The synthesized materials have thoroughly characterized for morphology, crystallinity, phase etc., using multitude of techniques been tested in diverse applications. The synthesized materials have also been tested in diverse applications. FLG was synthesized by microwave irradiation (MWI) of GO (in a household microwave oven without using any reducing agents) followed by a simple sonication step. This method does not evolve any unsafe by-product gases which is otherwise the case when reducing agents are used in the reduction of GO to graphene or FLG. Moreover, the innate nature of the procedure allows scalability and cost-effectiveness. The synthesized FLG was tested as an anode material in Li-ion batteries. S, N doped FLG was synthesized by MWI of acid treated graphite flakes which are obtained by just soaking the graphite flakes in a proper acid mixture. In a similar manner, different ZnO decorated doped FLG composites are synthesized by taking appropriate amounts of Zn containing precursor and by varying the amount of S, N doped FLG during the reaction. The synthesized S, N doped FLG was used as a catalyst for preparation of uracil and tetrahydropyrimidine biologically active molecules. ZnO decorated doped FLG exhibited unique photo luminescence at room temperature. MgO decorated FLG was synthesized using a rudimentary combustion process involving combusting of Mg in the presence of dry ice. Similarly NiO and MgO decorated FLG was also synthesized by taking an appropriate amount of NiO during the combustion reaction. MgO decorated FLG was used as an adsorbent to remove Safranin O dye and textile effluent from water. MgO decorated FLG was also used as an anode material in Li ion batteries and in other applications.

Chapter 1 Introduction

1.1 Carbon Allotropes

Natural carbon allotropic forms (Fig. 1.1) are graphite, diamond and amorphous carbon [1]. The other popular allotropic forms (Fig. 1.1) of carbon are fullerenes (C_{60}) [2], carbon nanotubes (CNTs) [3] and graphene [4]. With the advent of C_{60} [5], research on other carbon clusters such as C_{70}, C_{76}, C_{78} and C_{84} has also flourished. C_{60} has a closed cage structure with an icosahedral symmetry which consists of 20 hexagonal and 12 pentagonal rings as the basis. In C_{60} each C atom is sp^2 hybridized and is bound to three other C atoms. CNTs are hollow cylindrical structures [6] which can be assumed as constructed by rolling graphene sheets constituted by sp^2 and sp^3 hybridized carbon atoms. The diameter of a typical CNT will be on the order of few nm, while its length can be as high as few mm [7,8]. Graphene (Fig. 1.1(a)) is one atom thick structure in which sp^2 C atoms are bonded into hexagons similar to basal planes in graphite. In fact graphene is nothing but a single basal plane of graphite which is built by AB stacking [9,10] of numerous individual graphene layers.

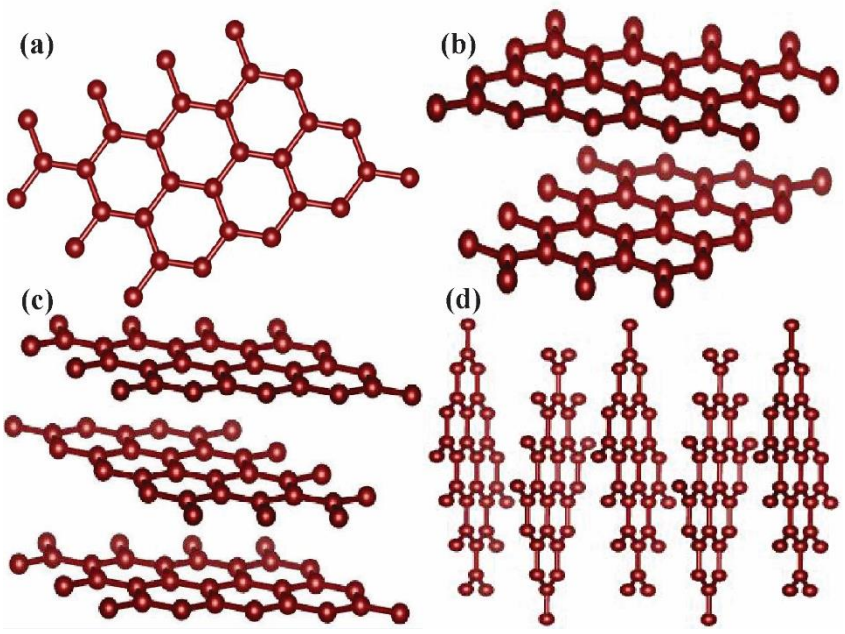

Figure 1.1. Schematic of (a) graphene and (b) bi-, (c) tri- and (d) few- layered graphene.

1.2 Layered Graphene

Graphene exhibits outstanding electronic and mechanical properties [11-13]. AB-stacked bi- [14] (Fig. 1.1(b)) and tri- [13] (Fig. 1.1(c)) layered graphenes also exhibit extraordinary properties owing to their distinct electronic band structures and are therefore touted as active materials for diverse applications. However, this is possible only if these materials are produced in bulk quantities. The existing methods such as manual peeling of highly-oriented pyrolytic graphite (HOPG) to obtain mono layer graphene or few-layered graphene (FLG) [15] (Fig. 1.1(d)) and epitaxial growth of graphene on suitable substrates [16] using chemical vapour deposition (CVD) and transfer of graphene on to different substrates [17-19] are even though very effective, they are complex and do not yield graphene in bulk quantities. On the other hand, chemical conversion of graphene oxide (GO) into FLG has been found to be much easier in comparison to mechanical cleavage and CVD methods of obtaining graphene. Moreover, when the experiment is carefully designed, chemical conversion of GO into FLG has the ability to give a high-yield of the end product [20-24]. GO was also converted to reduced-GO or FLG by thermal, laser, solar, gas and microwave treatments [25].

1.3 Doped Graphene

Graphene is a zero-bandgap material and therefore the devices fabricated out of it are difficult to be switched-off [26-28]. For practical applications, band gap is essential and therefore it is necessary to develop methods to precisely control the carrier type and concentration in graphene for further development of graphene-based devices [29]. In this context, research on doped graphene has gained a great attention [30,31]. Doping in graphene can be achieved by heteroatom doping, chemical modification and electrostatic field tuning (EFT). The heteroatom (O, B, N, P, S, etc.,) doping (Fig. 1.2) and chemical modification are utilized to alter graphene’s bandgap and to control its Fermi level.

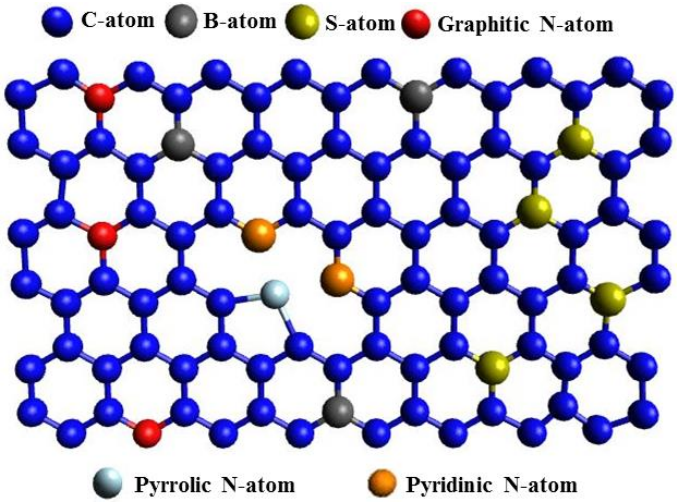

Figure 1.2. Schematic of heteroatom doped graphene.

Heteroatom doping mainly alters the electric properties of graphene [32]. B and N atoms can be easily doped in graphene owing to their comparable atomic size to that of C atom. Moreover the electron donor and hole acceptor characteristics of B and N atoms are helpful in their substitutional doping which not only alters the structure but also the electronic properties of graphene in such a way that the doped graphene exhibits an electronic band structure similar to that of pristine graphene [33-36]. Moreover, graphene has an extremely high specific surface area which gives a great opportunity to manipulate its electronic properties by chemically modifying its surfaces. For example, conversion of graphite into graphene oxide [37,38] by treating it with suitable oxidizing agents results in alteration of conductivity to a great extent [39-51] owing the alteration in the bonding nature due to oxidation. The alteration depends strongly on the nature of the oxidizing agent and the method used to oxidize graphite.

EFT can also be used to control transport properties in graphene [52,53]. The band structure of bi-layered graphene can be controlled (between zero and mid infrared energies) by applying an electric field along the zig-zag and arm-chair edges of the bi-layered graphene (Fig. 1.3) [54-57]. Similarly, the band structure of FLG can also be controlled in relation to the number of layers in FLG.

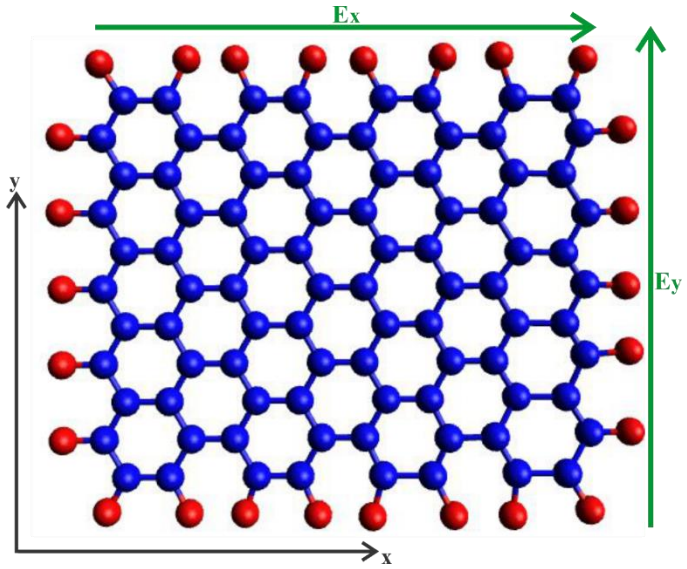

Figure 1.3. C atoms (blue) are passivated with H atoms (red) at both the arm-chair and zig-zag edges of graphene. The applied electric fields (green arrows) along the arm-chair and zig-zag edges are denoted as E_x and E_y, respectively.

1.4 Graphene Oxide

GO (Fig. 1.4) has oxygen-containing groups covalently bonded to its lattice [58,59]. Graphite oxide and GO differ in the number of layers contained in them. Graphite oxide is a many-layered structure whereas GO is few-layered or mono-layered structure. GO is a poor conductor compared to FLG. This is owing to the oxygen containing functional groups that are attached to the basal planes and edges of GO [60-62] distort the sp^3-hybridized C atoms thereby rendering insulating nature to GO [63]. However, when GO undergoes reduction [64,65] it can have properties at par with that of mono-layered graphene. The reduced GO or FLG contains residual oxygen and other heteroatoms as well as structural defects along with number of graphenaceous layers [66]. Chemically modified graphenaceous materials such as GO, reduced GO, functionalized GO and so on could be used in diverse applications [67] such as preparing novel nanocomposite materials [68], energy storage [69], biomedical [70], catalysis [71] and so on.

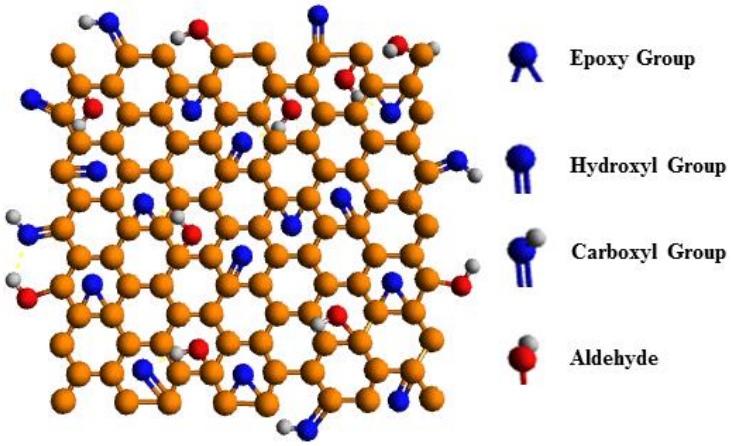

Figure 1.4. Schematic of Graphene Oxide contained various functional groups.

1.5 Metal Oxide Decorated FLG

It has been experimentally as well as theoretically proven that the intrinsic properties of different graphenaceous materials can be tuned by decorating well-distributed metal oxide nanoparticles (MO-NPs) at the edges and on the basal planes of graphene sheets (Fig. 1.5). This has led to the development of "tuneable graphene-MO nanocomposites" exhibiting a variety of novel properties [72-79].

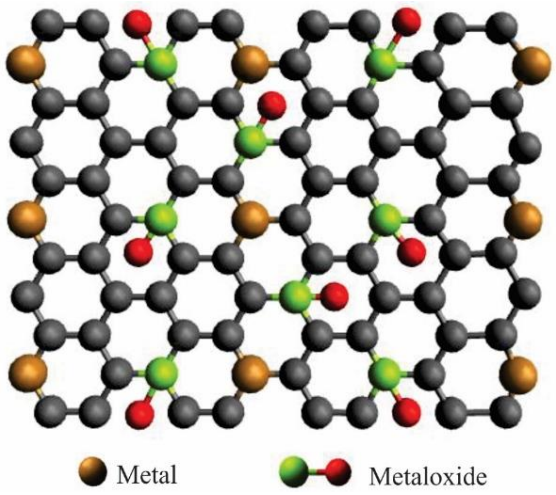

Figure 1.5. Schematic of graphene metal (brown colour) and metal oxide (green and red).

The decoration of MO-NPs on the graphene sheets helps in tuning surface morphology, specific surface area, bandgap, etc. Additionally MO-NPs could prevent the re-stacking of individual graphene sheets, which is generally caused by a strong Van der Waals interaction

between them. In graphene-metal oxide nanocomposites, graphene acts either as a functional constituent or a substrate for retaining MO-NPs. The large specific surface area and the controllable conductivity of graphene often enable charge transfer and redox reactions while graphene renders strength to the composite. As a result the MO-NPs decorated graphene structures are excellent materials for catalytic and energy applications [74-79]. The main drawbacks with these graphene-MO nanocomposites are non-uniform distribution of MO-NPs on the graphene sheets and unavailability of synthesis methods which can give bulk amounts of the final active material.

1.6 Problem Definition

After a thorough literature review (Chapter 2), problems associated with the existing synthesis methods of FLG and doped FLG have been identified and overcoming these problems is the motivation behind this thesis work. From the discussion presented in the 'Introduction', it is very clear that there is a requirement to develop new synthesis methods not only to effectively control the number of AB-stacked layers but also to obtain the material in bulk amounts. Similarly, even in the case with hetero-atom doped FLG there is a requirement to develop a method such as 'in-situ doping' while synthesizing FLG. Researchers have reported different chemical methods for conversion of GO to FLG. However, bulk synthesis of FLG without the use of any reducing agent is still a challenge. Another challenge is to synthesize materials using processes that are industrially viable i.e., the processes should allow up-scaling, should be environmental friendly, should be inexpensive and should be time-effective.

1.7 Objectives of the Thesis

Thesis objectives have been framed considering the challenges mentioned in the previous section and the literature review (Chapter 2). PhD thesis objectives are as follows: i)

development of a method to convert GO into FLG without using any reducing agent, ii) development of a method to synthesize doped FLG, iii) development of a chemical method to obtain ZnO decorated doped FLG, iv) development of a simple combustion method to obtain MgO decorated FLG and if possible another metal oxide decorated FLG, and v) use of the synthesized materials in diverse established applications.

1.8 Overview of the Thesis

The thesis work has been organized into 6 chapters. Chapter 1 describes the importance of graphene, bi- and tri- layered graphene, FLG, doped graphene and relevant composites. In addition, this chapter highlights the problem definition of the thesis and presents the objectives of this thesis work. Chapter 2 provides detailed and latest literature review on the development of synthesis methods of various graphenes. In Chapter 3, the experimental details of the synthesis methods developed as a part of this thesis work of various graphenes will be presented. The experimental details of basic characterization and testing of various materials synthesized in this thesis work will also be presented in Chapter 3. In Chapter 4, results and discussion pertaining to the general characteristics like morphology, structure and composition of all the synthesized materials will be presented. In the final section of Chapter 4, the use of the synthesized materials in various applications will be presented. Since the work related to certain applications has been taken up separately by other PhD students in our laboratory (at SEST, UoH) only a brief discussion will be presented in such cases. Chapter 5 includes the conclusions of this thesis work as well as the future outlook. All the references that have been cited in the thesis have been arranged and numbered in the order they appear in the main text under the heading “References” at the end of each chapter.

References

[1]. H. O. Pierson, “Graphite, Diamond and Fullerenes–Properties, Processing and Applications”, William Andrew Publishing/Noyes, (1993).

[2]. M. S. Dresselhaus, G. Dresselhaus and P. C. Eklund, “Science of Fullerenes and Carbon Nanotubes”, Academic Press, San Diego, (1995).

[3]. S. Iijima, Nature 354, 56-58 (1991).

[4]. A. K. Geim and K. S. Novoselov. Nat. Mater. 6, 183-191 (2007).

[5]. H. W. Kroto, J. R. Heath, S. C. O'Brien, R. F. Curl and R. E. Smalley, Nature 318(6042), 162-163 (1985).

[6]. M. Meyyappan, "Carbon Nanotubes: Science and Applications", CRC Press: Boca. (2005).

[7]. A. Jorio, R. Saito, J. H. Hafner, G. Dresselhaus and M. S. Dresselhaus, Phys. Rev. Lett. 86(6), 1118-1121 (2001).

[8]. A. Jorio, A. G. Souza Filho, G. Dresselhaus, M. S. Dresselhaus et al., Phys. Rev. B 65, 155412 (2002).

[9]. J. C. Charlier, X. Gonze and J. P. Michenaud, Carbon 32(2), 289-299 (1994).

[10]. D. D. L. Chung, J. Mater. Sci. 37, 1475-1489 (2002).

[11]. T. Ohta, A. Bostwick, T. Seyller, K. Horn and E. Rotenberg, Science 313(5789), 951-954 (2006).

[12]. Y. B. Zhang, T.-T. Tang, C. Girit, Z. Hao, M. C. Martin, et al., Nature 459, 820-823 (2009).

[13]. M. F. Craciun, S. Russo, M. Yamamoto, J. B. Oostinga, A. F. Morpurgo et al., Nat. Nanotechnol. 4, 383-388 (2009).

[14]. S. Y. Zhou, G. H. Gweon, A. V. Fedorov, P. N. First, et al., Nat. Mater. 6, 916 (2007).

[15]. K. S. Novoselov, D. Jiang, F. Schedin, T. J. Booth, et al., Proc. Natl. Acad. Sci. U.S.A. 102(30), 10451-10453 (2005).

[16]. C. Berger, Z. M. Song, T. B. Li, X. B. Li, et al., J. Phys. Chem. B 108, 19912-19916 (2004).

[17]. P. W. Sutter, J.-I. Flege and E. A. Sutter, Nat. Mater. 7, 406-411 (2008).

[18]. A. Reina, X. T. Jia, J. Ho, D. Nezich, et al., Nano Lett. 9, 30-35 (2009).

[19]. S. Lee, K. Lee and Z. H. Zhong, Nano Lett. 10(11), 4702-4707 (2010).

[20]. S. Stankovich, D. A. Dikin, R. D. Piner, K. A. Kohlhaas, et al., Carbon 45, 1558-1565 (2007).

[21]. D. Li, M. B. Müller, S. Gilje, R. B. Kaner, et al., Nat. Nanotechnol. 3, 101-105 (2008).

[22]. V. C. Tung, M. J. Allen, Y. Yang and R. B. Kaner, Nat. Nanotechnol. 4, 25-29 (2009).

[23]. S. Wang, P. K. Ang, Z. Wang, A. L. L. Tang, et al., Nano Lett. 10, 92-98 (2010).

[24]. C. Gomez-Navarro, J. C. Meyer, R. S. Sundaram, A. Chuvilin, et al., Nano Lett. 10, 1144-1148 (2010).

[25]. X. F. Gao, J. K. Jang and S. Nagase, J. Phys. Chem. C 114(2), 832-842 (2010).

[26]. K. S. Novoselov, S. V. Morozov, T. M. G. Mohinddin, L. A. Ponomarenko, et al., Phys. Status Solidi B 244(11), 4106-4111 (2007).

[27]. F. Schwierz, Nat. Nanotechnol. 5(7), 487-496 (2010).

[28]. A. Pospischil, M. Humer, M. M. Furchi, D. Bachmann, et al., Nat. Photonics 7, 892-896 (2013).

[29]. H. Lim, J. K. Lee, H.-J. Shin, H. S. Shin, et al., Langmuir 26(14), 12278-12284, (2010).

[30]. L. K. Randeniya, H. Q. Shi, A. S. Barnard, J. H. Fang, et al., Small 9(23), 3993-3999 (2013).

[31]. T. Wehling, K. Novoselov and S. Morozov, Nano Lett. 8(1), 173-177 (2008).

[32]. H.-J. Choi, S.-M. Jung, J.-M. Seo, D. W. Chang, et al., Nano Energy 1, 534–551 (2012).

[33]. L. S. Panchkula, K. S. Subramanian, S. K. Saha, A. Govindaraj, et al., Adv. Mater. 21(46), 4726-4730 (2009).

[34]. T. B. Martins, R. H. Miwa, A. J. R. da Silva and A. Fazzio, Phys. Rev. Lett. 98(19), 196803 (2007).

[35]. P. A. Denis, Chem. Phys. Lett. 492(4-6), 251-257 (2010).

[36]. O. Ü. Aktürk and M. Toma, Appl. Phys. Lett. 96(8), 081914 (2010).

[37]. S. Stankovich, D. A. Dikin, G. H. B. Dommett, K. M. Kohlhaas, et al., Nature 442, 282-286 (2006).

[38]. S. Gilje, S. Han, M. Wang, K. L. Wang and R. B. Kaner, Nano Lett. 7, 3394-3398 (2007).

[39]. C. Gomez-Navarro, R. T. Weitz, A. M. Bittner, M. Scolari, et. al., Nano Lett. 7, 3499-3503 (2007).

[40]. D. C. Elias, R. R. Nair, T. M. G. Mohiuddin, S. V. Morozov, et al., Science 323, 610-613 (2009).

[41]. R. N. Grass, E. K. Athanassiou and W. J. Stark, Angew. Chem. Int. Ed. 119, 4996-4999 (2007).

[42]. C. G. Tan and R. N. Grass, Chem. Commun. 4297-4299, (2008).

[43]. E. K. Athanassiou, F. Krumeich, R. N. Grass and W. J. Stark, Phys. Rev. Lett. 101, 4 (2008).

[44]. F. M. Koehler, A. Jacobsen, K. Ensslin, C. Stampfer, et al., Small 6(10), 1125-1130 (2010).

[45]. J. Q. Liu, J. G. Tang and J. J. Gooding, J. Mater. Chem. 22, 12435 (2012).

[46]. H. Pinto, R. Jones, J. P. Goss and P. R. Briddon, J. Phys.: Condens. Matter. 21(40), 402001 (2009).

[47]. D. Hsieh, Y. Xia, D. Qian, L. Wray, et al., Nature 460(7259), 1101-1105 (2009).

[48]. W. Chen, D. Qi, X. Gao and A. T. S. Wee, Prog. Surf. Sci. 84(9-10), 279-321 (2009).

[49]. J. B. Oostinga, H. B. Heersche, X. Liu, A. F. Morpurgo and L. M. K. Vandersypen, Nat. Mater. 7 (2), 151-157 (2008).

[50]. D. B. Farmer, R. Golizadeh-Mojarad, V. Perebeinos, Y.-M. Lin, et al., Nano Lett. 9(1), 388-392 (2009).

[51]. X. C. Dong, D. L. Fu, W. J. Fang, Y. M. Shi, et al., Small 5 (12), 1422-1426 (2009).

[52]. C. H. Ahn, A. Bhattacharya, M. Di Ventra, J. N. Eckstein, et al., Rev. Mod. Phys. 78(4), 1185 (2006).

[53]. C. Casiraghi, Phys. Rev. B 80(23), 233407 (2009).

[54]. E. McCann, Phys. Rev. B 74, 161403 R (2006).

[55]. E. V. Castro, K. S. Novoselov, S. V. Morozov, N. M. R. Peres, et al., Phys. Rev. Lett. 99, 216802 (2007).

[56]. M. J. Frisch, G. W. Trucks, H. B. Schlegel, G. E. Scuseria, et al., Gaussain 03, Revision C.02, Inc., Wallingford, CT, (2004).

[57]. H. X. Zheng and W. Duley, Phys. Rev. B 78, 155118 (2008).

[58]. D. R. Dreyer, S. Park, W. Bielawski and R. S. Ruoff, Chem. Soc. Rev. 39, 228-240 (2010).

[59]. B. Brodie, Ann. Chim. Phys. 45, 351-353 (1855).

[60]. H. C. Schniepp, J.-L. Li, M. J. McAllister, H. Sai, et al., J. Phys. Chem. B 110, 8535-8539 (2006).

[61]. D Pandey, R. Reifenberger and R. Piner, Surf. Sci. 602(9), 1607-1613 (2008).

[62]. D. W. Boukhvalov and M. I. Katsnelson, J. Am. Chem. Soc. 130(32), 10697-10701 (2008).

[63]. J. T. Robinson, F. K. Perkins, E. S. Snow, Z. Q. Wei and P. E. Sheehan, Nano Lett. 8(10), 3137-3140 (2008).

[64]. M. Yankowitz, J.-J. Wang, A. G. Birdwell, Y.-A. Chen, et al., Nat. Mater. 13, 786-789 (2014).

[65]. S. Pei and H.-M. Cheng, Carbon 50, 3210–3228 (2012).

[66]. C. K. Chua and M. Pumera, Chem. Soc. Rev. 43(1), 291-312 (2014).

[67].V. Georgakilas, M. Otyepka, A. B. Bourlinos, V. Chandra, et al., Chem. Rev. 112, 6156-6214 (2012).

[68]. X. Huang, X. Qi, F. Boey and H. Zhang, Chem. Soc. Rev. 41(2), 666-686 (2012).

[69]. I. V. Lightcap and P. V. Kamat, Acc. Chem. Res. 46(10), 2235-2243 (2013).

[70]. C. Chung, Y.-K. Kim, D. Shin, S.-R. Ryoo, et al., Acc. Chem. Res. 46(10), 2211-2224 (2013).

[71]. J. Pyun, Angew. Chem. Int. Ed. 50, 46-48 (2011).

[72]. H. Y. Koo, H.-J. Lee, H.-A. Go, Y. B. Lee, et al., Chem. Eur. J 17, 1214-1219 (2011).

[73]. C. Xu, X. Wang and J. W. Zhu, J. Phys. Chem. C 112, 19841-19845 (2008).

[74]. M. Shi, J. Shen, H. Ma, Z. Li, et al., Colloids Surf. A 405, 30-37 (2008).

[75]. N. R. Khalid, Z. L. Hong, E. Ahmed, Y. W. Zhang, et al., Appl. Surf. Sci. 258, 5827-5834 (2012).

[76]. B. Neppolian, A. Bruno, C. L. Bianchi and M. Ashokkumar, Ultrason. Sonochem. 19, 9-15 (2012).

[77]. S. Yang, X. Feng, S. Ivanovici and K. Mullen, Angew. Chem. Int. Ed. 49, 8408-8411 (2010).

[78]. N. L. Yang, J. Zhai, D. Wang, Y. S. Chen and L. Jiang. ACS Nano 4, 887-894 (2010).

[79]. F. Bonaccorso, Z. Sun, T. Hasan and A. C. Ferrari. Nat. Photonics 4, 611-622 (2010).

Chapter 2 Literature Review

2.1 Synthesis of Graphene and Few-Layered Graphene

2.1.1 Mechanical Exfoliation

Careful layer by layer manual peeling (commonly known as mechanical exfoliation) of highly ordered pyrolytic graphite (HOPG) with the aid of scotch tape results in graphene sheets [1-3] which are nothing but the basal planes (layers stacked along the c-axis) of the bulk graphite bonded by weak van der Waals energy of ~2 eV/nm^2. A small force of ~300 nN/μm^2 is enough to peel a monolayer of carbon atoms (i.e., graphene) from graphite [4]. Such a small force can be manually applied with the aid of the scotch tape. Mechanical exfoliation is a difficult process that gives a very low yield of good quality graphene sheets. Moreover there is a possibility of retaining scotch tape's residue which can be detrimental for transport properties [5,6]. To avoid this additional heat treatment is normally given [7,8]. Another drawback of mechanical exfoliation is the resultant graphene sheets' lateral size which is limited by the lateral size of the chosen HOPG.

2.1.2 Graphitization of SiC

When Silicon Carbide (SiC) is heated to ~1400 °C under vacuum, Si sublimes and as a result the surface becomes carbon rich surface resulting in the epitaxial nucleation of graphene layer [9-12]. It has been found that the growth rate of graphene depends on the crystal structure of the starting SiC [10-12]. For example: graphene nucleates faster on C-terminated (000-1) C-face in comparison to that on Si-terminated (0001) Si-face). It has also been observed that the use of C-face SiC results in poor coverage, uneven surfaces and agglomeration of graphene [10]. On the other hand, the use of S-face SiC results in enhanced uniform graphene coverage of 1 μm^2 without any agglomeration [11]. This has been further improved (i.e., coverage area as high as 50 μm^2 was achieved) by reducing the sublimation of

Si atoms from SiC by heating it to ~1650 °C in Ar atmosphere at atmospheric pressure [12]. The quality (w.r.t charge carriers' mobility) of graphene obtained by heating SiC was not at par with the graphene obtained using the exfoliation method [12]. The main drawbacks are the cost involved in procuring SiC substrates and the requirement for a special experimental set-up to achieve very high temperatures.

2.1.3 Chemical Vapor Deposition

Chemical vapour deposition (CVD) involves deposition of high quality graphene films on large area substrates from suitable gas phase species. CVD graphene films typically are either single layered or few layered while the common substrates are transition metals [13-17]. In CVD of graphene films, the deposition parameters are arranged in such a way that only heterogeneous nucleation (i.e., nucleation on the substrate) takes place thereby avoiding the formation (i.e., homogeneous/gas phase nucleation) of any soot [18]. The solubility of carbon in transition metals also plays an important role in determining the number of graphene layers that form during the CVD [18]. Lower is the solubility of carbon in a transition metal greater is the transition metal's suitability as a substrate for large area graphene deposition [17]. In this context Cu has been found to be an industrially viable substrate [19,20]. However, to realize the formation of monolayer of graphene across the whole Cu substrate's surface, the surface should be ultra-smooth [21]. If the Cu surface has small local variations in roughness/smoothness, non-uniform multi-layered graphene regions significantly form on the surface [22]. The quality (w.r.t charge carriers' mobility) of graphene obtained by CVD was not at par with the graphene obtained using the exfoliation method. This was due to the presence of many graphene domains with different crystallographic orientations and thereby the presence of many grain boundaries [23-25]. To encounter this problem, researchers have demonstrated the deposition of isolated single crystals of graphene on the substrates [26-28]. Another drawback of CVD of graphene is the cost involved in setting-up the experiments

because the temperatures involved are greater than 2500 °C. Another major drawback pertaining to CVD of graphene is the transfer of graphene from the top of the metal surface on which it is deposited to another surface to derive the properties for an intended application. For example, in the case of electronic devices, graphene needs to be transferred from the surface of a metal substrate to the surface of an insulating substrate. If the transfer process is not properly carried out, graphene might be structurally damaged which in turn might degrade the expected properties [29,30].

2.1.4 Unzipping of Carbon Nanotubes

Unzipping of Carbon Nanotubes (CNTs) along their length results in graphenaceous layered material named graphene nanoribbons (GNRs) [31,32]. Even before the edge, size, chirality and ribbon width effects on the behaviour of GNRs were critically studied through experiments, they were theoretically studied [33-36]. Longitudinal unzipping of CNTs is an effective method to obtain GNRs [31,37,38]. The unzipping is normally carried by exposing multi-walled CNTs to strong oxidizing solutions. Other methods such as anisotropic etching [39], sono-chemical cutting [40], anodic oxidation lithography [41] etc. Of late CNTs can be produced in bulk quantities using CVD and therefore GNRs can also be produced in bulk quantities. However, it should be noted that the quality of GNRs depends on the quality of CNTs. In the context of this thesis work, GRNs can be considered as FLG.

2.1.5 Wet Chemical Route

In wet chemical routes of obtaining FLG (also named reduced graphene oxide), the starting material is always graphite (typically in the form of flakes of few tens to hundreds of µm in lateral size) which is converted into graphite oxide by reacting it with strong oxidizing agents [42]. The reaction allows covalent bonding [43] of hydroxyl and epoxy groups in the oxidizing agents to the C atoms in graphite forming graphite oxide in such a way that the

graphite's layered structure (now with graphene oxide sheets) is retained but conjugated structure (along the c-axis of graphite) of C atoms is severely distorted [44]. In the next step, graphene oxide is reduced by using reducing agents such as hydrazine, dimethyl hydrazine and hydroquinone results in the formation of FLG of different lateral sizes and number of layers [42]. Allowing the above mentioned covalent bonding results in distorted sp^2 network of C atoms. To mitigate this problem, researchers have used 1-pyrene carboxylic acid [45] and 9-anthracene carboxylic acid [46] as the oxidizing agents and succeeded in non-covalent bonding (π-π stacking) of the functional groups with the conjugated C atoms in graphite. The schematic of graphite, graphite oxide and reduced graphene oxide (FLG) is shown in Fig. 2.1.

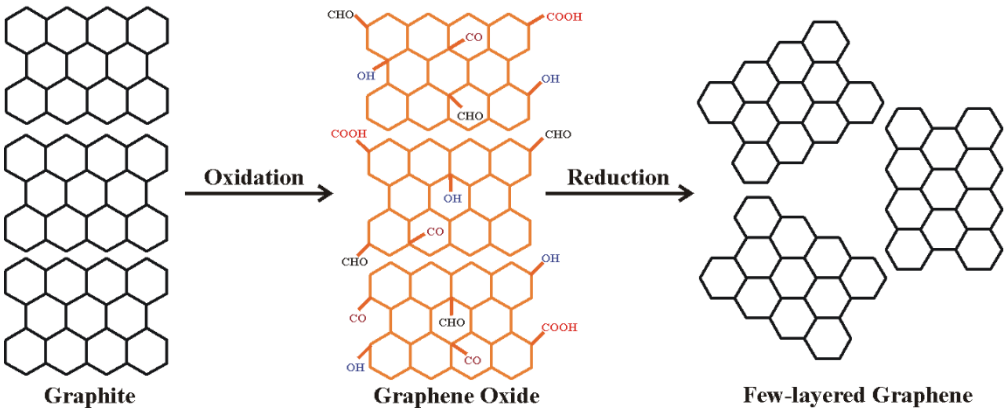

Figure 2.1. Schematic model of a graphite, graphene oxide and graphene.

Thermal reduction is another method to convert GO to reduced graphene oxide (RGO). In this method heat energy is used to heat GO above 1000 °C to remove the oxide functional groups from graphene oxide surfaces [47]. Besides thermal reduction, some other novel reduction methods such as the photo-catalytic [48], biomolecule-assisted [49], plant extract [50], supercritical fluid [51] and electrochemical [52] methods were demonstrated to convert GO to RGO. Even though there are several methods available to obtain FLG or RGO, researchers are still in the pursuit of developing methods which are eco-friendly, deliver high yields of end product and are cost-effective.

2.2 Synthesis of Heteroatom Doped FLG

2.2.1 Synthesis of N Doped FLG

Nitrogen (N) atom has a large electronegativity in comparison to that of C atom and therefore when it is doped in graphene, it polarizes the C atom network and thereby alters all the transport properties [53]. A doped N atom in graphene can have three types of bonds with the C atoms in the graphene lattice and accordingly the doped N atom is named as graphitic N, pyridinic N and pyrrolic N [54]. One very convenient method to dope heteroatoms in graphene is in-situ doping during the CVD growth (as discussed in section 2.1.3) of graphene films. This in-situ doping during CVD growth of graphene is initiated typically by introducing the precursor containing N atoms along with the carbon precursor into the reaction zone of the CVD reactor. Single precursor containing both C and N atoms can also be used. The co-doping of multiple species may also be achieved, aiming to create synergy between the co-dopants. During the reaction, these precursors dissociate and recombine into N-graphene by precipitating on the surface of the catalyst [55,56]. The nitrogen content in graphene can be controlled by changing the flow rate [55] and the ratio between carbon source and nitrogen source [57] during the reaction. However, it is very important to completely understand the relationship between the N atom bond formation with graphene and the practical constraints of CVD. In another method nitrogen doped graphene was synthesized by arc discharge of graphite in the presence of pyridine or NH_3 vapour [58]. In another unique method, nitrogen doped graphene was prepared by transforming nanodiamond surfaces [59]. This method resulted in higher nitrogen content than that synthesized by arc discharge of graphite. However in this method few single layered nitrogen doped graphenes are observed most of them are two or three layered graphenes.

Solvothermal process was also used to obtain nitrogen doped graphene. The reaction was carried out at ~300 °C to obtain the product in several grams. The solvothermal reaction was

facilitated by mixing Li_3N with CCl_4 or $N_3C_3Cl_3$ with Li_3N and CCl_4 [60]. In another method named segregation method, N-containing B layers and C-containing Ni layers are consecutively deposited on the SiO_2/Si substrate by e-beam evaporation method. In a subsequent process i.e., vacuum annealing process, the B atoms are trapped by Ni while the C atoms segregate out onto the Ni surfaces and combine to form N-graphene [61]. In this method, the N content is controlled by adjusting the thickness of the B and Ni layers.

In a simple chemical method, the oxygen functional groups and defects on GO were explored as active sites for doping heteroatoms. In this method, GO (or reduced GO) is thermally annealed in the presence of appropriate N-atom containing precursors (such as NH_3) and at suitable temperatures (≥800 °C) in such a way that the sp^2 carbon network is restored while N-doping is simultaneously achieved [62-64]. Here it should be noted that NH_3 is not only a source of N-atoms but also an effective reducing agent in comparison to H_2. In this context, the starting material to obtain N doped graphene could be GO. However, if the annealing temperature is low, only pyridinic- and pyrrolic- N doped graphenes are formed. When the defect density in the starting materials is low and/or the annealing temperatures are too high (and therefore C-N bonds break), low doping level is observed [65]. Here it is important to note that N doping is energetically favoured at defects and edges of the starting material [66].

Plasma processes [67-71] have also been used to dope N atoms in graphene. In these processes, the hexagonal rings of graphene are altered typically by bombarding graphene or GO with nitrogen ions and then N2 gas is introduced to fill C atom vacancies in the lattice. N doped graphene has been synthesized by exposing graphene or GO to N_2 plasma [67] and mechanically exfoliated to NH_3 gas [68]. N doping level is typically controlled by controlling the plasma density and plasma exposure time. During the plasma processes, it has been observed that substantial amount of oxygen species are introduced into graphene due to the creation of more number of reactive C atoms at the graphene edges [69]. The drawbacks of

plasma processes are the requirement of protective environment during the plasma exposure and the requirement of high temperatures.

In another unique method, GO was chemically reduced in a mixture solution of NH_3 and N_2H_4 to prepare N doped graphene [72]. The doping content can be controlled by controlling the reduction temperature. At high reduction temperatures (≥160 °C) N_2H_4 desorbs resulting in the decrease of doping content. It has also been observed that the morphology can also be altered with temperature. In another simple method, N doped graphene was prepared by ultra-sonication of graphene in the presence of N_2H_4 [73]. Careful analysis showed that N atoms are attached to only edges and defects in the starting graphene.

Even though some of the above presented methods are easy to execute, the control on the doping content is limited. On the other hand the methods which give a great control on the doping content demand stringent processing conditions and sophisticated equipment while the yield could be very low at a very high cost.

2.2.2 Synthesis of S Doped FLG

S atom doping is difficult than N atom doping. It requires higher energy than in the case of N atom doping. In the context of GO and reduced GO, S has a similar doping configuration as that of O [74,75]. The schematic of different bonding configurations between C and S [76] such as C–S–C, C–SO_x–C (x = 2, 3, and 4) and C–SH are shown in Fig. 2.1. It should be noted that the C–S bond length is ~25% longer than that of the C–C bond [77].

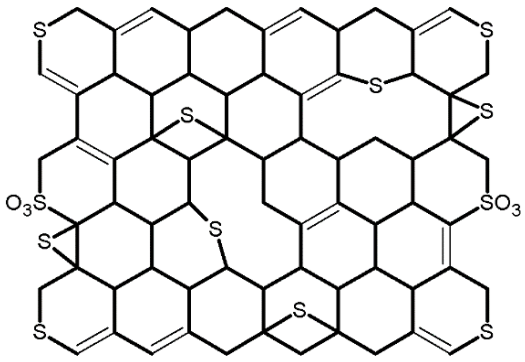

Figure 2.2. Typical configuration of S-doped graphene.

Theoretically it has been shown that S atom doping in graphene occurs by first formation of defect sites followed by the rupture of S=S bonds and depending on the doping level, the resultant S doped graphene can act as a narrow band-gap semiconductor or a metal [78]. S doped graphene is typically prepared by thermally annealing GO and S atoms containing precursor at high temperatures [79-84]. S doped graphene was also prepared by cycling lithium−sulphur batteries using graphene−sulphur composites as cathode materials and by using combined ion-exchange method [85,86]. It should be noted that the electronegativity of S and C are similar unlike in the case of N atom and C atom [87]. It has been theoretically shown that S doping occurs mainly at zigzag and armchair edges of graphene [88-90].

2.2.3 Synthesis of S, N Doped FLG

The idea behind co-doping S, N in graphene is to generate synergistic effects and to extract the advantages of both S and N doping together. CVD has been successfully used to prepare S, N doped graphene by carrying out the graphene deposition in the presence of pyrimidine and thiophene [91] and pyridine and thiophene [92] as the N and S doping sources, respectively. S atom doping in graphene through CVD occurs mainly in the form of sulphide groups (−C−S−C−) and to a less extent, in the form of oxidized S groups (−C−SO_x−C−) with pyrrolic/graphitic N structures. S doped graphene was also prepared by annealing GO at high temperatures (~900 °C) using different doping sources [89,93-95]. It has been observed that S, N doping in graphene is dependent on the temperature which controls the overall content of the independent dopants [96]. Hydrothermal synthesis method was also used to obtain S, N doped graphene [97,98]. In this process, GO and mercaptoacetic acid and DL-penicillamine as doping sources are allowed to react in the liquid phase.

2.3 Synthesis of Metal Oxide-Graphene Composites

In metal oxide-graphene composites, graphene acts as a functional component and/or a substrate for retaining metal oxide particles on its surfaces and edges. The large specific surface area and robust conductive configuration of graphene not only facilitate easy charge transfer and controllable redox reactions but also enhance the mechanical strength of the composite. Metal oxide-graphene composites are widely used in applications such as opto-electronics, electrochemical energy conversion and storage, solar energy harvesting, and so on [99-104]. In the recent past researchers have developed simple but effective synthesis methods to obtain a variety of oxide-graphene composites [105-109]. The synthesis methods namely *ex-situ* hybridization and *in-situ* crystallization have been well-understood methods to synthesize metal oxide-graphene composites [110]. In *ex-situ* hybridization, surface modified graphene (in the form of GO or reduced GO) and/or pre-synthesized or as-purchased metals or metal oxides are mixed in solution phase such that they bind through either the non-covalent bonding or any typical chemical bonding [110-113]. Due to the intrinsic nature of the method even though *ex-situ* hybridization allows pre-selection of the components and functional groups, it often results in low density and non-uniform distribution of metal oxide particles on graphene surfaces [114]. On the contrary, the *in-situ* crystallization [115-117] results in uniform surface distribution of metal oxide particles because the nucleation sites on the graphene surfaces can be controlled while the final form of graphene is formed along with the nucleation of metal oxide particles. Sol–gel method is a well-known chemical method to synthesize metal oxides from metal alkoxides or chlorides precursors which undergo a series of hydrolysis and poly-condensation reactions. Since GO and reduced GO offer reactive and anchoring sites for the nucleation and chemical bonding of metal oxide nanoparticles, *in-situ* sol-gel method was used to prepare TiO_2 and Fe_3O_4 [118,119] decorated graphene. Similar to sol-gel method, hydrothermal/solvothermal method is also a well-known method that results in

highly crystalline metal oxide particles even without the requirement of post-synthesis annealing or calcination. During this process if GO is simultaneously reduced, metal oxide-graphene composite can be formed. Using this method TiO_2, Fe_3O_4, Co_3O_4, and SnO_2 decorated graphene composites could be prepared [120-123]. In this method, concentration of the precursor solutions and the reaction time strongly influence the crystallinity of the metal oxide particles. This method is simple and effective but it involves dealing with solution synthesis which is not an industrially comfortable process. *In-situ* chemical and photochemical reduction of GO while metal oxides form is one interesting method to obtain metal oxide-graphene composites [124-127]. The microwave irradiation of suitable starting materials was also used to prepare metal oxide-graphene composites [128,129]. In this method microwaves provide the required energy to complete a chemical reaction. However, this method does not give the leverage on the control of metal oxide particle size and of the surface distribution of metal oxide particles on graphene surfaces. In the case of thin film based graphene applications, electrochemical deposition of metal oxides has been found to be an excellent method to obtain metal oxide-graphene composites [130]. On the other hand *in-situ* deposition of metal oxides has also been demonstrated while CVD growth of graphene films [130,131]. Careful observation of the synthesis methods of metal oxide-graphene composites shows that there is no solid state synthesis process that can co-form metal oxides and graphene.

References

[1]. K. S. Novoselov, A. K. Geim, S. V. Morozov, D. Jiang et al., Science 306, 666-669 (2004).

[2]. K. S. Novoselov, D. Jiang, F. Schedin, S. V. Morozov, A. K. Geim, et al., Proc. Natl. Acad. Sci. U.S.A. 102, 10451 (2005).

[3]. A. K. Geim and K. S. Novoselov. Nat. Mater. 6, 183-191 (2007).

[4]. Y. Zhang, J. P. Small, W. V. Pontius and P. Kim, Appl. Phys. Lett. 86, 073104 (2005).

[5]. J. -H. Chen, C. Jang, S. Xiao, M. Ishigami and M. S. Fuhrer, Nat. Nanotech. 3, 206-209 (2008).

[6]. K. I. Bolotin, K. J. Sikes, G. Fudenberg, P. Kim, et al., Solid State Commun. 146, 351-355 (2008).

[7]. M. Ishigami, J. H. Chen, W. G. Cullen, M. S. Fuhrer and E. D. Williams, Nano Lett. 7, 1643-1648 (2007).

[8]. J. Moser, A. Barreiro and A. Bachtold, Appl. Phys. Lett. 91, 163513 (2007).

[9]. I. Forbeaux, J. Themlin and J. Debever, Surf. Sci. 442, 9-18 (1999).

[10]. P. Sutter, Nat. Mater. 8, 171-172 (2009).

[11]. J. Hass, R. Feng, T. Li, X. Li, Z. et al., Appl. Phys. Lett. 89, 143106 (2006).

[12]. K. V. Emtsev, A. Bostwick, H. B. Weber, T. Seyller, et al., Nat. Mater. 8, 203-207 (2009).

[13]. K. S. Kim, Y. Zhao, H. Jang, B. H. Hong, et al., Nature. 457, 706-710 **(**2009).

[14]. A. Reina, X. Jia, J. Ho, D. Nezich and H. Son, Nano Lett. 9, 30-5 (2008).

[15]. X. Li, W. Cai, J. An, L. Colombo, R. S. Ruoff, et al., Science. 324, 1312-4 (2009).

[16]. X. Li, C. W. Magnuson, E. M. Vogel, L. Colombo, R. S. Ruoff, et al., J. Am. Chem. Soc. 133, 2816-2819 (2011).

[17]. X. Li, W. Cai, L. Colombo and R. S. Ruoff, Nano Lett. 9, 4268-4272 (2009).

[18]. C. Mattevi, H. Kim and M. Chhowalla, J. Mat. Chem. 21, 3324 (2011).

[19]. Z. Luo, Y. Lu, D. W. Singer, B. R. Goldsmith, A. T. C Johnson, et al., Chem. Mater. 23, 1441-1447 (2011).

[20]. W. Liu, H. Li, C. Xu, Y. Khatami and K. Banerjee, Carbon 49, 4122-4130 (2011).

[21]. H. Kim, C. Mattevi, M. R. Calvo, M. Chhowalla, E. Saiz, et al., ACS Nano 6, 3614-3623 (2012).

[22]. M. Congqin, Z. Churan, L. Owen and X. Ya-Hong, "Chemical Vapor Deposition of Graphene. In Physics and Applications of Graphene – Experiments", S. Mikhailov, Ed. In Tech: Rijeka 37-54 (2011).

[23]. K. Kim, Z. Lee, W. Regan, C. Kisielowski, M. F. Crommie and A. Zettl, ACS Nano 5(3), 2142-2146 (2011).

[24]. P. Y. Huang, C. S. Ruiz-Vargas, A. M. Van der Zande, J. W. Kevek, D. A. Muller, et al., Nature. 469, 389-92 (2011).

[25]. L. Tapasztó, P. Nemes-Incze, G. Dobrik, K. Jae Yoo, et al., Appl. Phys. Lett. 100, 053114 (2012).

[26]. D. Geng, B. Wu, Y. Guo, L. Jiang, W.Hu, Y. Liu, et al., Proc. Natl. Acad. Sci. U.S.A. 109(21), 7992-7996 (2012).

[27]. W. Wu, L. A. Jauregui, Z. Su, Z. Liu, et al., Adv. Mater. 23, 4898-4903 (2011).

[28]. Q. Yu, L. A. Jauregui, R. Colby, T. F. Chung, et al., Nat. Mater. 10, 443-449 (2011).

[29]. T. Yoon, W. C. Shin, T. Y. Kim, J. H. Mun, et al., Nano Lett. 12, 1448-1452 (2012).

[30]. Z. Sun, D. K. James and J. M. Tour, J. Phys. Chem. Lett. 2, 2425-2432 (2011).

[31]. D. V. Kosynkin, A. L. Higginbotham, A. Sinitskii, J. R. Lomeda, et al., Nature 458, 872-876 (2009).

[32]. B. W. Xiao, X. F. Li, X. Li, B. Q. Wang, X. L. Sun, et al., J. Phys. Chem. C 118(2), 881 (2014).

[33]. H. Bu, Y. F. Chen, M. Zou, H. Yi, et al., Phys. Lett. A 373(37), 3359-3362 (2009).

[34]. E. V. Castro, K. S. Novoselov, J. Nilsson, F. Guinea, et al., J. Phys. Condens. Matter 22, 175503 (2010).

[35]. A. Yamashiro, Y. Shimoi, K. Harigaya and K. Wakabayashi, Phys. Rev. B 68, 193410 (2003).

[36]. M. Y. Han, B. Ozyilmaz, Y. B. Zhang and P. Kim, Phys. Rev. Lett. 98, 206805 (2007).

[37]. B. Shinde, J. Debgupta, A. Kushwaha, M. Aslam and V. K. Pillai, J. Am. Chem. Soc. 133, 4168-4171 (2011).

[38]. M. Saghafi, F. Mahboubi, S. Mohajerzadeh, M. Fathi and R. Holze, Current Appl. Phys. 14(10), 1335-1343 (2014).

[39]. L. C. Campos, V. R. Manfrinato, J. D. Sanchez-Yamagishi, J. Kong and P. Jarillo-Herrero, Nano Lett. 9, 2600-2604 (2009).

[40]. Z.-S. Wu, W. Ren, L. Gao, B. Liu, et al., Nano Res. 3, 16-22 (2010).

[41]. S. Masubuchi, M. Ono, K. Yoshida, K. Hirakawa and T. Machida, Appl. Phys. Lett. 94, 082107 (2009).

[42]. S. Park and R. S. Ruoff, Nat. Nanotechnol. 4, 217-224 (2009).

[43]. A. Lerf, H. He and M. Forster, J. Phys. Chem. B 5647, 4477-4482 (1998).

[44]. A. Buchsteiner, A. Lerf and J. Pieper, J. Phys. Chem. B 110, 22328 (2006).

[45]. S. Bose, T. Kuila, A. K. Mishra, N. H. Kim and J. H. Lee, Nanotechnol. 22, 405603 (2011).

[46]. X. An, T. Simmons, R. Shah, C. Wolfe, et al., Nano Lett. 10, 4295-301 (2010).

[47]. A. Nikolakopoulou, D. Tasis, L. Sygellou, V. Dracopoulos, et al., Electrochim. Acta 111, 698-706 (2013).

[48]. G.Williams, B. Serger and P. V. Kamat, ACS Nano 2, 1487-1491 (2008).

[49]. Z. Xing, Q. Chu, X. Ren, J. Tian, et al., Electrochem. Commun. 32, 9-13 (2013).

[50]. O. Akhavan, E. Ghaderi, E. Abouei, S. Hatamie and E. Ghasemi, Carbon 66, 395-406 (2014).

[51]. C. Kong, W. Song, M. J. Meziani, A. Anderson, et al., J. Supercrit. Fluids 61, 206-211 (2012).

[52]. M. Zhou, Y. Wang, Y. Zhai, J. Zhai, et al., Chem. Eur. J. 15, 6116-6120 (2009).

[53]. P. Wu, P. Du, H. Zhang and C. Cai, Phys. Chem. Chem. Phys. 15, 6920-6928 (2013).

[54]. D. Usachov, O. Vilkov, A. Gruneis, D. Haberer, et al., Nano Lett. 11, 5401-5407 (2011).

[55]. A. L. M. Reddy, A. Srivastava, S. R. Gowda, H. Gullapalli, et al., ACS Nano 4, 6337-6342 (2010).

[56]. Z. Jin, J. Yao, C. Kittrell and J. M. Tour, ACS Nano 5, 4112-4117 (2011).

[57]. D. Wei, Y. Liu, Y. Wang, L. Huang, G. Yu, et al., Nano Lett. 9, 1752-1758 (2009).

[58]. L. S. Panchakarla, A. Govindaraj, H. R. Krishnamurthy, U. V. Waghmare, C. N. R. Rao, et al., Adv. Mater. 21, 4726-4730 (2009).

[59]. K. S. Subrahmanyam, L. S. Panchakarla, A. Govindaraj, C. N. R. Rao, et al., J. Phys. Chem. C 113, 4257 (2009).

[60]. D. Deng, X. Pan, Q. Xue, G. Sun, X. Bao, et al., Chem. Mater. 23, 1188 (2011).

[61]. C. Zhang, L. Fu, N. Liu, M. Liu, et al., Adv. Mater. 23, 1020-1024 (2011).

[62]. X. L. Li, H. L. Wang, J. T. Robinson, H. J. Dai et al., J. Am. Chem. Soc. 131, 15939-15944 (2009).

[63]. B. Guo, Q. Liu, E. Chen, H. Zhu, L. Fang and J. R. Gong, Nano Lett. 10, 4975 (2010).

[64]. D. Geng, Y. Chen, X. Sun, S. Ye, S. Knights, et al., Energy Environ. Sci. 4, 760 (2011).

[65]. K. Kinoshita, "Carbon: Electrochemical and Physicochemical Properties", Wiley, New York, (1988).

[66]. X. Wang, X. Li, L. Zhang, Y. Yoon et al., Science 324(5928), 768-771 (2009).

[67]. Y. Shao, S. Zhang, Y. Wang, Y. Lin, et al., J. Mater. Chem. 20, 7491-7496 (2010).

[68]. Y. C. Lin, C. Y. Lin and P. W. Chiu, Appl. Phys. Lett. 96, 133110 (2010).

[69]. Y. Shao, S. Zhang, I. A. Aksay, Y. Lin, et al., J. Mater. Chem. 20, 7491 (2010).

[70]. Y. Wang, Y. Shao, D. W. Matson, J. Li and Y. Lin, ACS Nano 4, 1790 (2010).

[71]. Y. H. Lu, Y. Huang, M. J. Zhang and Y. S. Chen, J. Nanosci. Nanotechnol. 14, 1134-1144 (2014).

[72]. D. Long, W. Li, L. Ling, J. Miyawaki, et al., Langmuir 26, 16096, (2010).

[73]. D. W. Wang, I. R. Gentle and G. Q. Lu, Electrochem. Commun. 12, 1423 (2010).

[74]. K. A. Mkhoyan, A. W. Contryman, S. Miller and M. Chhowalla, Nano Lett. 9, 1058-1063 (2009).

[75]. J. Y. Dai and J. M. Yuan, J. Phys. Condens. Matter. 22, 225501 (2010).

[76]. Z. Yang, Z. Yao, X. M. Zhou, X. Chen, et al., ACS Nano. 6, 205-211 (2012).

[77]. P. A. Denis, Chem. Phys. Lett. 492, 251-257 (2010).

[78]. P. A. Denis, R. Faccio and A. W. Mombru, Chem. Phys. Chem. 10, 715-722 (2009).

[79]. J. C. Wang, R. Ma, Z. Z. Zhou, G. H. Liu and Q. Liu, Sci. Rep. 5, 9304 (2015).

[80]. M. Li, C. Liu, H. Zhao, H. An, et al., Carbon 86, 197-206 (2015).

[81]. R. Wang, D. C. Higgins, F. Hassan, Z. Chen, et al., Sci. Rep. 3, 2431-2437 (2013).

[82]. X. Chen, X. Xu, Z. Yang, X. Xu, S. Huang, et al., Nanoscale 6, 13740-13747 (2014).

[83]. J. E. Park, Y. J. Jang, Y. J. Kim, S. Kim, Phys. Chem. Chem. Phys, 16, 103-109 (2014).

[84]. H. L. Poh, P. Simek, Z. Sofer and M. Pumera, ACS Nano 7, 5262-5272 (2013).

[85]. Z. Ma, S. Dou, A. Shen, S. Wang, et al., Angew. Chem., Int. Ed. 54, 1888-1892 (2015).

[86]. Y. Zhang, M. Chu, W. Deng, M. Ma, et al., Chem. Commun. 50, 6382-6385 (2014).

[87]. S. Glenis, A. J. Nelson and M. M. Labes, J. Appl. Phys. 86, 4464-4466 (1999).

[88]. Z. Yang, Z. Yao, G. F. Li, X. Chen and S. M. Huang, ACS Nano 6, 205-211 (2012).

[89]. J. Liang, Y. Jiao, M. Jaroniec and S. Z. Qiao, Angew. Chem. Int. Ed. 51, 11496-11500 (2012).

[90]. L. Zhang, J. Niu, M. Li and Z. Xia, J. Phys. Chem. C 118, 3545-3553 (2014).

[91]. J. Xu, G. Dong, C. Jin, M. Huang and L. Guan, Chem. Sus. Chem. 6, 493-499 (2013).

[92]. Y. Ito, W. Cong, T. Fujita, Z. Tang and M. Chen, Angew. Chem. 54, 2131-2136 (2015).

[93]. W. Ai, Z. Luo, J. Jiang, L. Xie, H. Zhang, et al., Adv. Mater. 26, 6186-6192 (2014).

[94]. A. G. Kannan, J. Zhao, Y. S. Kang, D. W. Kim, et al., J. Mater. Chem. A 2, 12232-12239 (2014).

[95]. H. Zhang, X. Liu, X. Zhang, W. Hu, et al., J. Power Sources. 279, 252-258 (2015).

[96]. P. Xiao, Y. Yan, J. Y. Wang, X. Wang, et al., Appl. Catal. B 154-155, 232-237 (2014).

[97]. B. Feng, J. Xie, C. Dong, S. Zhang, et al., RSC Adv. 4, 17902-17907 (2014).

[98]. Q. Luo, F. Hao, M. Grätzel and H. Lin, J. Phys. Chem. C. 118, 17010-17018, (2014).

[99]. Q. Wu, Y. X. Xu, Z. Y. Yao, A. R. Liu and G. Q. Shi, ACS Nano 4, 1963 (2010).

[100]. W. J. Hong, Y. X. Xu, C. Li, G. Q. Shi, et al., Electrochem. Commun.10, 1555 (2008).

[101]. Y. H. Ng, A. Iwase, A. Kudo and R. Amal, J. Phys. Chem. Lett. 1, 2607 (2010).

[102]. S. Yang, X. Feng, S. Ivanovici and K. Mullen, Angew. Chem. Int. Ed. 49, 8408-8411 (2010).

[103]. N. L. Yang, J. Zhai, D. Wang, Y. S. Chen and L. Jiang. ACS Nano 4, 887-894 (2010).

[104]. Y. Q. Sun, C. Li, Y. X. Xu, G. Q. Shi, et al., Chem. Commun. 46, 4740 (2010).

[105]. B. X. Li, T. X. Liu, L. Y. Hu and Y. F. Wang, J. Phys. Chem. Solids 74, 635-640 (2013).

[106]. Q. Guo, Z. Zheng, H. L. Gao, J. Ma and X. Qin, J. Power Sources 240, 149-154 (2013).

[107]. J. Y. Son, Y.H. Shin, H. Kim and H. M. Jang, ACS Nano 4, 2655-2658 (2010).

[108]. D. Marquardt, C. Vollmer, E. Redel, C. Janiak, et al., Carbon 49, 1326-1332 (2011).

[109]. Y. J. Yun and K. B. Song, J. Nanosci. Nanotechnol. 11, 7376-7380 (2013).

[110]. X. Huang, X. Qi, F. Boey and H. Zhang, Chem. Soc. Rev. 41(2), 666-686 (2012).

[111]. J. Liu, S. Fu, B. Yuan, Y. Li and Z. Deng, J. Am. Chem. Soc. 132, 7279-7281 (2010).

[112]. S. R. Sun, L. Gao, Y. Q. Liu, Appl. Phys. Lett. 96, 083113 (2010).

[113]. J. Liu, H. Bai, Y. Wang, D. D. Sun, et al., Adv. Funct. Mater. 20, 4175-4181, (2010).

[114]. J. Huang, L. Zhang, Y. Zhang, Z. Zhang, et al., Nanoscale 2, 2733-2738 (2010).

[115]. D. Wang, R. Kou, M. A. Pope, I. A. Aksay, et al., ACS Nano 4, 1587-1595 (2010).

[116]. H. Kim, S.W. Kim, D. H. Seo, Y. Kim, K. Kang, et al., Nano Res. 3, 813-821 (2010).

[117]. J. S. Lee, K. H. You and C. B. Park, Adv. Mater. 24, 1084-1088 (2012).

[118]. X. Y. Zhang, H. P. Li, X. L. Cui and Y. H. Lin, J. Mater. Chem. 20, 2801-2806 (2010).

[119]. G. Zhou, D. W. Wang, L. Wen, H.-M. Cheng, et al., Chem. Mater. 22, 5306-5315 (2010).

[120]. J. F. Shen, B. Yan, H. W. Ma, N. Li, et al., J. Mater. Chem. 21, 3415-3421 (2011).

[121]. J. Z. Wang, C. Zhong, Z. X. Wang, H. K. Liu, et al., Chem. Eur. J. 17, 661-667 (2011).

[122]. J. X. Zhu, Y. K. Sharma, Q. Y. Yan, et al., J. Phys. Chem. C 115, 8400-8406 (2011).

[123]. X. Huang, X. F. Zhou, K. Qian, C. Z. Yu, et al., Chem. Phys. Chem. 12, 278-281 (2011).

[124]. I. V. Lightcap, T. H. Kosel and P. V. Kamat, Nano Lett. 10, 577-583 (2010).

[125]. F. H. Li, H. F. Yang, C. S. Shan, L. Niu, et al., J. Mater. Chem. 19, 4022-4025 (2009).

[126]. Y.-K. Kim, H.-K. Na and D.-H. Min, Langmuir 26, 13065-13070 (2010).

[127]. K. Jasuja and V. Berry, ACS Nano 3, 2358-2366 (2009).

[128]. J. Yan, Z. J. Fan, T. Wei, W. Z. Qian, et al., Carbon 48, 3825-3833 (2010).

[129]. J. Yan, T. Wei, L. J. Zhang, Z. J. Fan, et al., Electrochim. Acta 55, 6973-6978 (2010).

[130]. S. X. Wu, Z. Y. Yin, Q. Y. He, H. Zhang, et al., J. Phys. Chem. C 114, 11816-11821 (2010).

[131]. Z. Y. Yin, S. X. Wu, X. Z. Zhou and X. Huang, Small 6, 307-312 (2010).

Chapter 3 Experimental Work

3.1 Synthesis of Materials

3.1.1 Synthesis of Few-Layered Graphene

Graphene oxide (GO) was first prepared from graphite flakes (flake size ~300 μm, lower flake size could also be used) by adopting Hummers method [1]. Graphite flakes (3 g) were added to 69 ml of concentrated H_2SO_4 (98%, Merck) and stirred for 12 h at moderate speed at room temperature to intercalate graphite layers. To this mixture, 1.5 g of $NaNO_3$ (98%, Merck) was added and stirred for 15 min. Till this stage all the steps are carried out under room conditions. The idea behind oxidation is to increase the inter-planar spacing between two basal plans in graphite. Subsequently $KMnO_4$ (9 g) was added very slowly and reaction temperature during this addition was maintained at 0 °C with the aid of ice bath as this oxidation process is highly exothermic. The reactions carried out in ice bath for ~2 h. Then the reaction mixture was removed from the ice bath and was allowed to cool under stirring. As the reaction progressed, the mixture gradually thickened with decreasing effervescence. At the end of 3 h, the mixture became a brownish grey thick paste. Subsequently distilled water (138 ml) was added drop by drop to the mixture causing violent effervescence and a rise in temperature of the resultant solution to 98 °C. The reaction mixture was maintained at this temperature for 15 min. After cooling the mixture to room temperature it was further diluted with warm distilled water (420 ml) and a small amount of 30% H_2O_2 (3 ml) was added to reduce the residual permanganate and manganese dioxide to colourless soluble manganese sulphate. Upon treatment with the peroxide, the suspension turned bright yellow. The obtained mixture was then subjected to multiple washes with warm distilled water by discarding the supernant every time and finally the filtrate was collected and kept in hot oven at 100 °C for 12 h to obtain GO powder. GO was then subjected to microwave irradiation (MWI) (900 W and 2.45 GHz) inside a household microwave oven for few secs for

exfoliation of graphene sheets and removal of attached functional groups which are mostly epoxide and hydroxyl groups, in addition to carbonyl and carboxyl groups during the synthesis. Microwave irradiation results in the formation of graphene worms (GWs) which are further ultra-probe sonicated in ethanol for 1 h to obtain a uniform suspension of graphene sheets.

3.1.2 Synthesis of S, N Doped FLG

The graphite flakes (flake size ~150 µm, lower flake size could also be used) were mixed to a solution mixture (3:1 by volume) of sulfuric acid (98%) and nitric acid (65%) for 15 h. Nitric acid serves as an oxidizer and sulfuric acid as a source for intercalation. The mixture was stirred from time to time to facilitate uniform intercalation of each graphite flake. The resultant mixture was then subjected to multiple washes with distilled water by discarding supernant every time until the pH of solution reached 7 (neutral). After washing, acid-treated graphite flakes (ATGFs) were dried at 100 °C in a vacuum oven for 12 h to avoid remove any water. Thus prepared ATGFs were subjected to MWI to obtain GWs (same as in the case of FLG described in the previous section) which are further ultra-probe sonicated in ethanol for 1 h to obtain a uniform suspension of S, N doped FLG sheets. The schematic of the formation of S, N doped FLG is shown in Fig. 3.1. Here the yield is 98% by weight in comparison to 90% in the case of FLG.

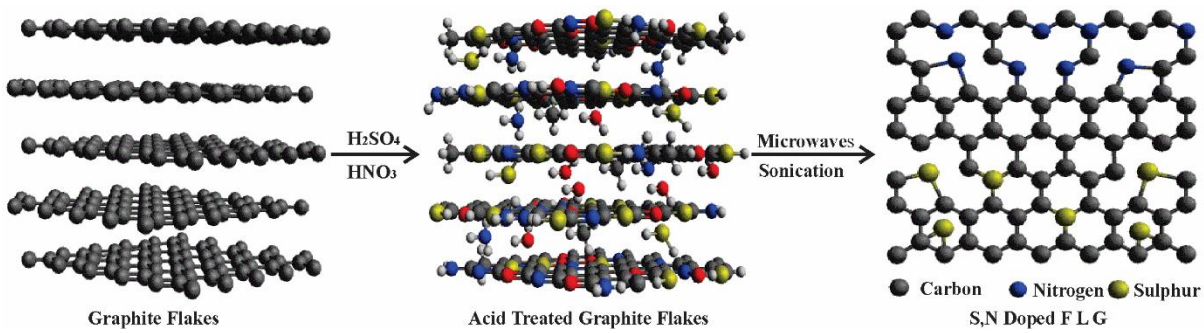

Figure 3.1. Schematic diagram of obtaining S, N doped FLG from graphite flakes.

The logic behind the use of microwave irradiation to obtain FLG and S, N doped FLG is explained here. Microwave irradiation typically results in homogeneous and volumetric heating of polar materials [2]. The molecular dipoles are induced to oscillate by microwaves. These oscillations cause high rate of molecular collisions which generate heat throughout the irradiated volume unlike in the case of conventional heating wherein there can be a temperature gradient between the heat source and the mass to heat. The other advantage of microwaves is their help in enhancement of chemical reactions. This is due to the interaction between the electromagnetic irradiation and chemical structure [3].

3.1.3 Synthesis of ZnO Decorated S, N Doped FLG

In preparing ZnO decorated S, N doped FLG, a certain amount of GWs (section 3.1.2) were sonicated in absolute ethanol until attaining a proper dispersion of GWs. Then Zinc Acetate ($Zn(Ac)_2 \cdot 2H_2O$ from Alfa Easer) was added and the mixture was heated at 100 °C under stirring and room conditions to allow proper dissolution of Zinc Acetate and subsequent precipitation. The precipitate was calcined at 300 °C for 12 h in a muffle furnace to obtain ZnO decorated S, N doped FLG. Pure ZnO was prepared by following the same procedure except for the addition of GWs. In all experiments the molarity of solution ($Zn(Ac)_2 \cdot 2H_2O$ + ethanol) was maintained at 0.03 $mol.L^{-1}$ while 1, 2 and 3 wt% of GWs are added in separate experiments to prepare ZnO decorated S, N doped FLG.

3.1.4 Synthesis of MgO Decorated FLG

A green synthesis method [4] is adopted to prepare MgO decorated FLG. In this method magnesium (Mg) ribbons are burnt in dry ice resulting in FLG and MgO are products. Unreacted species and MgO are removed by treating the sample with concentrated HCl. However, traces of MgO nanoparticles can be intentionally left over as decoration on FLG by controlling the concentration of the HCl, MgO nanoparticles are retained as a decoration on

FLG instead of making an effort to remove MgO. This was done here because MgO is electrochemically inactive [5-7] while its adsorbing and liquid electrolyte retaining capability [8] functions as a protective coating and its role in enhancing ionic conductivity encourages the use of MgO decorated FLG, for example, as an anode material in Li ion batteries (LIBs) [9-12]. In addition, the presence of MgO nanoparticles with surface defects may become alternative doping components in FLG, which may be a promising solution to stop the clustering or electroplating and subsequent dendritic growth of Li atoms at the anode of LIBs [13]. Additionally owing to the characteristics of both MgO and FLG, adsorption based applications can be achieved. The synthesis of MgO decorated FLG is as follows: Mg turnings (99.9% pure and those typically used in Grignard reaction) are ignited in the presence of dry ice. A groove is made in a block of dry ice and 3 g of the Mg turnings are placed in it. The turnings are then ignited. Immediately after ignition the groove is covered with another block of dry ice (Fig. 3.2(a)) until the combustion process is completed. After combustion, the product (Fig. 3.2(b)) was transferred to a beaker containing 100 ml of 1 M HCl. The resultant mixture was stirred at room temperature for 12 h to remove any unreacted Mg (HCl easily reacts with metals to form metal chlorides, which are easily dissolved in aqueous solutions). The mixture was then filtered and washed with deionized water several times until the pH of the solution was 7. The product was dried for 12 h under vacuum at 100 ºC. If the concentration of HCl is high, more of MgO is removed and there is also a possibility of damaging the FLG.

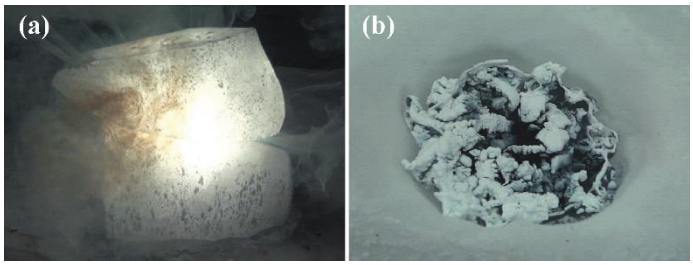

Figure 3.2. Photographs of (a) combustion of Mg metal turnings in dry ice and (b) combustion product in the groove in one of the dry ice blocks.

3.1.5 Synthesis of MgO and NiO Decorated FLG

Mg metal turnings (same as in section 3.1.4), NiO (Sigma Aldrich), hydrochloric acid (Merck) and ethanol, were used as-received. 1 g of Mg metal turnings and 0.5 g of NiO powder were mixed together by using planetary ball mill (Retch PM 400). The powder (NiO+Mg) to ball ratio was fixed at 1:5 while ethanol (13.37 ml) was used as a process control agent during ball milling. The optimal milling time was 10 h which is the time required for the Mg turnings to flatten. The ball-milled blend of NiO powder and Mg was combusted in the presence of dry ice (solid CO_2) and the combustion product was washed with an acid (1 M HCl) to remove any impurities and/or free-standing metal oxides' residue. The mixture was then filtered, washed with deionized water several times until the filtrate turned out to be of neutral pH. Finally, the isolated solid NiO-MgO carbon product was dried under vacuum for 12 h at 100 °C.

3.2 Characterization

3.2.1 Electron Microscopy

Scanning electron microscopy was mainly used to obtain secondary electron (SE) images of the samples. For imaging purposes, the sample surface must be electrically conducting, otherwise the electron beam would charge up the surface. In the present study all the samples are electrically conductive and therefore conducting coating (like Au) was not used on the surfaces prior to the examination. Zeiss Ultra55 ultra high resolution field emission scanning electron microscope (FESEM) was used to obtain SE images at working distance (typically 4 mm), at accelerating voltage (5 kV), and at a very high magnification. Also, for energy-dispersive x-ray (EDX) analysis working distance and accelerating voltages were 10 mm and 10 kV, respectively. EDX analysis was carried out to obtain the elemental composition of the samples' surfaces.

Morphology was also studied by transmission electron microscope (Model FEI Technai G^2 S-Twin) operated at an accelerating voltage of 200 kV. High resolution TEM images were also recorded. Electron diffraction patterns from appropriate areas of the samples were collected and indexed to understand the crystallinity of the samples. Standard indexing was followed to index different diffraction patterns. The electron diffraction results were complemented with X-ray diffraction results. For TEM studies samples had to be specially prepared. The powder sample was first dispersed in 10 ml of ethanol by sonication for 30 min in a typical ultrasonic bath. A small volume of this solution was then dropped onto carbon coated or lacey carbon formvar Cu TEM grids using a micro-pipette. Upon evaporation of ethanol the sample to be studies would be retained on the TEM grid.

3.2.2 X-ray Diffraction

To determine the crystallinity of the samples considered in this study, powder x-ray diffraction measurements were performed in the 2θ (θ is the angle of diffraction) range of 5-100° with a step size of 0.02°. GIXRD patterns in this work have been measured using Bruker D8 Discover diffractometer which uses X-rays of the Cu Kα line (λ = 1.54 Å), produced by impinging an 40 mA electron beam on a Cu target. Standard indexing was followed to index different diffraction peaks. JCPDS data files have also been referred to confirm the crystallinity. In some cases Rietveld refinement of the XRD patterns were carried out using TOPAS software (version 3.0). In the Rietveld method, the least squares approach was used to refine the theoretical line profile (height, width and position of the Bragg's reflections of a powder X-ray diffraction pattern) until it matches the experimental pattern.

3.2.3 Micro Raman Scattering

Micro Raman scattering study was carried out using CRM spectrometer. Raman spectra have been collected by using 532 nm green line of Nd-YAG LASER as the excitation source. The

LASER power was kept at minimum in all the measurements in order to avoid any thermal influences. The LASER beam was focused onto the sample surfaces by means of 100x (for LASER spot diameter ~1 μm). The scattered light was collected using charge coupled device (CCD) detector (model alpha 300 of WiTec, Germany) in the spectral range 500 to 4000 cm^{-1} in a back scattering geometry perpendicular to (100) face of the Si standard. LASER is focused on the sample placed under the microscope that excites the sample and the scattered light is collected in the same path as the incoming LASER. The scattered light is dispersed on to a CCD detector. Before every measurement the spectrometer was calibrated using the Si standard sample.

3.2.4 X-Ray Photoelectron Spectroscopy

X-Ray Photoelectron Spectroscopy (XPS) was used to understand the precise compositional details of the samples. In this study, XPS measurements were performed using VG Scientific ESCALab Mark II X-ray photoelectron spectrometer using a monochromatic Al Kα x-ray source (~1486.6 eV). Survey spectra were collected covering the full binding energy range 0-1200 eV using a step size of 1 eV and pass energy of 50 eV, whereas the high resolution spectra of C1s, Al 2p and Al KLL were collected using a step size of 0.2 eV and pass energy of 20 eV. To compensate for any surface charging, all binding energies were corrected with reference to the C1s peak at 284.5 eV. Peak fitting and deconvolution of the high resolution spectra were achieved using XPS peak fit 4.0 software and were fitted according to mixed Gaussian–Lorentzian components and a non-linear Shirley background.

3.2.5 UV-Visible Spectroscopy

Typical UV-Visible (UV-Vis) spectroscopy was used to understand the bonding characteristics in certain samples. In this work, minute quantity of the synthesized material was taken in a glass beaker containing ethanol. The mixture was then sonicated in an

ultrasonic bath for 30 min for proper dispersion. The solution was then transferred to the cuvettes for measurement. The prepared solutions were characterized with Perkin Elmer Lambda 35 UV/Vis spectrophotometer. The absorbance scanning wavelength ranged from 200 nm to 900 nm. The measurements were made with ethanol as a reference. The results were directly transferred to Excel for calculating the band gap using the absorption coefficient from the data.

3.2.6 Fourier Transform Infrared Spectroscopy

Fourier Transform Infrared (FTIR) spectroscopy was used to understand the composition of the samples. In this study, FTIR spectra of the samples was collected using Perkin Elmer FT-IR X 1760 instrument. Typical potassium bromide (KBr) pellet procedure was followed. In brief, a small quantity of the sample was mixed with KBr and finely crushed to get a homogeneous mixture. This mixture was then taken in a 10 mm diameter die and pressed under pressure into pellet before recording the spectra. Spectra were taken in the transmission mode. Changes in the absorption bands were investigated in the 400-4000 cm^{-1} region.

3.2.7 Specific Surface Area Measurement

Standard specific surface area and porosity distribution are determined from results of N_2 physisorption at 77 K with Micromeritics (Tristar 3000, USA) using BET and Barrett-Joyner-Halenda (BJH) multipoint methods. Samples were preheated under N_2 flow for 1 h at 150 °C. During surface area measurements, normal temperature and pressure conditions were maintained while N_2 gas flowed continuously.

Other experiments related to the applications are mentioned along with the discussion on the applications in section 4.6.

References

[1]. W. S. Hummers and R. E. Offeman, J. Am. Chem. Soc. 80(6), 1339 (1958).

[2]. P. Lidström, J. Tierney, B. Wathey and J. Westman, Tetrahedron, 57, 9225-9283 (2001).

[3]. J. T. Senise and L. A. Jermolovicius, J. Microw. Optoelectron. 97, 97-112 (2004).

[4]. B. Z. Shakhashiri, Chemical Demonstrations: A Handbook for Teachers of Chemistry, Vol. 1, pp. 90-92 (1983).

[5] W. Zhou, S. Upreti and M. S. Whittingham, Electrochem. Commun. 13, 1102-1104 (2011).

[6]. Z. Wang, C. Wu, L. Liu, F. Wu, et al., J. Electrochem. Soc. 149, A466-A471 (2002).

[7]. J. Chen, H. Zhao, J. He and J. Wang, Rare Met. 30, 166-169 (2011).

[8]. M.-S. Song, S.-C. Han, H.-S. Kim, J.-H. Kim, et al., J. Electrochem. Soc. 151, A791-A795 (2004).

[9]. M. Mladenov, R. Stoyanova, E. Zhecheva and S. Vassilev, Electrochem. Commun. 3, 410-416 (2001).

[10]. J. S. Gnanaraj, V. G. Pol, A. Gedanken and D. Aurbach, Electrochem. Commun. 5, 940-945 (2003).

[11]. H. Zhao, L. Gao, W. Qiu and X. Zhang, J. Power Sources 132, 195-200 (2004).

[12]. C. J. Leo, G. V. Subba Rao and B. V. R. Chowdari, Solid State Ionics 159, 357-367 (2003).

[13]. Y. Liu, V. I. Artyukhov, M. Liu, A. R. Harutyunyan and B. I. Yakobson, J. Phys. Chem. Lett. 4, 1737-1742 (2013).

Chapter 4 Results and Discussion

4.1 Few-Layered Graphene

Field emission scanning electron micrographs of graphite flakes (GFs), graphene worms (GWs) and few-layered graphene (FLG) (Fig. 4.1) clearly show that the microwaves fragmented GO into many GWs and within each GW, graphene layers are observed to be intact (indicating only partial exfoliation). Further, sonication of GWs resulted in the formation (indicating further exfoliation) of FLG sheets with a lateral size of at least 1 μm^2. Figs. 4.1(a) and (b) show the typical plane and cross-sectional morphology of the GFs, respectively. Fig. 4.1(b) clearly shows that GFs are very thick and consist of numerous graphene layers which are stacked together along the c-axis of graphite.

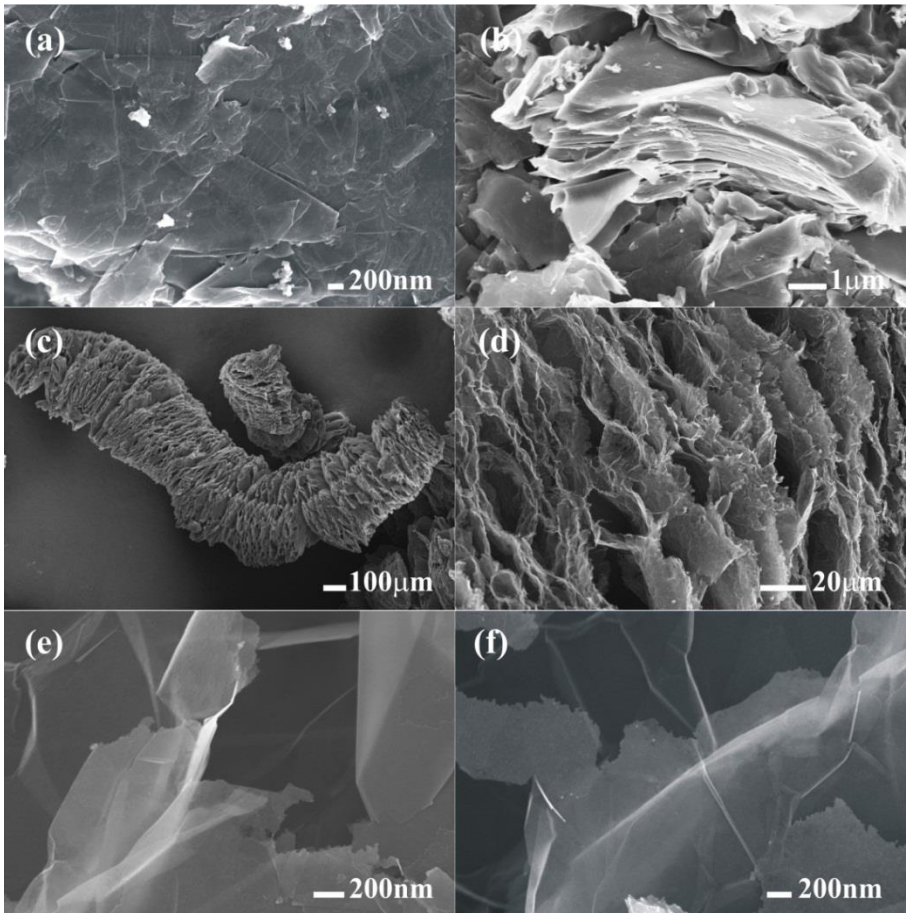

Figure 4.1. Secondary electron micrographs showing the morphology of graphite flakes ((a) and (b)), graphene worms ((c) and (d)), and few-layered graphene sheets ((e) and (f)).

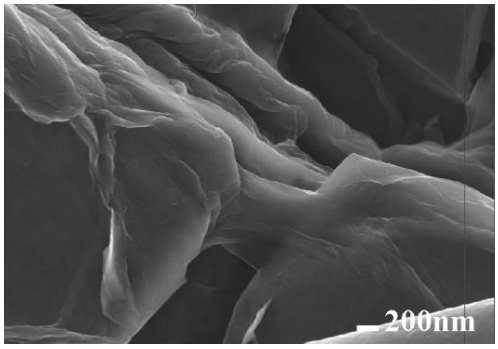

Figure 4.2. Secondary electron micrograph of graphene oxide.

Swollen and crumpled GO (owing to the intercalation and oxidation of graphite) [1,2] could be observed in Fig. 4.2. Formation of fluffy GWs was observed (Figs. 4.1(c) and (d)) due to the microwave irradiation of GO. Figs. 4.1(c) and (d) show partial exfoliation of graphene layers. Ultra-sonication results in further exfoliation of graphene layers as shown in Figs. 4.1(e) and (f) which clearly indicate that the layers are transparent to electrons even in scanning electron microscope (in other words even low energy electrons can pass through the layers). FLG sheets are transparent to the electron beam as observed in transmission electron micrographs (Figs. 4.3(a) and (b)) indicating the presence of only several sheets in each FLG unit. Electron diffraction (Fig. 4.3(c)) from FLG indicated a multi-layered system [3,4]. High intensity diffraction spots are indexed to crystal planes of hexagonal multi-layered graphene. The outer and inner hexagon diffraction patterns with varied intensity of the diffraction spots that constitute the electron diffraction pattern as shown in Fig. 4.3(c) indicate few-layered system that is built-in with A-B type of atomic stacking as in graphite.

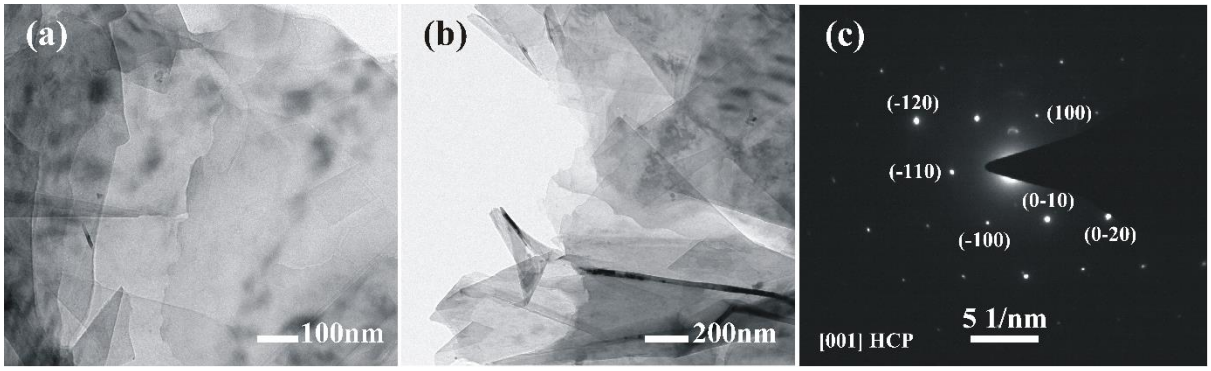

Figure 4.3. (a) and (b) Transmission electron micrographs and (c) diffraction pattern of FLG.

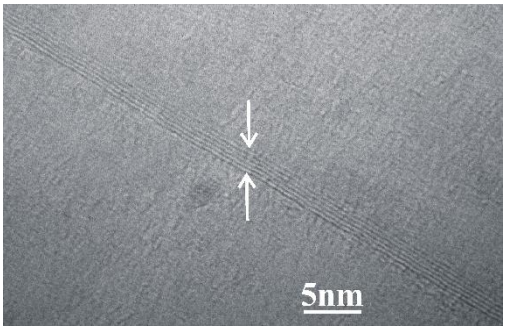

Figure 4.4. High resolution transmission electron micrograph of FLG.

The number of layers in each FLG was further confirmed using high resolution transmission electron microscope (HRTEM) image (Fig. 4.4). HRTEM images show that each FLG has ~6-7 graphene layers. The d spacing as measured from the HRTEM images is ~0.34 nm. To further understand the crystal structure of the above mentioned materials, x-ray diffraction (XRD) analysis was carried out. XRD patterns of different materials under discussion are shown in Fig. 4.5. As shown in Fig. 4.5, graphite flakes exhibit a strong and sharp (002) basal reflection at 2θ = 26.2° (corresponding to a d-spacing of 0.335 nm). Due to the oxidation of graphite, the (002) diffraction peak in the case of GO appears at a lower angle of 11.8° (corresponding to a d-spacing of 0.62 nm). In the case of FLG, (002) reflection is broad and appears at a higher angle of 24. 2° (corresponding to a d-spacing of 0.35 nm).

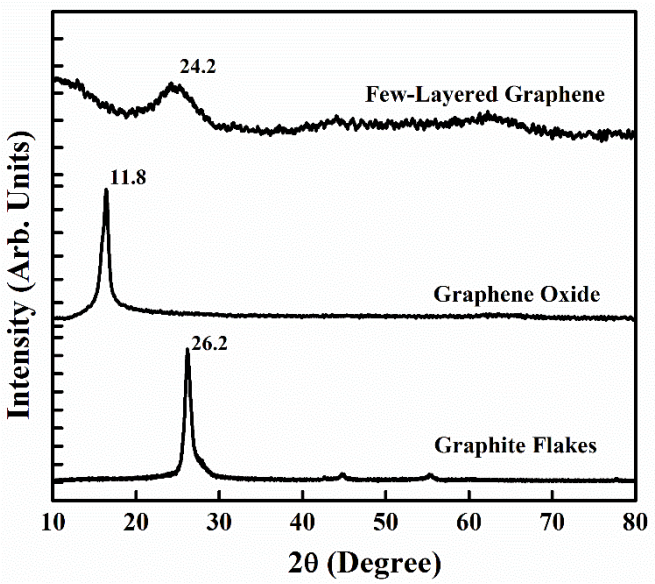

Figure 4.5. X-ray diffractograms obtained from graphite flakes, GO and FLG.

The relatively larger d-spacing of GO than that of pristine graphite is due to the intercalation of various species and attachment of several oxygen-containing functional groups (-OH,-COOH, C=O,-CHO) on the basal plane and the edges of the graphite flakes [5]. However, after reduction, the d-spacing was greatly decreased, indicating the removal of the oxygen-containing functional groups. Raman scattering analysis further confirmed the structure configurations of the samples and especially the few layered nature of FLG. Raman spectra (Fig. 4.6) obtained from the samples showed distinctive D and G bands representative of graphitic materials. FLG showed D band at 1352 cm^{-1}, G band at 1578.6 cm^{-1}, M-K scattering band 2445 cm^{-1}, 2D band at 2702 cm^{-1} and 2D' band at 3234 cm^{-1}. These peak positions commensurate to Raman scattering from folded graphene, single, double and few layer graphene [6,7]. In the case of FLG, the intensity ratio I_D/I_G which is a measure of the extent of disorder was ~0.6 indicating higher graphitization degree while I_G/I_{2D} was ~1.2 corresponding to less than 20 graphene layers in FLG [8]. Raman spectrum of FLG clearly shows the evolution of the characteristic 2D Raman band at ~2700 cm^{-1} confirming the formation of graphene. The shifting of 2D band towards higher wave numbers is related to number of layers and different number of layers set gives different band shapes.

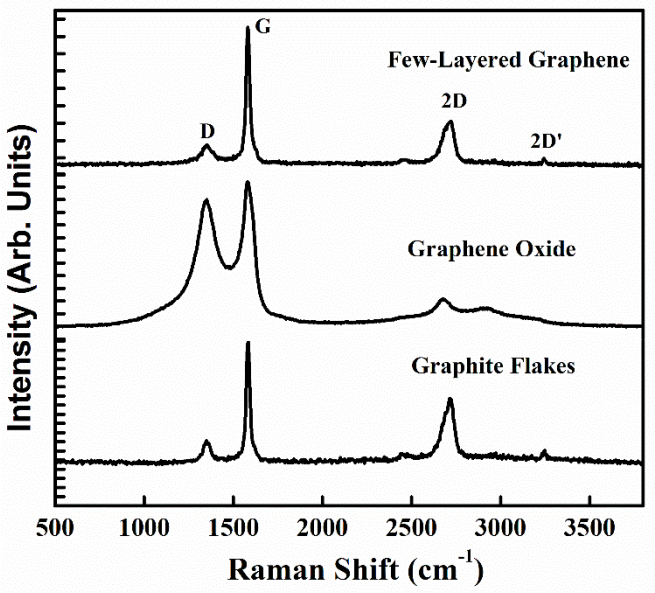

Figure 4.6. Raman spectra obtained from GFs, GO and FLG.

The apex of the 2D band peak obtained for graphite as shown in Fig. 4.6 corresponding to maximum intensity was observed around 2715.6 cm^{-1}. Also this peak is lacking symmetry as there is a shoulder with increasing wave number towards apex of the peak. 2D band in the case of FLG has good centre of symmetry around ~2700 cm^{-1} [9]. This type of symmetry indicates that FLG contains very few graphene layers as shown in Fig. 4.4. XRD and Raman scattering features of GWs were found to be similar to that of FLG (Fig. 4.8). The features clearly indicated that GWs are constituted with many graphene layers. Subjecting GWs to sonication induces acoustic cavitations near their surfaces which in turn creates localized erosion that leads to ripping or shearing of the layers [10,11]. Inertial cavitations due to the violent collapse of bubbles can also rip layers apart, thus releasing graphene nanosheets [10,11]. Increase of MWI time results in further breaking of the exfoliated graphene nanosheets. However, here it appears that all the three-steps mentioned above have occurred simultaneously. FTIR spectrum of GO [12] shows a strong peak at ~1623 cm^{-1} corresponding to C=C. It also exhibits a peak at ~1721 cm^{-1} due to the C =O stretching as well as peaks corresponding to carboxy C–O (1442 cm^{-1}), epoxy C–O (1259 cm^{-1}), and alkoxy C–O (1015 cm^{-1}) groups attached to the edges of GO [12-14]. In the case of FLG, the peaks at 1721 and 1442 cm^{-1} decrease significantly in intensity, suggesting the reduction of GO [13,14].

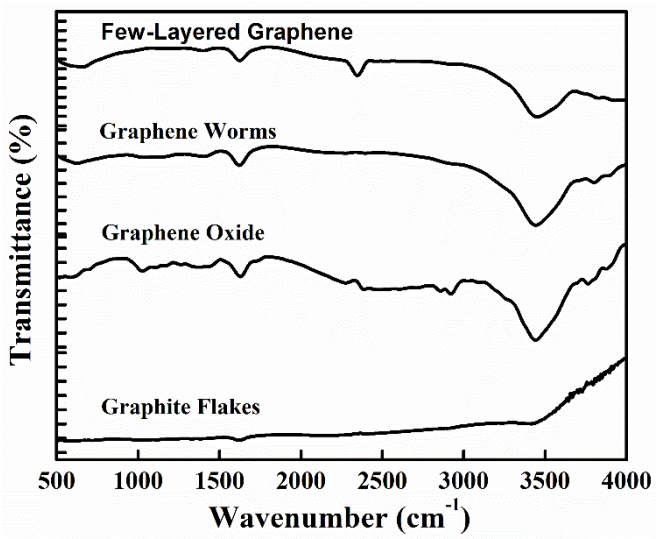

Figure 4.7. FTIR spectra obtained from GFs, GO, GWs and FLG.

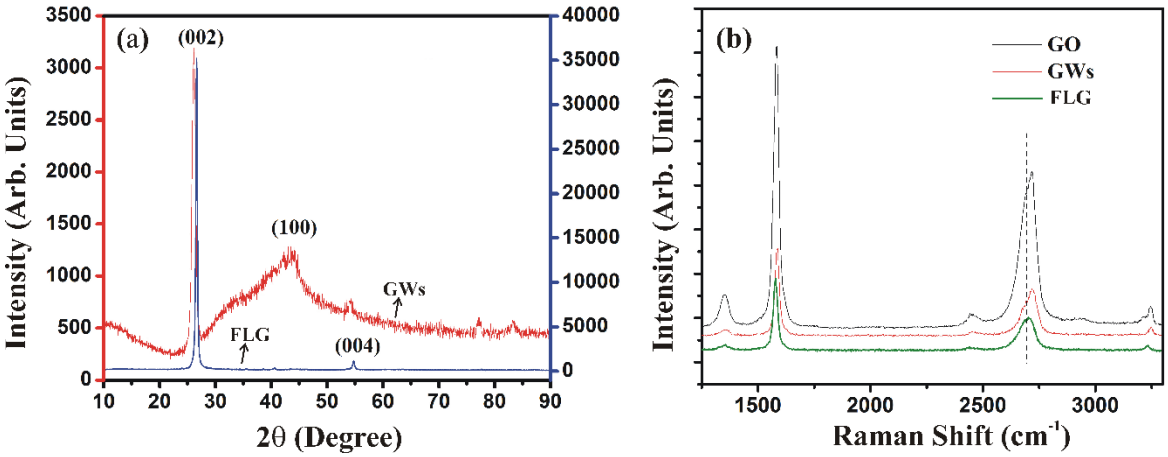

Figure 4.8. (a) XRD patterns and (b) Raman spectra of GWs and FLG.

The measured BET and Langmuir surface areas of FLG are 8.1 and 12.4 (±0.2) m^2/g, respectively. Average pore volume and size obtained from BET analysis were ~0.047 cm^3/g and ~23.53 nm, respectively. Isotherm of N_2 gas adsorption and desorption followed the type III isotherm among the BET classification types I-VI (Fig. 4.9). The specific surface area of FLG is very low when compared with other graphene materials [15]. The low BET surface area is a combined result of high flake size (~300 µm) of the staring graphite material, less oxidation time (~2 h), only partial exfoliation and reordering of individual graphene (basal planes) of FLG over long range (the size crystallite of FLG as measured using (002) x-ray diffraction line is ~27 nm, which is high).

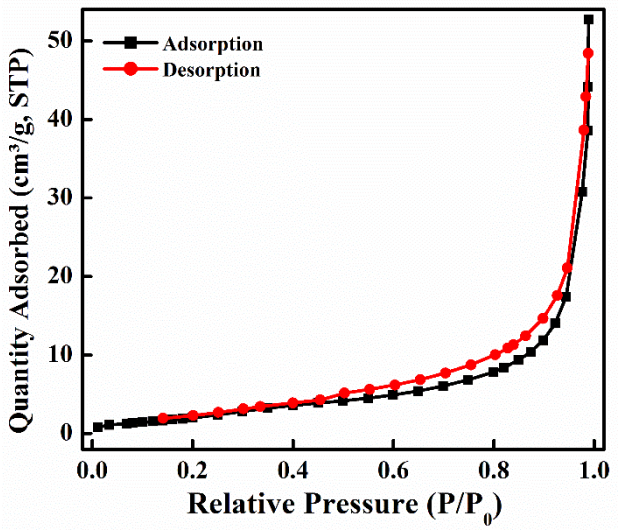

Figure 4.9. BET Isotherm of FLG for N_2 gas adsorption and desorption.

4.2 S, N Doped FLG

Secondary electron micrographs of GFs (starting material, here the flake size is ~150 μm), ATGFs, GWs and S, N doped FLG are shown in Fig. 4.10. Figs. 4.10(a) and (b) show the typical plane and cross-sectional morphology of the GFs, respectively.

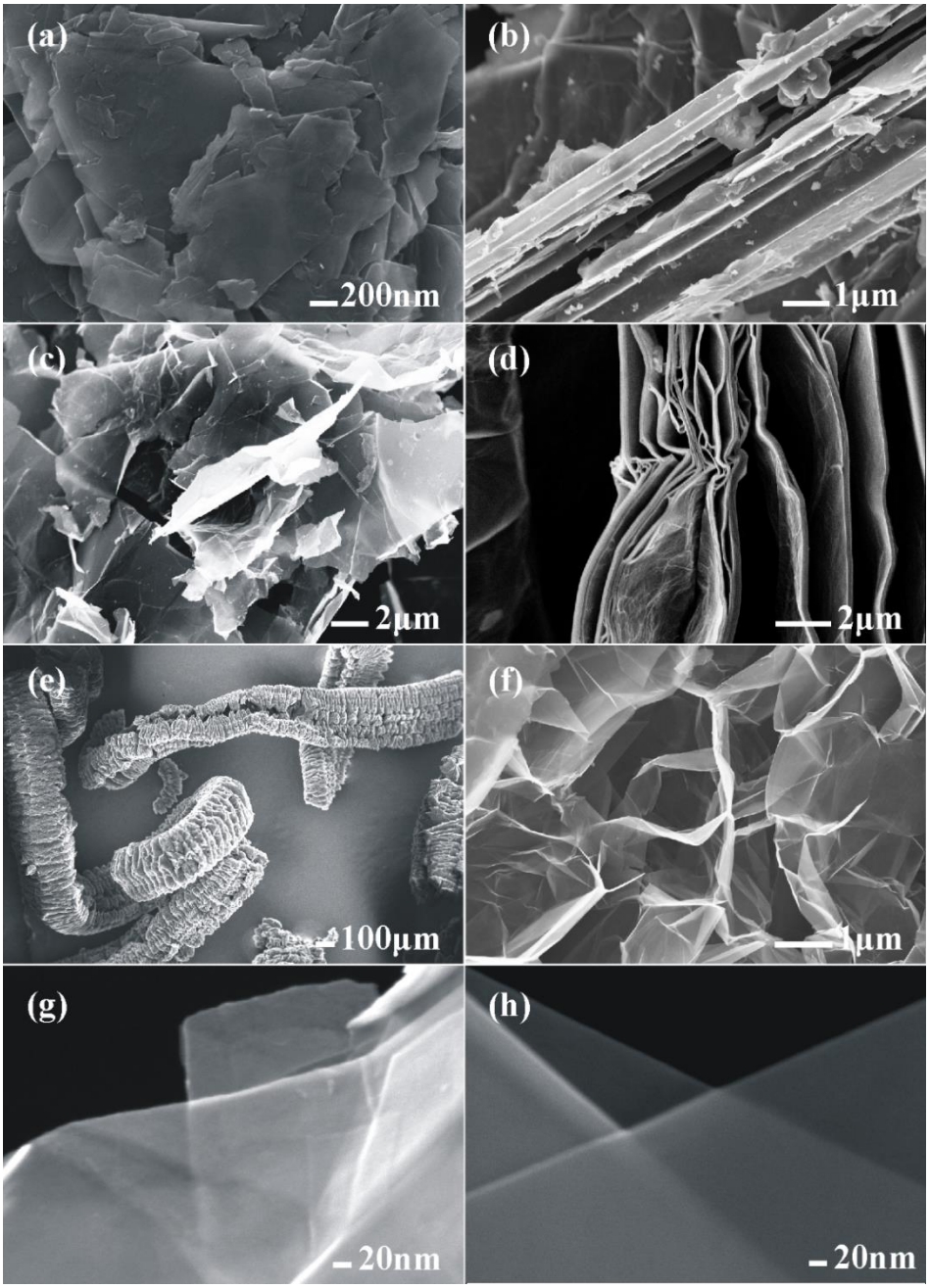

Figure 4.10. Secondary electron micrographs showing the morphology of graphite flakes (GFs) ((a) and (b)), acid treated graphite flakes (ATGFs) ((c) and (d)), graphene worms (GWs) ((e) and (f)), and S, N doped few-layered graphene (FLG) sheets ((g) and (h)).

The morphology of GFs in the case of preparing S, N doped FLG is similar to the GFs used in preparing FLG. Fig. 4.10(b) clearly shows that GFs are very thick and consist of numerous graphene layers which are stacked together along the c-axis of graphite. In the case of ATGF (Fig. 4.10(d)), swelling along the c-axis is clearly observed. This is because of the intercalation of sulphate and nitronium ions (as confirmed from XPS analysis, to be discussed) between the graphene layers constituting the graphite flakes and also due to the typical oxidation as in GO. Due to the microwave irradiation of ATGFs, here too (similar to the case discussed in section 4.1) fluffy GWs have formed (Fig. 4.10(e)). However in this case the graphene sheets seem to be loosely bond to each other and severely crumpled as shown in Fig. 4.10(f). Finally ultra-sonication results in exfoliation of graphene layers as shown in Figs. 4.10(g) and (h) which clearly indicate that the layers are transparent to low energy electrons in scanning electron microscope. S, N doped FLG sheets are transparent to the electron beam as observed in transmission electron micrograph (Fig. 4.11(a)) indicating the presence of only several sheets in each S, N doped FLG unit. Electron diffraction (Fig. 4.11(b)) from S, N doped FLG indicated a multi-layered system [3,4] similar to the case of FLG. The presence of few graphene layers was further confirmed by HRTEM image shown in Fig. 4.11(c) and clearly in Fig. 4.12. HRTEM images show that each S, N doped FLG has ~4-7 graphene layers. The d spacing as measured from the HRTEM images is ~0.35 nm.

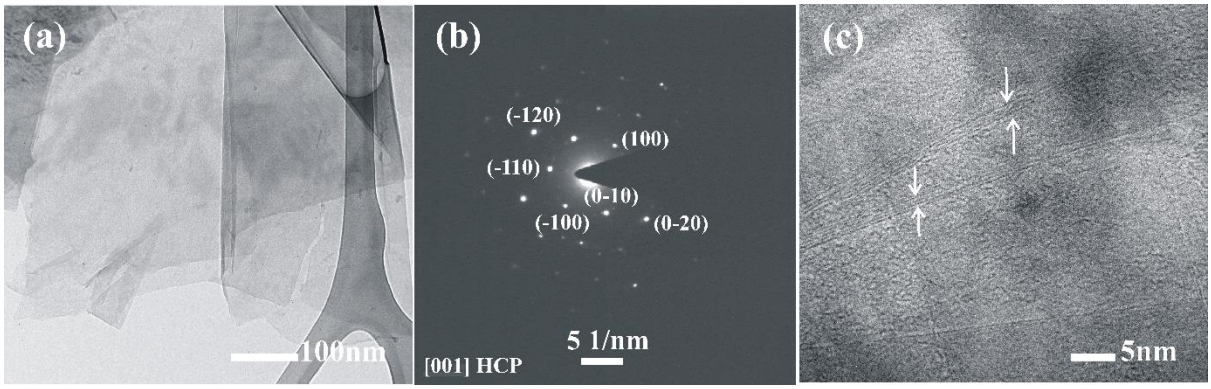

Figure 4.11. (a) Transmission electron micrograph, (b) electron diffraction pattern and (c) HRTEM image of S, N doped FLG.

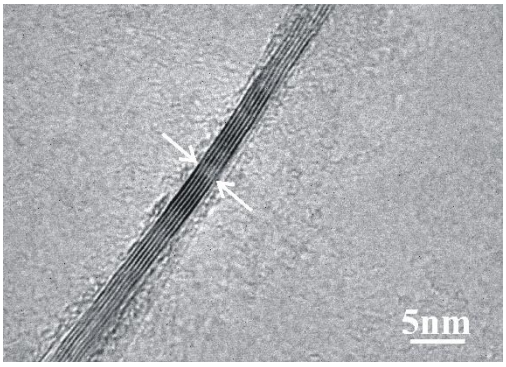

Figure 4.12. High resolution transmission electron micrograph of S, N doped FLG.

X-ray diffractograms of GFs, ATGFs, GWs and S,N doped FLG are shown in Fig. 4.12. The signature carbon (002) peak is observed in all cases. For better understanding, carbon (002) peak has been enlarged (Fig. 4.14). As shown in Fig. 4.13, GFs exhibit a strong and sharp (002) basal reflection at 2θ = 26.2° (corresponding to a d-spacing of 0.335 nm). Due to the oxidation of graphite, the (002) diffraction peak in the case of ATFGs appears at a lower angle (corresponding to an increase in the d-spacing). In the case of S, N doped FLG, (002) reflection is broad and appears at an angle greater than 26.2°. On the other hand GWs showed almost the same characteristics as that of GWs in the case of obtaining FLG.

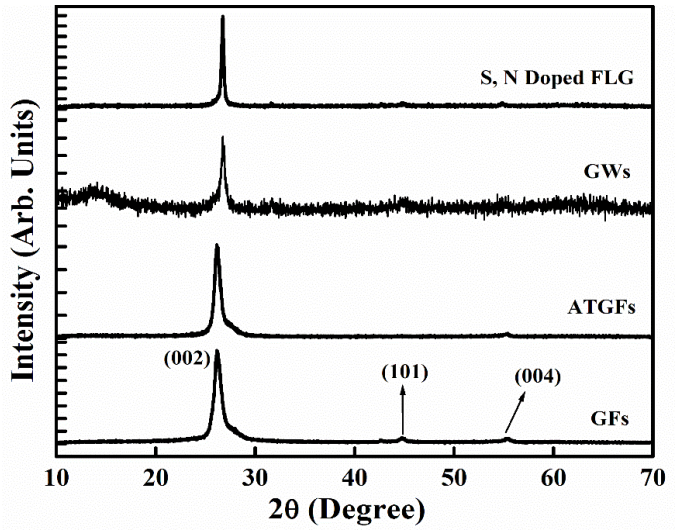

Figure 4.13. X-ray patterns of (a) Graphite Flakes, (b) Acid treated Graphite Flakes, (c) Graphene worms, (d) S, N doped FLG.

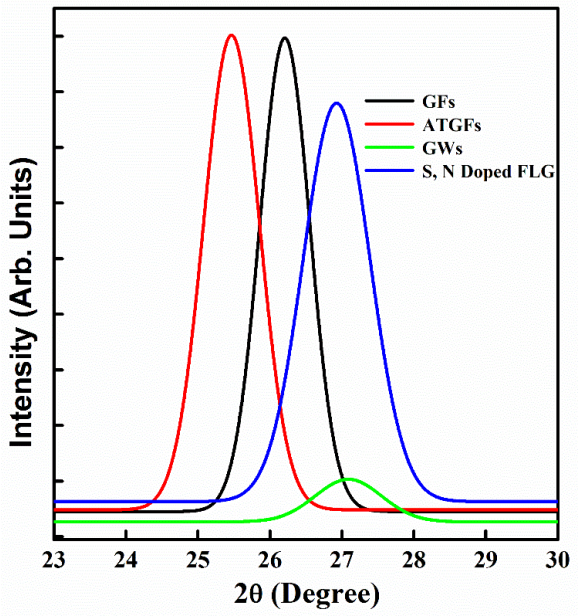

Fig: 4.14. Gaussian fit of (002) diffraction peak of GFs, ATGFs, GWs and S, N Doped FLG.

Raman spectra of GFs, ATGFs, GWs and S, N doped FLG are shown in Fig. 4.15. In all the spectra typical intensities (I_x, where x = G, D and 2D) and peak positions corresponding to graphitic materials are observed [16,17]. Raman spectra of GFs, ATGFs, GWs and S, N doped FLG are similar to that of Raman spectra of GFs, GO, GWs and FLG, respectively as discussed in section 4.1. However some subtle differences have been observed.

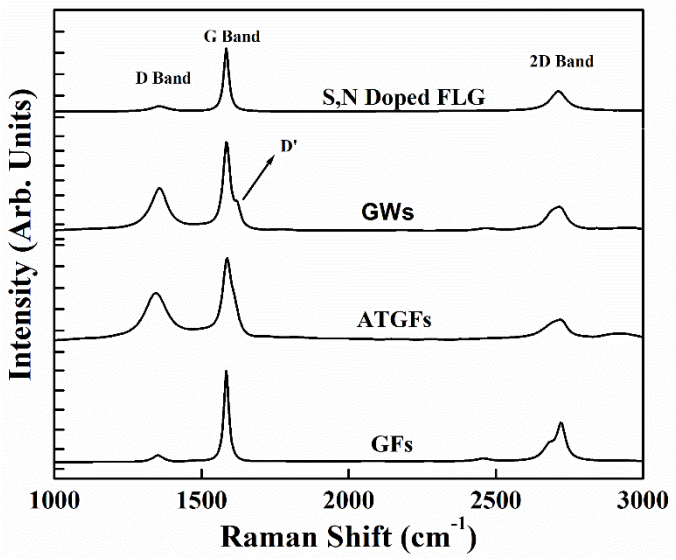

Figure 4.15. Raman spectra of (a) graphite flakes (GFs), (b) acid treated graphite flakes (ATGFs), (c) graphene worms (GWs) and (d) S, N doped FLG.

In the case of ATGFs the intensity of D band is high in comparison to that in the case of GFs. This clearly indicates the presence of defects in ATGFs due to intercalation and oxidation. In the case of GWs (which have expanded along the c-axis of graphite after microwave irradiation of ATGFs), a strong G band at ~1580 cm^{-1} and a weak D band are observed. Similar is the case with S, N doped FLG. However in this case the D band is much weaker indicating the good quality of graphene layers in S, N doped FLG. D′ band observed in the case of GWs is often observed in layered carbon nanostructures which are formed owing to ripping or unzipping of another carbon nanostructures such as in the case of unzipped CNTs [18,19]. In the case of S, N doped FLG, the simultaneous observation of high intensity G band, low intensity D band and the single 2D band with an intensity lower than that of G band are an indication of the presence of few-layered graphene [9]. The intensity ratio I_D/I_G which is a measure of disorder in the material was ~0.6 indicating high graphitization degree while I_G/I_{2D} was ~1.3 corresponding to the presence of less than 15 graphene layers in S, N doped FLG. The broad 2D band at 2700 cm^{-1} is also consistent with the few layered feature of FLGs. Raman scattering analysis clearly shows that the exfoliation process was effective.

FTIR spectra of GFs, ATGFs, GWs and S, N doped FLG are shown in Fig. 4.16. As expected, GFs did not show any absorbance signal. In the other cases: The bands at 3435, 2928 and 2846, and 1630 cm^{-1} correspond to O-H stretching in COOH [13], C-H stretch, and O-H bending and aromatic C=C stretch [12,14], respectively. The strong bands at 1384 and 586 cm^{-1} correspond to N-O stretch [20] and C-S stretch in disulphides [21], respectively. CO_2 stretch is observed at 2362 cm^{-1}, C=O stretching in COOH at 1714 cm^{-1}, while the bands in the range 1000-1300 cm^{-1} correspond to C-O in oxidized carbons like alcohols, acid and esters. CH_2 twist is observed at 1227 cm^{-1} while C-N/C-O stretch at 1102 cm^{-1} [22]. The band at 584 cm^{-1} corresponds to partial C-S. All in all, FTIR spectroscopic analysis shows that the samples (especially ATGFs and S, N doped FLG) have the expected functional groups.

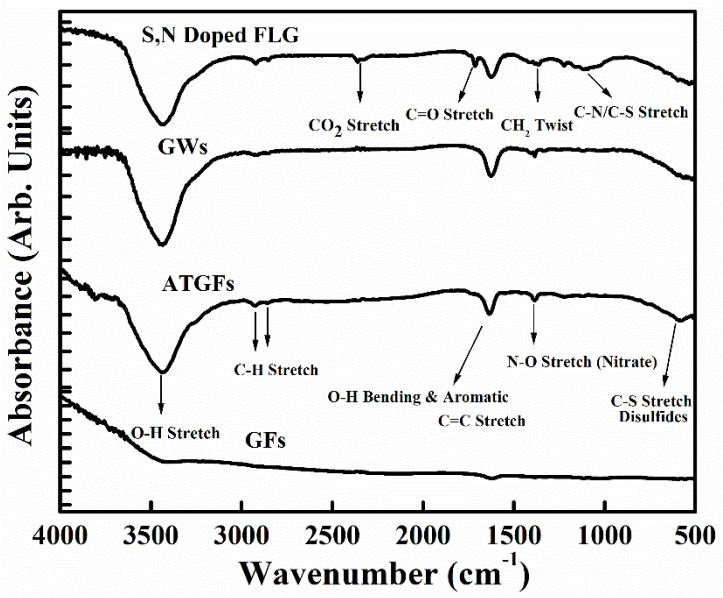

Figure 4.16. FTIR spectra of (a) graphite flakes (GFs), (b) acid treated graphite flakes (ATGFs), (c) graphene worms (GWs) and (d) S, N doped FLG.

To further ascertain the bonding characteristics of ATGFs and S, N doped FLG XPS analysis was carried out. XPS survey spectra of ATGFs and S, N doped FLG are shown in Fig. 4.17. The evident signals from C (1s), O (1s), N (1s), S (2s) and S (2p) are detected and shown along with the corresponding binding energies in Fig. 4.17.

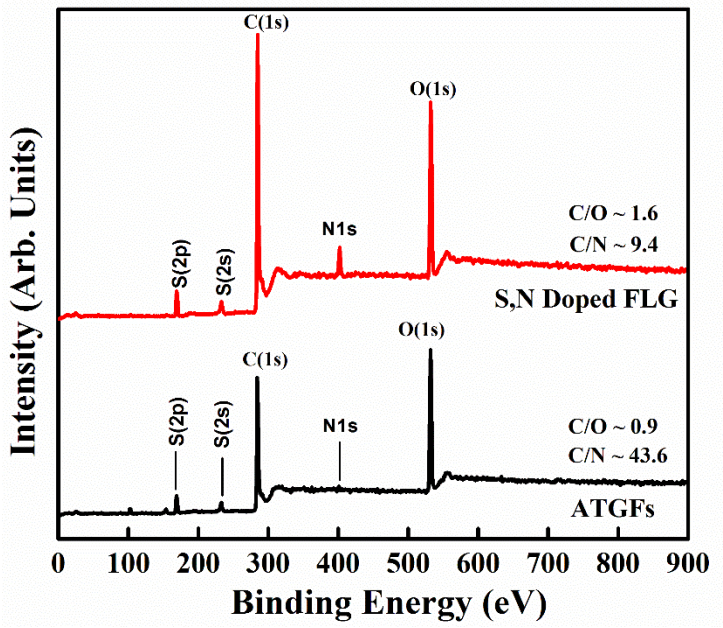

Figure 4.17. XPS survey spectra of ATGFs and S, N doped FLG.

C signal was analysed to accurately distinguish sp^2 and sp^3 hybridized bonds of the C atoms and to know the corresponding binding energies. Strong intensity N and S signals even after reduction of ATGF using microwave irradiation indicate S, N doping in FLG. However the peak positions and intensities corresponding to O, N and S atoms in the case of S, N doped FLG are different than those in the case of ATFGs owing to functionalization and reduction of ATGFs as shown in Fig. 4.17 from which it can be clearly observed that C:O ratio increased in the case of S, N doped FLG in comparison to ATGFs due to increase in O functionalities while C:N ratio noticeably decreased because N atoms are involved in bond formation with C atoms in graphene. Peak fitted XPS signals pertaining to C (1s) of ATGFs and S, N doped FLG are shown in Figs. 4.18(a) and (b), respectively, from which the following are very clearly observed: In the case of ATGFs (Fig. 4.18(a)), five characteristic peaks at 283.8, 284.5, 285.2, 286.3, 287.5 and 290.6 eV ascribed to sp^2-hybridized carbon [23,24], sp^3-hybridized carbon [25], -C–O, -C=O [26,27] and π–π* plasmon [28], respectively are observed. This is a clear indication of characteristic of layered-like graphitic carbon. This observation complements well with the corresponding FTIR spectral analysis confirming the presence of abundant oxygen functional groups in ATGFs. However in the case of S, N doped FLG (Fig. 4.18(b)) the C peak appeared at 284.5 eV [23] (graphite-like sp^2 C) and it could be deconvoluted into seven different components. The bands at 283.8, 284.2, 286.1, 288.1, 289.9, and 291.4 eV ascribed to C-C, C–C/C=C in the aromatic rings, C–OH of alkoxy and C-S, C=O of carbonyl and carboxylic acidic and π–π* transition [29-32], respectively are observed. This is owing to increase in the amount of functional groups at C sites. This made the C peak asymmetric and narrowed toward low and high binding energy sides. The peak at ~284.5 eV (C–C/C=C) is more intense in the case of S, N doped FLG in comparison to that in ATFGs. This clearly indicates the restoration of the π-electronic conjugated network structure after reduction. In addition, a new peak at ~284.8 eV

corresponding to the C–N/C–S bond [33] could be identified in the case of S, N doped FLG. The band at ~284.2 eV signifies carbon rich material while the weaker oxygen peaks are ascribed to impurities that could have come-in due to ambient air oxidation and/or acid treatment during synthesis [34].

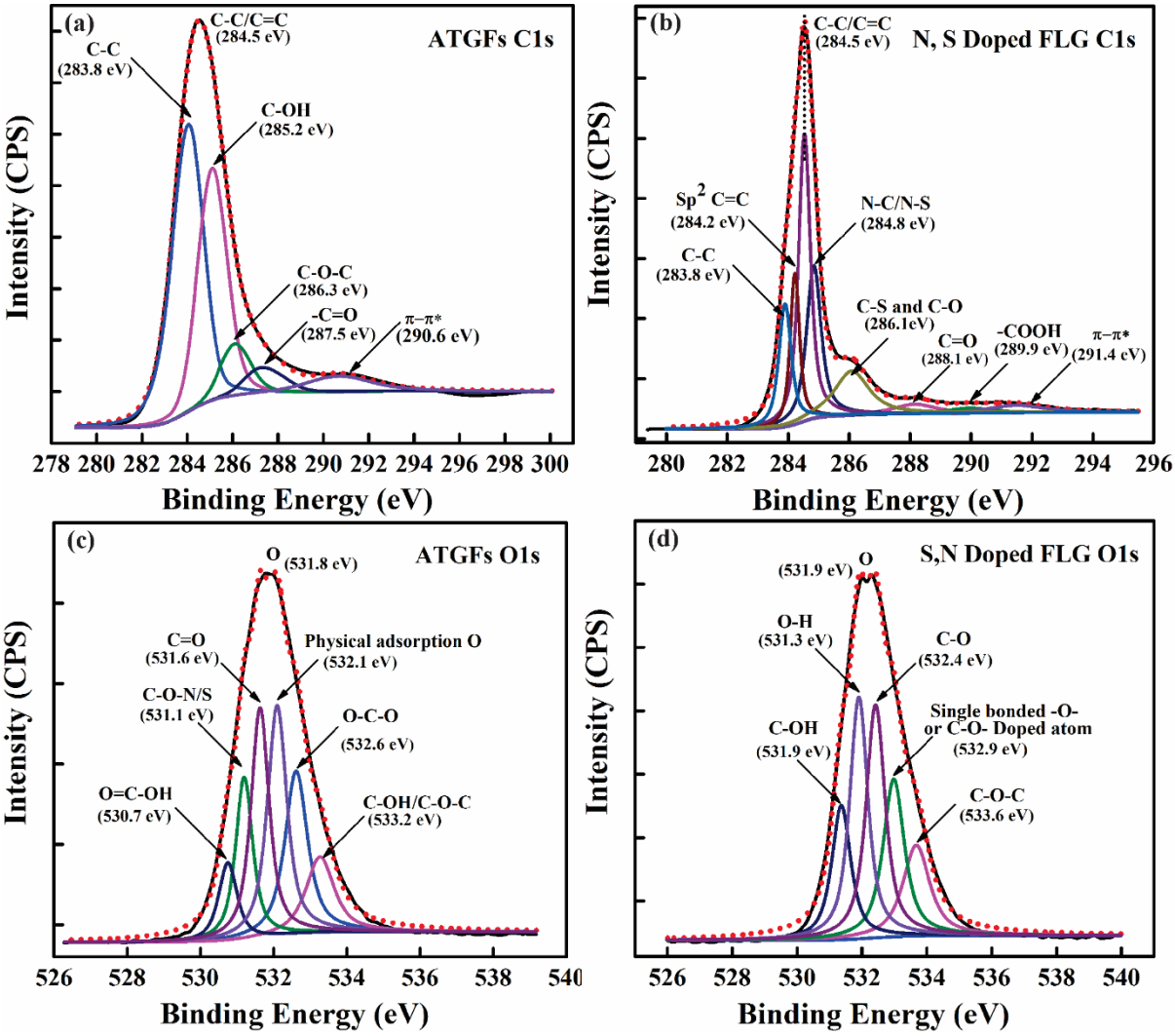

Figure 4.18. Peak fitted XPS signals: (a) ATGFs C (1s), (b) S, N doped FLG C (1s), (c) ATGFs O (1s) and (d) S, N doped FLG O1(s).

Differences in the peak positions and intensities of O related signal have also been analysed. Peak fitted XPS signals pertaining to O (1s) of ATGFs and S, N doped FLG are shown in Figs. 4.18(c) and (d), respectively, from which the following are clearly observed: In case of ATFGs, the peak at ~531.8 eV attributed to oxygen bonded to carbon through aliphatic sp^3 orbitals [35]

has been identified. The other peaks at 530.7, 531.1, 531.6, 532.1, 532.6 and 533.2 eV ascribed to Quinone [36], C-O-N/S, C=O (Oxygen doubly bonded to aromatic Carbon), C-OH, O-C-O and C-O-C [37-40], respectively are identified. Significant contributions from the $\pi^*(p_z)$ resonance of epoxide bonds appeared as a peak at ~533.2 eV [41,42]. In the case of S, N doped FLG, O (1s) peak shifted to a higher binding energy value indicating the presence of adsorbed oxygen, because C-OH in residual −COOH groups can be consumed completely by the acid-base reaction [43]. The peaks at 531.3, 531.9, and 532.4 eV assigned to different oxygen functional groups [44-46] are also clearly identified. The peak at ~532.9 eV is assigned to combine effects of singly bonded oxygen (-O-) in C-O and in C-O-P [47]. The peak at ~533.6 eV is ascribed to chemisorbed oxygen and H_2O [42].

Differences in the peak positions and intensities of N related signal have also been analysed. Peak fitted XPS signals pertaining to N (1s) of ATGFs and S, N doped FLG are shown in Figs. 4.19(a) and (b), respectively, from which the following are clearly observed: In the case of ATFGs, the peaks at 400.1, 401.1 and 401.9 eV ascribed to pyrrolic (N in a five membered ring), quaternary and oxidized nitrogen cations [48,49], respectively could be identified. The peak at ~401.9 eV can also be due to the presence of oxidized nitrogen cations [50,51]. In the case of S, N doped FLG, the quaternary peak at 401.1 eV shifts to lower binding energy side because of the presence of other dopants. The other peaks at 402 and 402.5 eV corresponding to the pyridine N oxides and bipolaron = NH^+-bond [52,53] are easily identified. The appearance of the peak at ~397.2 eV clearly indicates that the graphene is N doped [54].

Differences in the peak positions and intensities of S related signal have also been analysed. Peak fitted XPS signals pertaining to S (2p) of ATGFs and S, N doped FLG are shown in Figs. 4.19(c) and (d), respectively, from which the following are clearly observed: The broad peak centred at ~168.8 eV ascribed to the sulphate species [55] could be identified. The oxidized sulphur (namely in the bonding configuration $C–SO_2–C$) signal at 167.9 eV

indicating that S was also doped into the carbon network of graphene [56] could also be identified. The peak at ~170.3 eV ascribed to sulphur contained in $-SO_2^-$, which is associated with the sulfonic acid groups [57] could also be identified. The peaks at 168.3 and 169.3 eV arising from -C-SO_x (x=2.3) associated with sulphate or sulphonate [58,59] are also identified. The signal from sulphone bridges (–C–SO_2–C–) appeared at 170.1 eV. These bridges form due to the oxidizing conditions present during the synthesis process [60]. The peak at 170.6 eV ascribed to chemisorption of oxygen and formation of SO_4^{2-} [61].

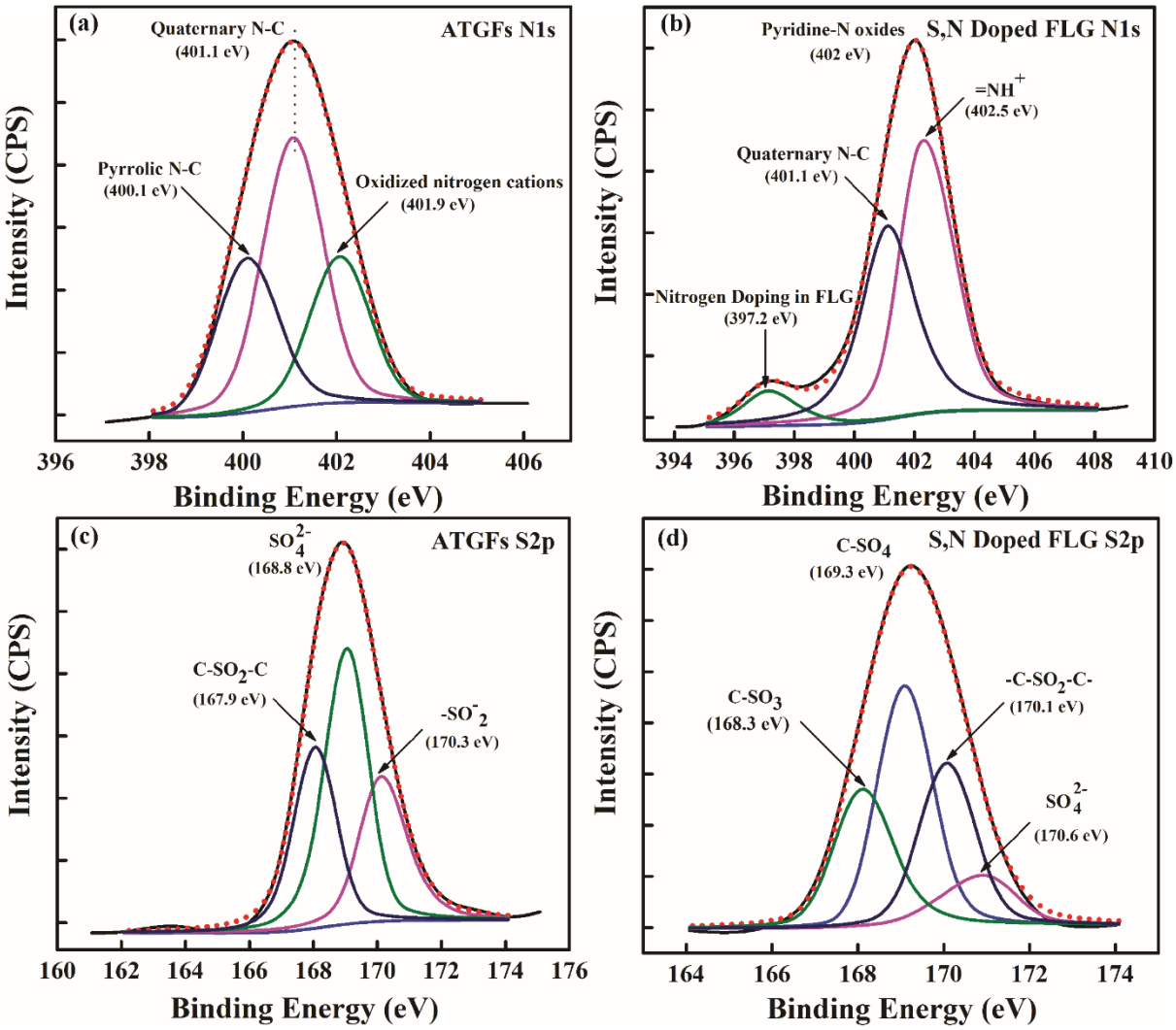

Figure 4.19. Peak fitted XPS signals: (a) ATGFs N (1s), (b) S, N doped FLG N (1s), (c) ATGFs S (2p) and (d) S, N doped FLG S (2p).

4.3 ZnO Decorated S, N Doped FLG

XRD patterns of ZnO and different ZnO–S, N doped FLG composites are shown in Fig. 4.20. The diffraction peaks in the case of all the samples are well indexed to different diffraction planes in hexagonal ZnO (JCPDS No. 89-1397)). Low intensity carbon (002) peak marked at 26.8° could be indexed only in the case of the ZnO-2wt% S, N doped FLG and ZnO-3wt% S, N doped FLG samples. This indicates the presence of FLG in these samples. In the case of ZnO-1wt% S, N doped FLG, carbon (002) peak was not discernible because the FLG content was too less while the diffraction signals from ZnO dominated the pattern. However, electron microscopy (to be discussed) showed the presence of FLG even in the case of ZnO-1wt% S, N doped FLG sample. The diffraction peaks corresponding to ZnO are broad, indicating that the ZnO crystallites are small in size. This was further confirmed by HRTEM analysis. The crystallinity was further confirmed by electron diffraction analysis.

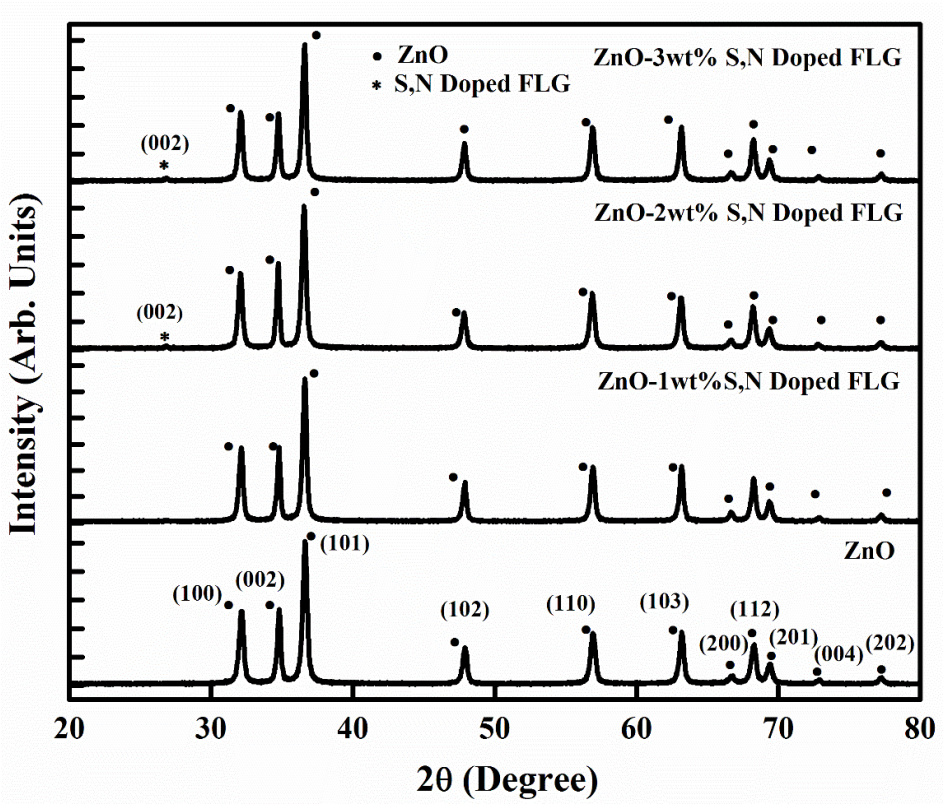

Figure. 4.20. X-ray patterns of ZnO, ZnO-1wt% S, N doped FLG, ZnO-2wt% S, N doped FLG and ZnO-3wt% S, N doped FLG.

FESEM images of ZnO and different ZnO–S, N doped FLG composites are shown in Fig. 4.21. Bare ZnO particles are fine and quasi-spherical (Fig. 4.21(a)). In the other cases, morphology of ZnO particles changed with increase in GWs content during the synthesis. This is plausibly due to the change in C-O-ZnO bonding character and the increased S and N contributions (more GWs more is the presence of S and N). With the increase in GWs content, the morphology of ZnO changed from quasi-spherical to rod-like. These changes are clearly presented in Fig. 4.22, which shows TEM and HRTEM micrographs and the representative electron diffraction patterns of ZnO, ZnO-1wt% S, N doped FLG, ZnO-2wt% S, N doped FLG and ZnO-3wt% S, N doped FLG. The size of the ZnO particles ranged from 40 nm to 80 nm. It can also be observed that the particles are uniformly decorating the graphene sheets in the case of ZnO-1wt% S, N doped FLG, ZnO-2wt% S, N doped FLG and ZnO-3wt% S, N doped FLG. The electron diffraction patterns are indexed to different diffraction planes in ZnO. Diffraction signals from S, N doped FLG were not discernible due to either poor intensity of diffraction spots or improper diffraction conditions.

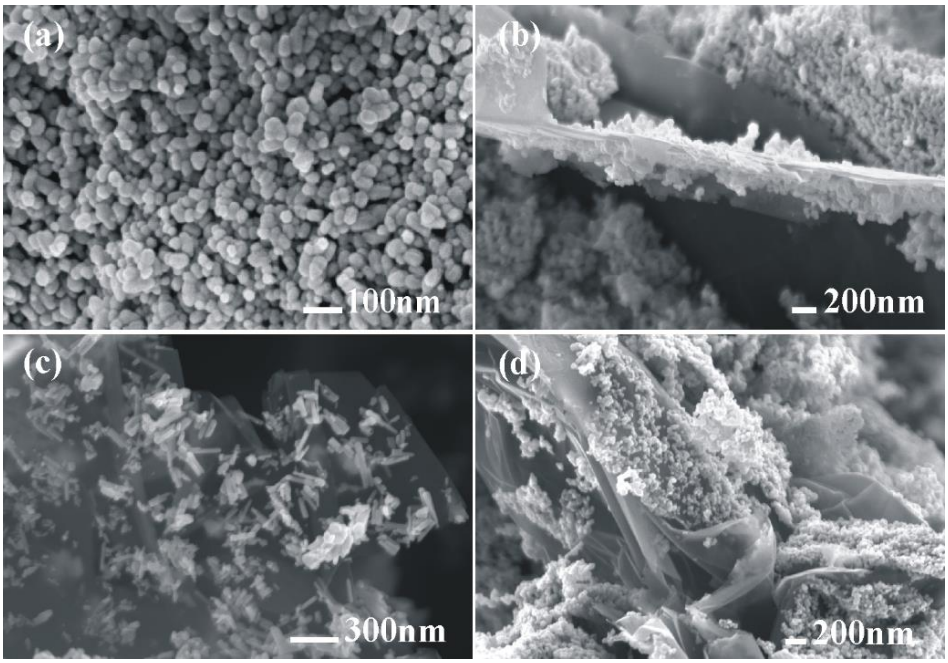

Figure 4.21. FESEM of (a) ZnO, (b) ZnO-1wt% S, N doped FLG, (c) ZnO-2wt% S, N doped FLG and (d) ZnO-3wt% S, N doped FLG.

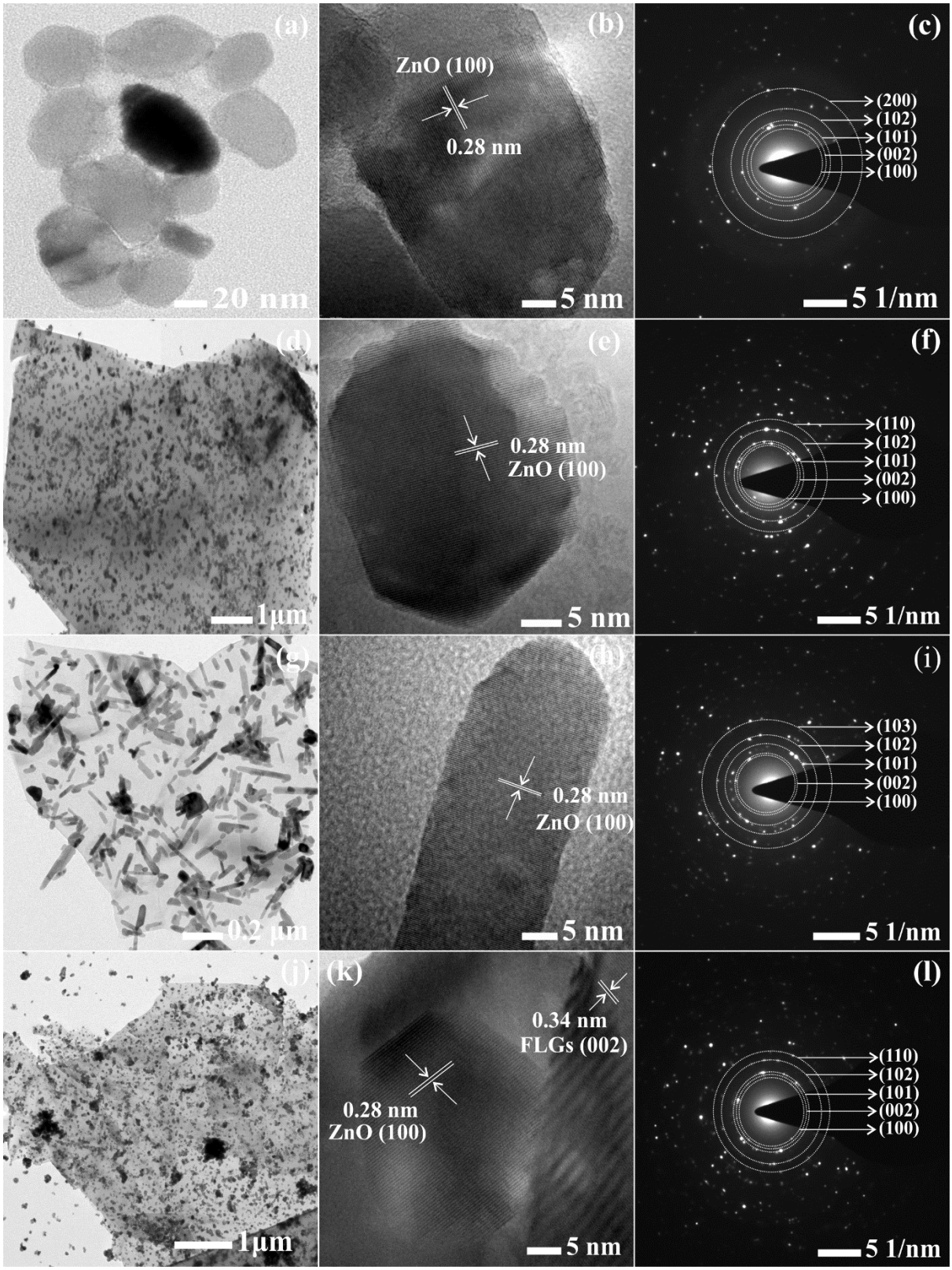

Figure 4.22. TEM and HRTEM images and corresponding electron diffraction pattern of (a,b,c) Bare ZnO, (d,e,f) ZnO-1wt% S, N doped FLG (g,h,i) ZnO-2wt% S, N doped FLG, and (j,k,l) ZnO-3wt% S, N doped FLG, respectively.

4.4 MgO Decorated FLG

Secondary electron micrograph of MgO decorated FLG (MDFLG) is shown in Fig. 4.23. It can be clearly observed from this micrograph that small MgO fragments (bright spots) are decked onto FLG structures (cube and cuboid features in the micrograph). Energy dispersive x-ray spectrum (Fig. 4.24) obtained from MDFLG clearly shows the presence of C, Mg and O elements in the probed area. At some probed locations negligible amounts of Fe and Si (even though signals are not prominent) are also detected. In order to further understand the morphology of MDFLG, TEM images at different magnifications are obtained and presented in Fig. 4.25. In addition to the cube and cuboid shaped FLG features high resolution TEM images (Figs. 4.25(c)–(f)) reveal thin wavy sheets (annotated by arrows) of graphene running over MgO fragments (annotated by dotted ellipses). The number of graphene layers in each FLG structure ranged from 3 to 9 at different locations. Interplanar spacing corresponding to <111> in MgO and <002> in FLG (in MDFLG) is ~0.24 and ~0.38 nm, respectively.

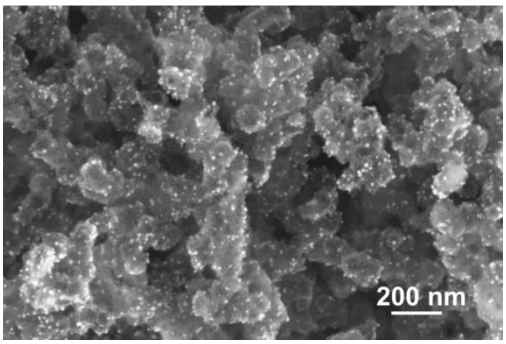

Figure 4.23. Plane view field emission secondary electron micrograph of MDFLG.

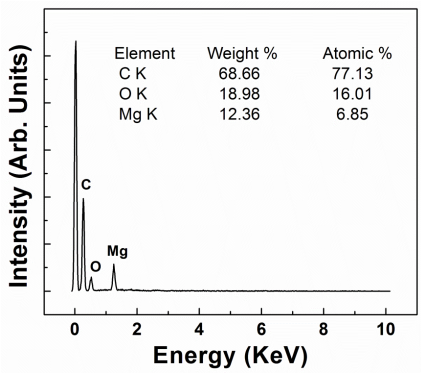

Figure 4.24. Energy dispersive x-ray spectrum obtained from MDFLG.

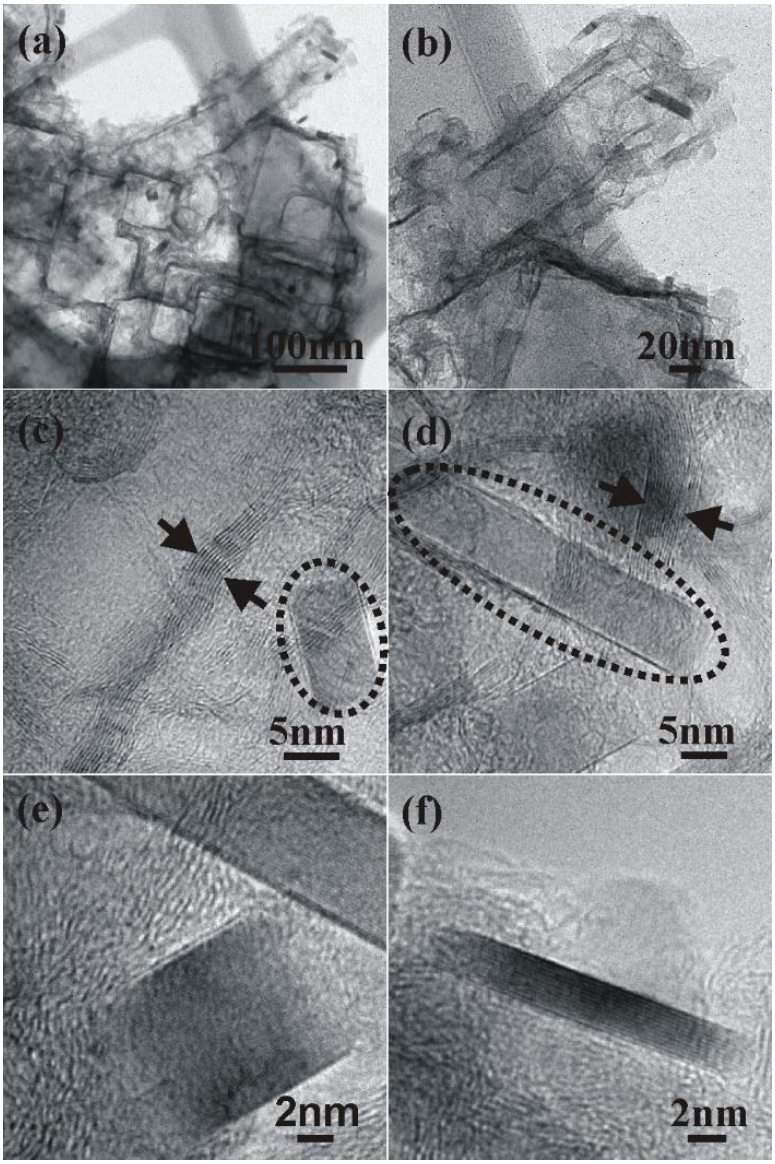

Figure 4.25. (a) TEM image of MDFLG, (b) magnified image of the area shown in (a), (c) and (d) high resolution transmission electron micrographs showing graphene layers (annotated by arrows) and MgO fragments (annotated by dotted ellipse), (e) magnified high resolution TEM image of the area shown in (d) and (f) high resolution transmission electron micrograph showing graphene layers and MgO fragment at a different location.

X-ray diffractrogram obtained from MDFLG is shown in Fig. 4.26(a). The broad x-ray diffraction peak at 2θ = ~26.3° is indexed to (002) FLG in MDFLG. Other prominent diffraction peaks at ~37.2°, ~62.5° and ~72.50° are indexed to different (111), (220) and (311) crystal planes, respectively in cubic MgO (Inorganic Crystal Structure Database-

159377). The diffraction peak at 2θ = ~43.1° is a resultant of the overlap of (100) FLG and (200) MgO. However, the peak at 2θ = ~94.3° is easily indexed (assuming it to be the 2nd order diffraction peak) to (400) MgO, which shows that that the peak at 2θ = ~43.1° corresponds to (200) MgO. X-ray diffractogram shown in Fig. 4.26 (a) does not indicate the presence of any other phases. Raman spectrum (Fig. 4.26(b)) of MDFLG depicts typical bands related to the presence of FLG namely G band (~1578 cm^{-1}), which is due to the vibrations of stretching bonds of carbon atoms constituting the basal plane of layered graphene, D band (~1345 cm^{-1}), which is indicative of defects/disorderness in the material and G′/2D band (~2678 cm^{-1}, second overtone of D-band), which is indicative of number of layers present in FLG. In graphene a sharp and symmetric G′/2D band appears at ~2700 cm^{-1}. But the broad, asymmetric and red-shifted G′/2D band in the case of MDFLG indicates the presence of multi-layers of graphene stacked together along their c-axis (direction perpendicular to the basal plane in graphene). The typical inter-valley scattering band G* and D+G band could also be identified. The presence of FLG in MDFLG is already confirmed by transmission electron microscopy. This discussion complements well with that presented in section 4.1. UV-visible absorption spectrum obtained from MDFLG is shown in Fig. 4.26 (c). The spectrum depicts a strong absorption peak at ~232 nm. Graphene should typically show an absorption band at 266 nm [61]. However, the red-shift observed in the case of MDFLG is indicative of MgO decking onto FLG. Similar observation was also made in the case of graphene/CdS nanocomposite [63]. High BET and Langmuir surface areas of ~394±2.4 and ~921±43 m^2/g, respectively are measured for MDFLG [64]. The calculated average pore volume and pore diameter are ~0.8689 cm^3/g and ~9 nm, respectively. A net volume (area under curves) difference of ~43.6 cm^3/g was observed between adsorption and desorption of N_2. These values indicate the availability of enough surface sites for any possible adsorption.

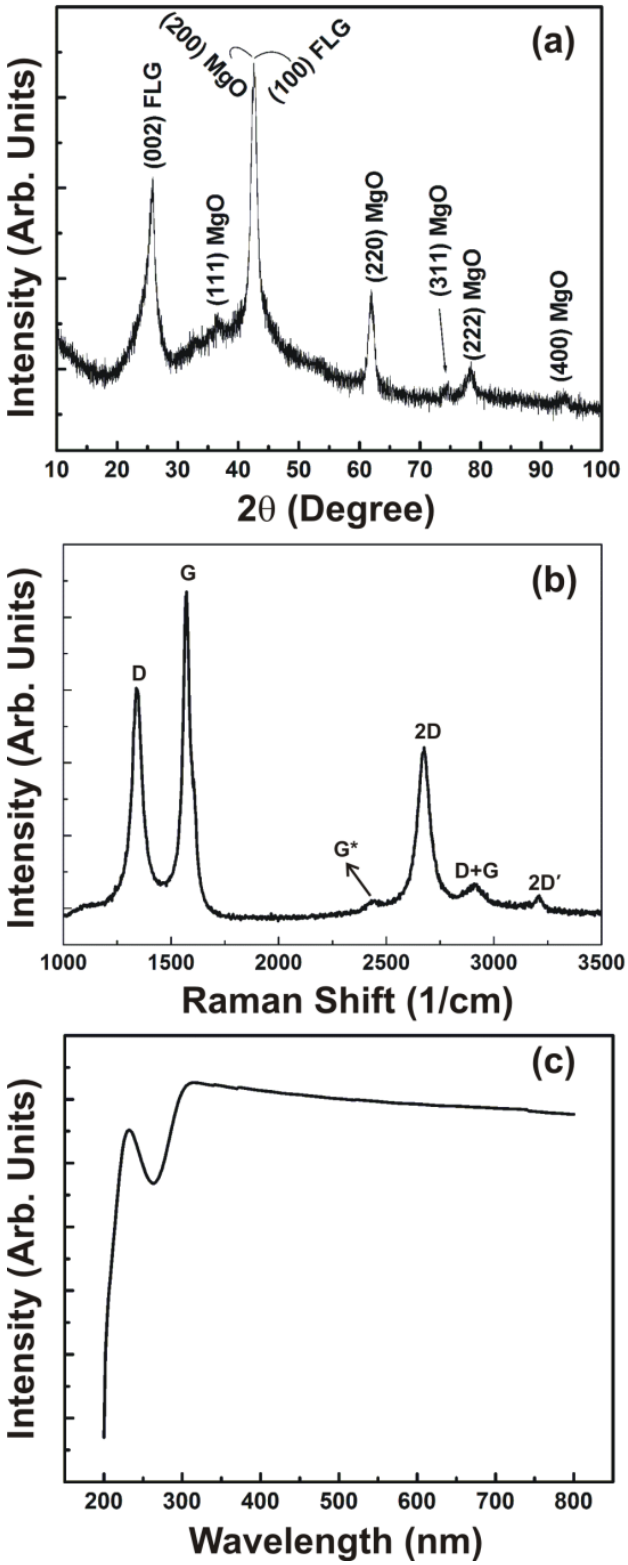

Figure 4.26. (a) X-ray diffractogram, (b) Raman spectrum and (c) UV-visible absorption spectrum obtained from MDFLG.

4.5 MgO and NiO Decorated FLG

Secondary electron micrographs of MgO and NiO decorated FLG are shown in Fig. 4.27. It can be clearly observed from this micrograph that small fragments (bright spots) are decorated onto FLG structures (long features in the micrographs). For clarity an ultra-high magnification image is shown in Fig. 4.27(b). To further understand the morphology of the sample, TEM images (Figs. 4.28 and 4.29) at different magnifications are obtained. Representative electron diffraction pattern in also shown in Fig. 4.28(b). TEM micrograph (Fig. 4.28(a)) depicted the same morphology as that shown in Fig. 4.27. From Fig. 4.28(a) it is clear that the long features are transparent to electrons and that they are decorated with small particles (regions of darker contrast in the micrograph).

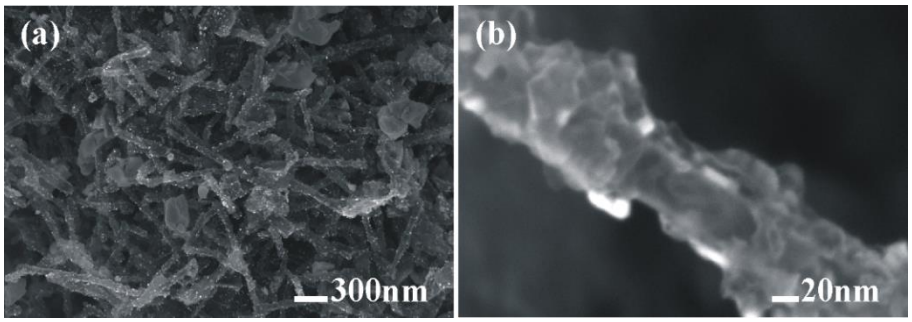

Figure 4.27. Field emission secondary electron micrographs of MgO and NiO decorated FLG at different magnifications.

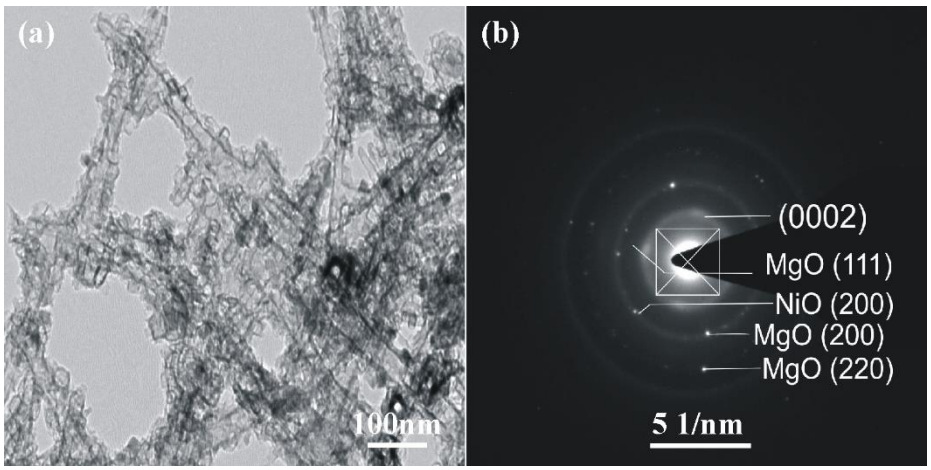

Figure 4.28. (a) TEM micrographs and (c) electron diffraction pattern of MgO and NiO decorated FLG.

Diffraction spots in the electron diffraction pattern (Fig. 4.28(b)) are indexed to (111), (200) and (220) crystal planes in MgO, (200) NiO and (0002) C diffraction planes. (0002) C diffraction signals are indicative of the presence of hexagonal multi-layered graphene in the sample. For more clarity HRTEM images (Fig. 4.29) of the sample have also been recorded. From Fig. 4.29(a) it can be clearly observed that the long features are hollow (resembling long and wide carbonaceous multi-walled tubes). The walls of these hollow features are constituted by 15 to 20 graphene layers (circularly annotated in Fig. 4.29(a)). Apart from the graphene layers constituting the walls of the tubular features there are also graphene layers (wavy features in the micrographs) throughout the sample as observed in Figs. 4.29(a) and (b). MgO and NiO particles are decorated at different locations of the walls of the tubular features and surfaces of the graphene layers in the sample.

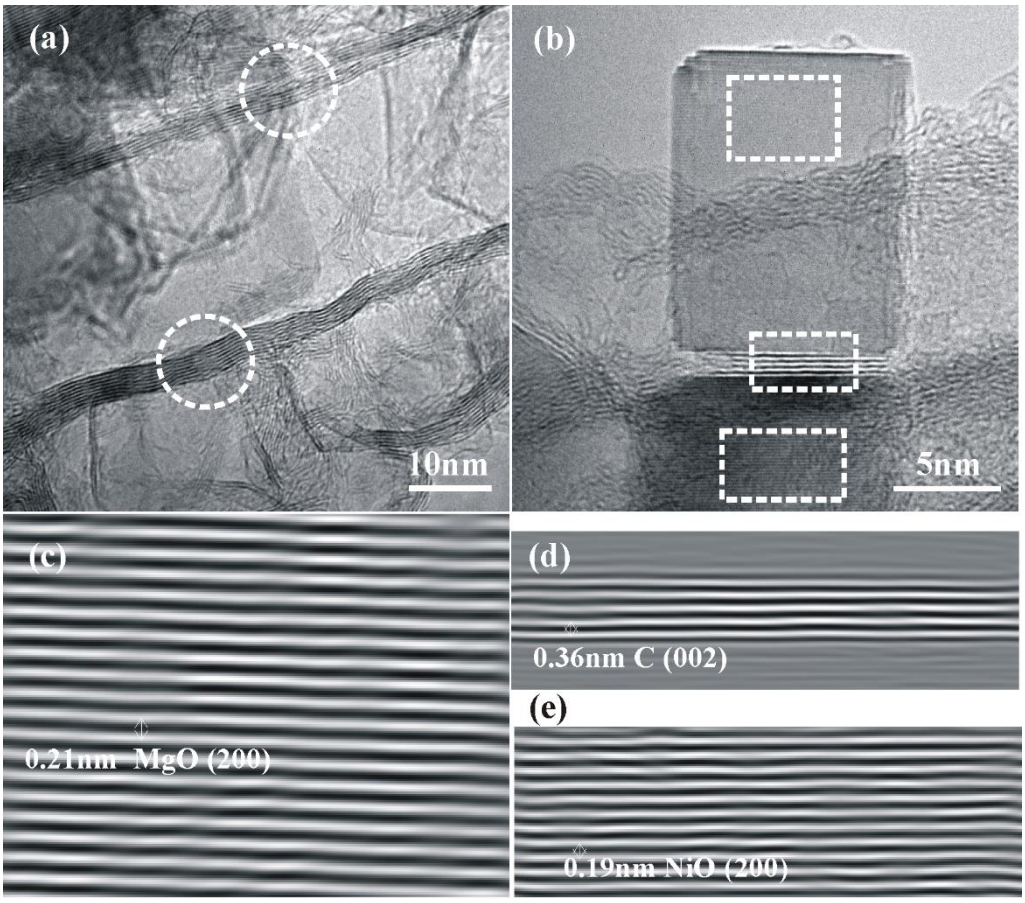

Figure 4.29. (a,b) HRTEM images of MgO and NiO decorated FLG; (c), (d) and (e) are the IFFT images of top, middle and bottom rectangular annotations in (b), respectively.

A representative HRTEM image depicting MgO particle (top rectangular annotation), NiO particle (bottom rectangular annotation) and graphene layers (middle rectangular annotation) is shown in Fig. 4.29(b). MgO and NiO particles are cuboidal in shape with different sizes. IFFT images of the top, middle and bottom rectangular annotations in Fig. 4.29(b) areshown in Figs. 4.29(c), (d) and (e), respectively. Interplanar spacing of <200> MgO, <002> graphene and <002> NiO are measured as 0.21, 0.36 and 0.19 nm, respectively from the corresponding IFFT images.

To understand the presence of crystalline MgO, NiO and graphene XRD analysis was considered. XRD pattern of the sample is shown in Fig. 4.30. The diffraction peaks from MgO and NiO could not separately discernible because the diffraction angles in both the crystal structure cases are very close to each other. The diffraction peaks at ~37.3°, ~43.3°, ~62.9°, ~75.4° and ~79.4° could be indexed to (111), (200), (220), (311) and (222) crystal planes in cubic MgO (JCPDS No. 1-1235 (inorganic mineral alloy PHR)). The same peaks could also be indexed with high confidence to different crystal planes in cubic NiO (JCPDS No. 65-5745 (inorganic alloy NST)). The broad diffraction peak at ~26.4° was indexed to (002) carbon. Here it should be mentioned that the presence of MgO, NiO and graphene in the sample was confirmed beyond doubt by electron diffraction and HRTEM images.

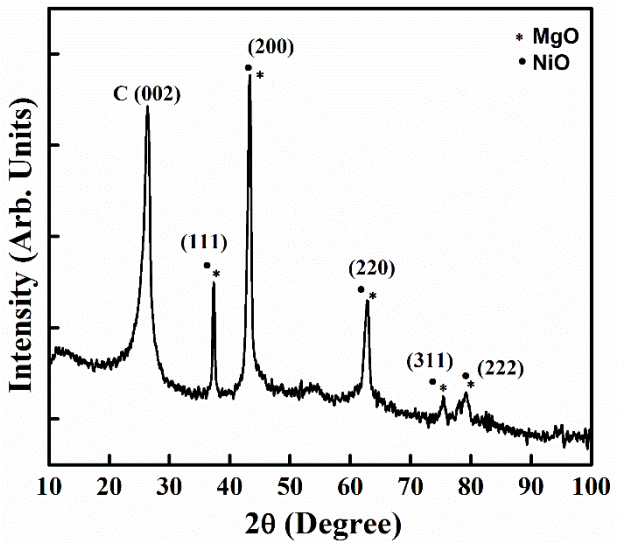

Figure 4.30. X-ray diffraction pattern of MgO and NiO decorated FLG.

In order to understand the nature of carbon present in the sample Raman scattering analysis was considered. Raman spectrum of the sample is shown in Fig. 4.31 in which D, G, G^*, 2D, D+G and 2D' bands representative of typical multi-walled carbon nanotubes [17,65-69] are clearly identified. This is consistent with the tubular features observed in the electron micrographs (Figs. 4.27 and 4.28). Further, the I_G/I_{2D} ratio was measured as ~1.4 which indicates the presence of 15 to 20 graphene walls in the tubular structures [8]. This is consistent with the observations made from the HRTEM images (Fig. 4.29).

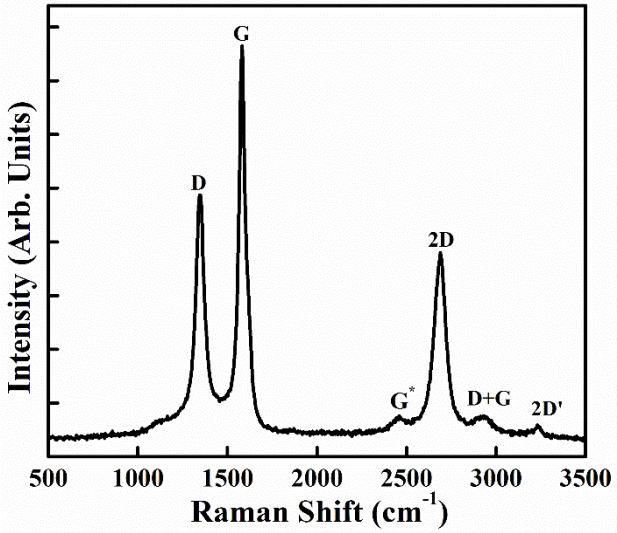

Figure 4.31. Raman spectrum of MgO and NiO decorated FLG.

4.6 Applications and Unique Properties

4.6.1 FLG as Anode Material in Li Ion Battery

FLG synthesized in this thesis work was extensively tested as an anode material in Li ion battery in another work [70] owing to its suitable characteristics as discussed in section 4.1. Careful electrochemical characterization was done to measure anodic response of FLG in a typical Li ion battery. Reversible capacity Vs. Li/Li^+ was measured as ~400 mAh/g at a low current rate of 0.1 C and this value fluctuated around ~250 mAh/g for high current rate of 1 C. Average capacity of 385 $mAhg^{-1}$ was measured at low current rate (0.1 C, over 60 Cycles). At high current rate (1 C), for initial 30 cycles, the average capacity was measured as ~270

$mAhg^{-1}$ while it decreased to ~225 $mAhg^{-1}$ over 60 cycles. Cyclic voltammetry studies also confirmed few layered nature of graphene as shown by current versus Voltage histograms with clear difference in shifting of cathodic and anodic current peaks to higher voltages similar to the case of commercial graphite. High capacity of graphene versus theoretical value of graphite and capacity above 0.5 V in charge-discharging profile was due to unknown Li ion storage mechanism which could be related to structural disorders like defects, crumpling and folding of individual exfoliated graphene layers etc. as discussed in section 4.1. Overall performance of FLG was found to be better than that of commercial graphite.

4.6.2 S, N Doped FLG as a Catalyst to Synthesize Uracil and Tetrahydropyrimidine

Pyrimidine and its derivatives play an important role in several biological processes and have considerable chemical and pharmacological importance. In particular pyrimidine ring can be found in nucleoside antibiotic, antibacterial and cardio-vascular products as well as agro-chemical and veteran products [71]. One of the possible reasons for growing interest in pyrimidine heterocyclic compound is that, it comprises the base for thiamine, and uracil and cytosine nitrogen bases which are building blocks of the nucleic acids. Among these bases, uracil and tetrahydropyrimidine and their analogues gained importance in medicinal chemistry. Derivatives of uracil are well known for their enzyme inhibition and antiretroviral properties [72]. It is well known fact that the C5 substituted derivatives possess excellent biological activities, for example: 5-Fluoro-uracil is an important anticancer agent widely used in oncology [73]. Several unique procedures were used to prepare such uracil derivatives with the aid of catalysts such as sodium ethoxide, potassium carbonate (under additional microwave irradiation) and acetic acid [74-76]. On the other hand 5-Cyano-2-thiouracils can be readily prepared by a number of methods [77,78]. Synthesis of 6-substituted analogues (R. aryl, heteroaryl or tert-alkyl) involves condensation of an aldehyde with ethyl cyanoacetate and thioureas in the presence of potassium carbonate [77,78].

With regards to tetrahydropyrimidines, they are important intermediates in the catabolism of pyrimidines and their derivatives play an important role in the synthesis of nucleic acid [79,80]. A known method for the synthesis of dihydropyrimidines is through the condensation of α, β-unsaturated acids with urea [81]. Tetrahydropyridines have outstanding biological properties and are widely used in preparing pharmaceutical compounds and synthetic intermediates [82]. Although there are some reports for the synthesis of tetrahydropyridines, these methods are not always satisfactory with respect to ease of operation, yield, applicability and the regio-selectivity of the products [83-89]. Besides, very few efficient methods of formation of 1,2,3,4-tetrahydropyridines are described in the literature [83-97]. The products are often isolated by acidification followed by crystallization of the resultant precipitates. The above mentioned methods have certain limitations such as involving costly catalysts, drastic reaction conditions, need excess of catalysts and requirement of extended reactions times. Hence the development of new, eco-friendly and convenient reagents to obtain high yield of the product. In this context, catalysts are very helpful. However they are derived from heavy or rare metals and they have several draw backs for large scale applications. In contrast, graphene related materials could be the most inexpensive and environmental friendly catalysts owing to their catalytic characteristics. Pertaining to this thesis work, S, N doped FLG was considered as a catalyst to prepare 6-aryl-5-cyano-2-oxo uracil and 1,2,3,4-tetrahydropyridine. S, N dope FLG was considered owing to the characteristics it exhibited as discussed in the section 4.2

6-aryl-5-cyano-2-oxo uracil was synthesized as follows: A mixture of 10 mmol of ethyl cyanoacetate, 10 mmol of benzaldehyde, 10 mmol of urea and catalytic amount (15 mmol) of S, N dope FLG in 50 ml dry ethanol were refluxed. The completion of the reaction was monitored by thin layer chromatography using hexane:ethyl acetate as eluents. After completion of the reaction, the reaction mixture was cooled, filtered to remove the catalyst

and solvent was removed under reduced pressure. The solid residue was washed with water and dried under vacuum conditions. Then the solid compound was subjected to filter column to remove methoxide impurities and recrystallized in ethanol to obtain the pure compound. The product was confirmed by comparing with authenticate and found that the present catalyst initiated the reaction and minimized the reaction time from above 6 h to 2-3 h, which shows the catalytic action of S, N doped FLG. The time factor for conversion of the reaction is not varied even when the catalyst is reused for several times (more than 4-5 times). But the recovery in catalyst showed little variation that may be due to the filtration processes. The yields of the compound synthesized were also studied where the product formation showed small variation when the catalyst is reused consecutively (Table 4.1).

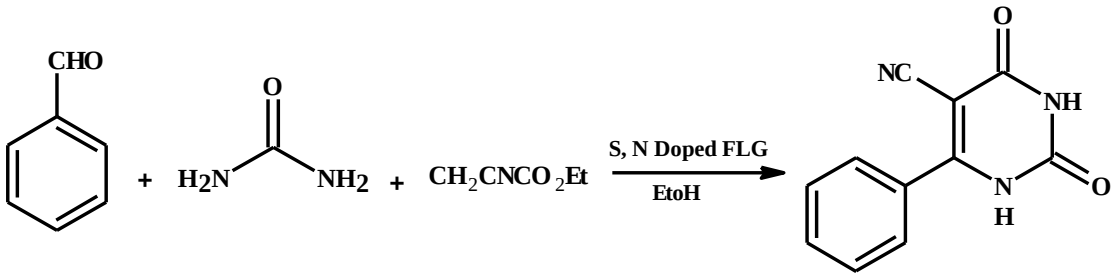

Figure 4.32. Synthetic procedure for Uracil using S, N doped FLG.

Tetrahydropyridine was synthesized as follows: In a 50 ml RB flask, 20 mmol of benzaldehyde, 10 mmol of 2-acetylphenone, 1.5 ml of 7N NH_3/MeOH and catalytic amount (15 mmol) of S, N doped graphene in a 10 ml of dried ethanol were mixed and stirred the reaction at 40 °C for 1 h. The completion of reaction was monitored by thin layer chromatography. After completion of the reaction, the reaction mixture was cooled, filtered to remove the catalyst and solvent was removed under reduced pressure. Then the solid compound was subjected to filter column to remove impurities and recrystallized in ethanol to afford the pure compound. The product was confirmed by advanced spectroscopic data (NMR) and found that the present catalyst initiated the reaction and the reaction time recorded was below to 3 h, which shows the catalytic action of the present compound. The

time factor for conversion of the reaction is not varied even the catalyst is reused for several times (more than 4-5 times) also recovery in catalyst is same as for Uracil synthesis.

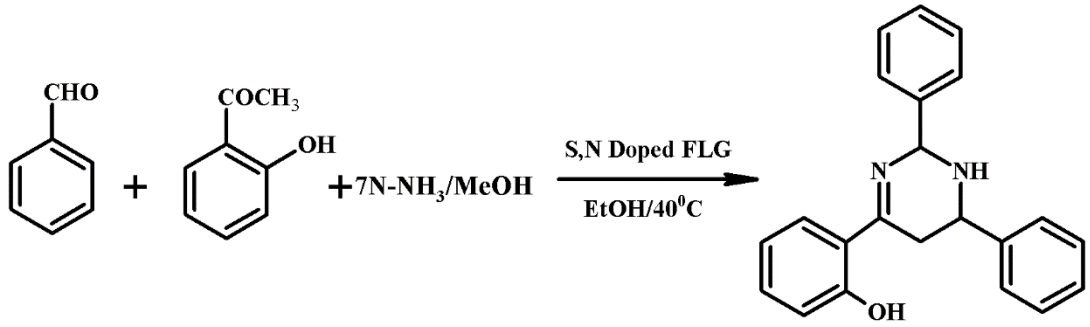

Figure 4.33. Synthetic procedure for tetrahydropyrimidine using S, N doped FLG.

The time factor for conversion of the reaction is not varied even the catalyst is reused for several times. But the recovery in catalyst showed little variation that may be due to the filtration processes. The yield of the tetrahydropyrimidine was also studied where the product formation showed small variation when the catalyst is reused consecutively (Table 4.1).

Table 4.1. The percentage of catalyst recovered and isolated yield for uracil and tetrahydropyrimidine compounds.

Entry	[a]% of catalyst recovered		[b]Isolated yield (%)	
	Uracil	tetrahydropyrimidine	Uracil	tetrahydropyrimidine
1	98	99	92	89
2	98	97	90	84
3	95	95	91	86
4	92	97	87	85
5	90	95	88	82

[a] Calculated weights compared with initial weight of catalyst taken

[b]Isolated yield on the basis of the weight of the pure product obtained.

Spectral data for Uracil: mp: 295-298 °C; IR (KBr): 3350, 3132, 3030, 2220, 1630, 1590, 1320 cm^{-1}; ^{1}H NMR (DMSO-d_6 400 MHz)δ: 7.2-8.0(m, 5H, Ar-H), 11.4(s, 1H, NH); ^{13}C NMR (DMSO-d_6 100-MHZ)δ: 82.0, 119.1, 127.8, 128.1, 129.3, 135.1, 163.3, 167.5, 171.1.

Spectral data for tetrahydropyrimidine: mp:160-162 °C; $^{1}HNMR$ ($CDCl_3$ 400MHz) δ2.67 (m, 2H, 5CH), 4.32 (m,1H, 6CH), 5.80 (1H, 2CH), 2.01 (bs-OH), 6.81-7.54 (m, 14Haromatic); ^{13}C-NMR ($CDCl_3$, 100MHz): 34.4, 55.7, 118.1, 119.3, 126.7, 127.1, 127.3, 128.1, 128.3, 128.6, 128.8, 129.2, 132.4, 141.6, 142.5, 162.2, 169.5.

4.6.3 Removal of SO Dye and Textile Effluent from Water Using MgO Decorated FLG

Textile, pharmaceutical, leather, paper, printing, cosmetic etc., industries use dyes of various kinds in their respective processing procedures. During these procedures the dyes invariably enter the effluents which in turn contaminate the surrounding water bodies and/or ground water. Adsorption (with the aid of efficient adsorbents) has been a well-practiced method to remove dyes from contaminated water. Activated carbon [98-103], carbon nanospheres [104] and MgO-loaded porous carbon [105] have been used as efficient adsorbents. MgO alone in different forms has been an excellent adsorbent [106-115]. In this section demonstration of 'MgO decked few-layered graphene (MDFLG)' as an excellent adsorbent will be presented. Here it should be noted that synthesis of MDFLG does not involve i) complicated procedures and ii) use of harmful starting materials. This is very important to consider any material as an adsorbent material. More importantly the characteristics of MDFLG as discussed in section 4.4 are found to be suitable for it to be considered an adsorbent. Safranine O (SO), a basic dye has been considered as the adsorbate in this study. Stock solution of SO dye was prepared in double distilled water. All the test solutions are prepared by diluting the stock solution with double distilled water. Batch experiments are carried out in 100 ml volumetric flasks with 50 ml of dye solution agitated for 120 min using water bath shaker. A set of

experiments is performed to study the effect of adsorbent dose, initial dye concentration, contact time, and pH of the solution. After adsorption, the treated solution was centrifuged and the absorbance of the supernatant solution was determined at λ_{max} 520 nm for SO dye.

The percentage removal of SO dye was calculated by the following equation:

$$\text{Percentage Removal (\%)} = \frac{C_0 - C_e}{C_0} \times 100$$

where C_o and C_e are the initial and equilibrium liquid-phase concentration of the SO dye (mol /L), respectively. To study the adsorption kinetics, a series of 50 ml samples of SO dye of known concentrations (4.0 x 10^{-4}, 4.5 x 10^{-4} and 5.0 x 10^{-4} M) are prepared in air-tight 100 ml volumetric flasks containing 0.05 g of MDFLG. The entire set of flasks with the mixture was mechanically agitated in water bath shaker. The samples are collected at predetermined time intervals from 5 to 120 min. After centrifugation, the final dye concentration was analyzed using UV–visible spectrophotometer. The amount of dye adsorbed at a time (t) was calculated using the following equation:

$$\text{Amount Adsorbed } (q_t) = (C_0 - C_t) \times \frac{V}{m}$$

where q_t is the amount of adsorbed dye (mol/g), C_o and C_t are the concentrations of the SO dyes (M) at initial and time t (min), respectively, whilst V is the volume of the dye solution (L) and m is mass of the added adsorbent (g). Regeneration of SO dye and reusability of MDFLG as adsorbent was tested by considering SO dye concentration of 5 x10^{-4} M and adsorbent dose of 0.1 g. Desorption experiments are conducted by immersing SO dye loaded MDFLG in 50 ml of acetone and ethanol separately at room temperature. Percentage desorption of dye was obtained using the following equation:

$$\text{Percentage Desorption} = \frac{\text{Concentration of desorbed dye}}{\text{Concentration of dye loaded on MDFLG}} \text{ x } 100$$

Desorption study is helpful to elucidate the nature of adsorption mechanism and to regenerate the adsorbate. To check the reusability of MDFLG in removing SO dye from aqueous

solution, 3 cycles of the above desorption experiment are repeated and after each cycle percentage removal was calculated. To determine the effect of adsorbent dose on the percentage removal of SO dye, the amount of MDFLG was varied from 0.01 g to 0.1 g per 50 ml of SO dye solution keeping the initial dye concentration at 4 x 10^{-4} M. The percentage removal increased with the adsorbent dosage up to a certain limit and then attained saturation. Figure 4.34(a) shows that the dye removal efficiency has increased from 27.87% to 99.83% as the adsorbent dose increased from 0.01 g to 0.1 g. The optimum adsorbent dose is 0.05 g. The increase in percentage removal of SO dye with increase in dosage is typically a characteristic of large number of adsorption sites' availability [116]. This was already indicated by large surface area of MDFLG. To determine the effect of initial dye concentration on the adsorption process, the initial concentration of SO dye was varied from 3.0 x 10^{-4} M to 8.0 x 10^{-4} M. Adsorbent dose used for this study was the optimum value of 0.05 g. As shown in Fig. 4.34(b), the percentage removal of SO dye decreased from 99.52% to 52.14% as the molar concentration increased. The percentage removal of SO decreased due to the non-availability of adsorption sites for the increased number of SO dye molecules. This trend is as-expected. The inference from this study is that for 0.05 g of adsorbent dose and SO dye's concentration of ~4.0 x 10^{-4} M (or less) will result in more than 90% of SO dye removal. To determine the effect of contact time on the adsorption process, adsorption experiments with a fixed adsorbent dose of 0.05 g and three SO dye concentrations namely 4.0 x10^{-4}, 4.5 x10^{-4} and 5.0 x10^{-4} M are conducted for different contact times. The results are shown in Fig. 4.34(c). It was found that more than 70% removal of SO dye occurred in the first 20 min and thereafter the rate of adsorption was found to be slow but effective. It can be observed from Fig. 4.34(c) that the adsorption of SO dye onto MDFLG increased with increase of contact time. The percentage removal curves are continuous and distinct but leading to saturation after a certain time, suggesting possible monolayer coverage of SO dye

on the surface of adsorbent. The optimum contact time was found to be 120 min for more than 90% removal for SO dye concentration of 4.0 x10^{-4} M.

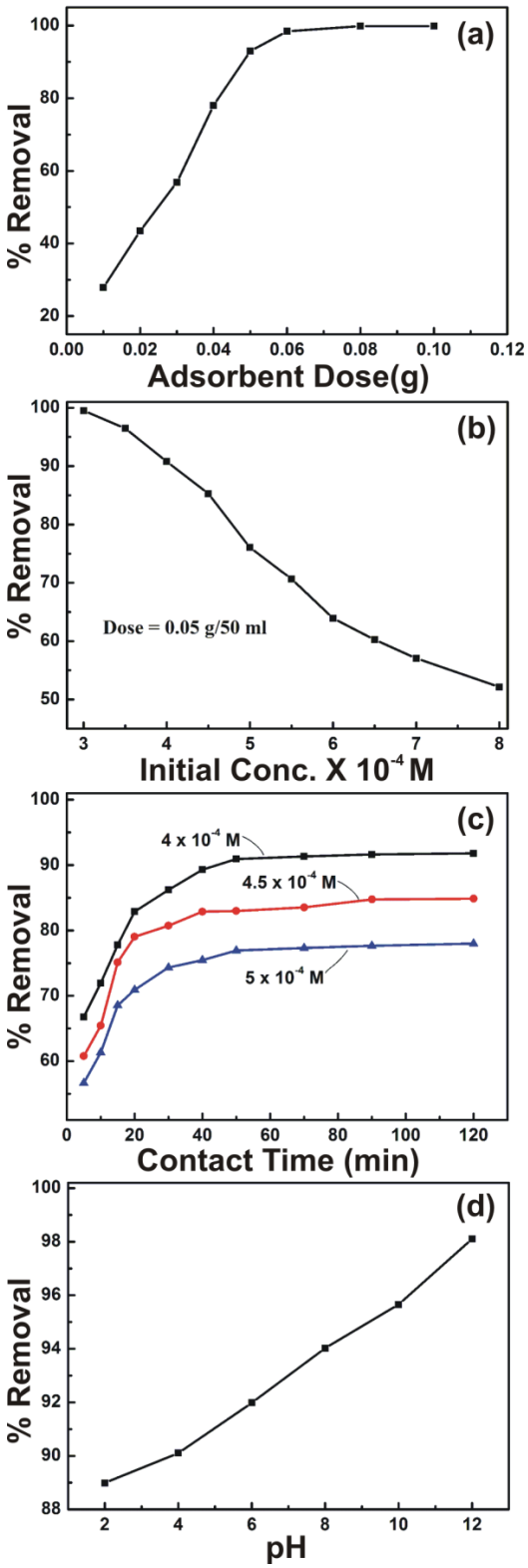

Figure 4.34. % Removal of SO dye Vs. (a) adsorbent dose, (b) SO dye concentration, (c) contact time of SO with MDFLG and (d) pH of SO dye solution.

The effect of pH was studied with SO dye concentration of 4.0 x 10^{-4} M, adsorbent dose of 0.05 g/50 ml and varying the pH by adding 0.1 N of NaOH or HCl solutions and then shaking the solution until equilibrium was reached. Figure 4.34(d) shows that as the pH of the SO dye solution increased from 2 to 12 the percentage adsorption of SO dye onto MDFLG increased from ~89% to 98%. At low pH, SO dye may be protonated and therefore only partial adsorption occurred. As the pH increased, [H^+] plausibly decreased resulting in less protonation of SO which in turn increased the adsorption of SO onto MDFLG.

The adsorption capacity of any adsorbent and adsorption mechanism can be predicted from equilibrium adsorption isotherms [117]. Langmuir, Freundlich and Dubinin-Radushkevich (D-R) adsorption isotherms are used to understand the adsorption of SO dye onto MDFLG. Langmuir adsorption isotherm assumes that monolayer adsorption occurs at the binding sites of uniform surface [118]. Equation representing Langmuir adsorption is:

$$\frac{C_e}{q_e} = \frac{1}{Q_m K_L} + \frac{1}{Q_m} C_e$$

where q_e (mol/g) and C_e (M) are the amount of dye adsorbed per unit weight of adsorbent and the concentration of the dye solution at equilibrium, respectively. Q_m (mol/g) is the adsorption capacity and K_L (L/mol) is the Langmuir equilibrium constant. The values of Q_m and K_L are calculated from the intercept and slope of the linear plot of C_e Vs. $\frac{C_e}{q_e}$ (Fig. 4.35) and are shown in the Table 4.1. Langmuir constant can be used to determine applicability of MDFLG for the removal of SO dye by using dimensionless constant called separation factor or equilibrium parameter (R_L) which is defined as [119,120]:

$$R_L = \frac{1}{1 + K_L C_0}$$

where C_0 is the initial SO dye concentration (M). If R_L value is between 0 and 1, the adsorption is favorable. R_L value of 0.0057 indicates a favorable adsorption of SO onto

MDFLG. The maximum adsorption capacity of SO dye-MDFLG system is found to be ~3.929 x10^{-4} mol/g.

Freundlich adsorption isotherm is empirical in nature and assumes heterogeneous adsorbent surface (that is adsorption sites at varied energy levels). Equation representing Freundlich adsorption can be expressed as [121]:

$$\log(q_e) = \log(K_F) + \frac{1}{n}\log(C_e)$$

where q_e and C_e are the same as discussed above whilst K_F (mol/g) and n (dimensionless) are constants for a given adsorbate and adsorbent combination at a particular temperature.

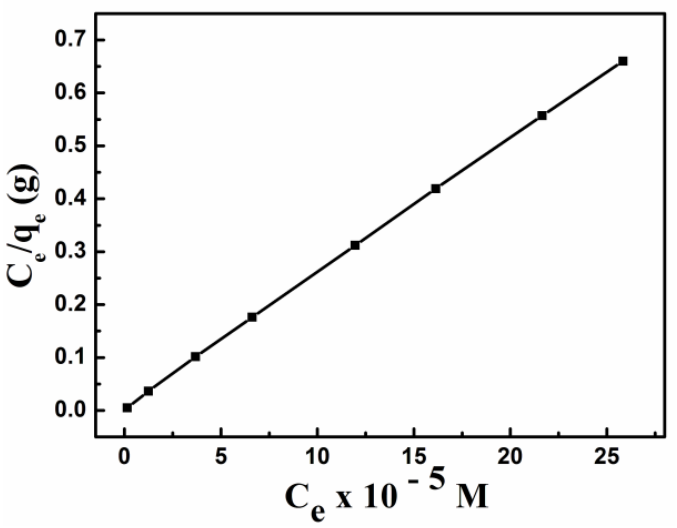

Figure 4.35. Langmuir adsorption isotherm of SO dye-MDFLG system.

The values of K_F and $\frac{1}{n}$ are obtained from the slope and the intercept of the plot of log (q_e) Vs. log (C_e) (Fig. 4.36). The value of $\frac{1}{n}$ in the range 0-1 indicates favorable adsorption [122]. The obtained K_F and $\frac{1}{n}$ values are given in Table 4.1. $\frac{1}{n}$ value of 0.0527 indicates a favorable adsorption of SO dye onto MDFLG.

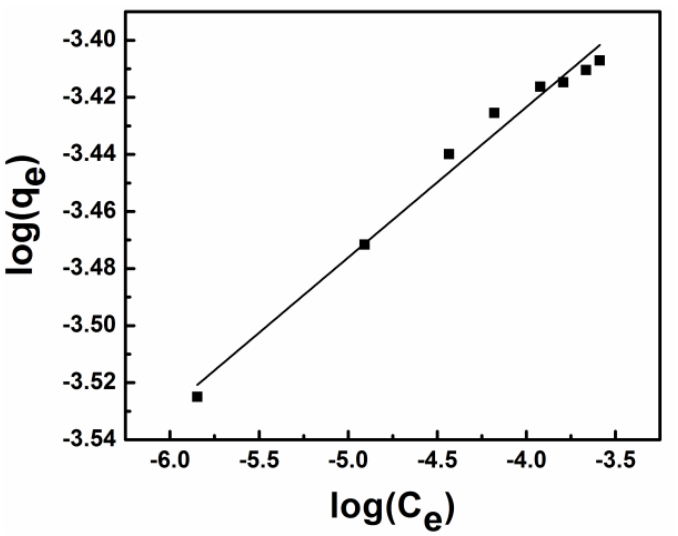

Figure 4.36. Freundlich adsorption isotherm of SO dye-MDFLG system.

D-R isotherm determines if the adsorption is by physical or chemical process. Equation representing D-R adsorption [123-125]:

$$\ln(q_e) = \ln(Q_m) - K\varepsilon^2$$

where K (mol^2/KJ^2) is a constant related to the adsorption process whilst ε is the Polanyi potential that can be calculated using the following equation:

$$\varepsilon = RT \ln(1 + \frac{1}{C_e})$$

where T is the temperature in Kelvin whilst R is the universal gas constant (8.314 J/mol/K). The slope of $\ln(q_e)$ Vs. ε^2 (Fig. 4.37) gives K whilst the intercept gives the adsorption capacity. The mean adsorption energy, E (kJ/mol) is obtained using the following equation:

$$E = \frac{1}{\sqrt{(2K)}}$$

A high E value of 36 kJ/mol is measured. This clearly indicates that adsorption of SO dye onto MDFLG is mainly through chemisorption. The values of different parameters obtained in different isotherm models are given in Table 4.2. Comparing the correlation coefficients (R^2) of the considered adsorption isotherms, Langmuir provided the highest R^2 of 0.999 which implies that it is the best fit in describing the adsorption of SO dye onto MDFLG.

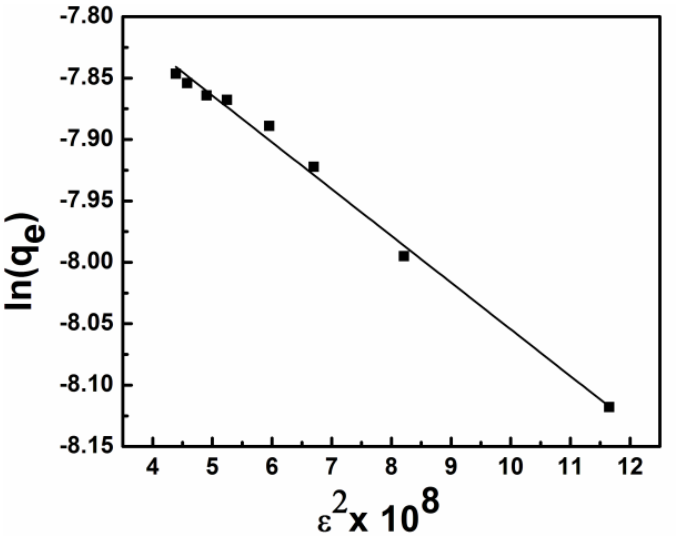

Figure 4.37. D-R adsorption isotherm of SO dye-MDFLG system.

Table 4.2. Values of different parameters in the considered adsorption isotherm models.

Isotherm	Parameter	Value	R^2
Langmuir	K_L (L/mol)	4.395×10^5	0.999
	Q_m (mol/g)	3.929×10^{-4}	
	R_L	0.0057	
Freundlich	K_F (mol/g)	6.128×10^{-4}	0.982
	$\frac{1}{n}$	0.0527	
D-R	K (mol^2/KJ^2)	0.03808×10^{-8}	0.992
	Q_m (mol/g)	4.648×10^{-4}	
	E (kJ/mol)	36.235	

In order to evaluate the adsorption kinetics, pseudo 1st and 2nd order models are applied to the experimental data and the fit between experimental data and model predicted values is expressed in terms of R^2. The pseudo 1st order equation is expressed as follows [126]:

$$\log(q_e - q_t) = \log q_e - \frac{k_1 t}{2.303}$$

where k_1 (/min) is the rate constant. k_1 and q_e can be calculated from the slope and intercept, respectively of $\log(q_e - q_t)$ Vs. t plot. If the calculated q_e is not equal to the experimentally obtained q_e value, then the reaction is not likely to be a pseudo 1st order reaction even when R^2 values are high [127,128]. $\log(q_e - q_t)$ Vs. t plots (Fig. 4.38) for different SO dye concentrations are straight lines with high R^2 values ranging from 0.961 to 0.978, which are

relatively high, but the calculated q_e values are not equal to the experimentally obtained q_e values (Table 4.3). This indicates that the adsorption of SO dye onto MDFLG does not follow the pseudo 1st order reaction.

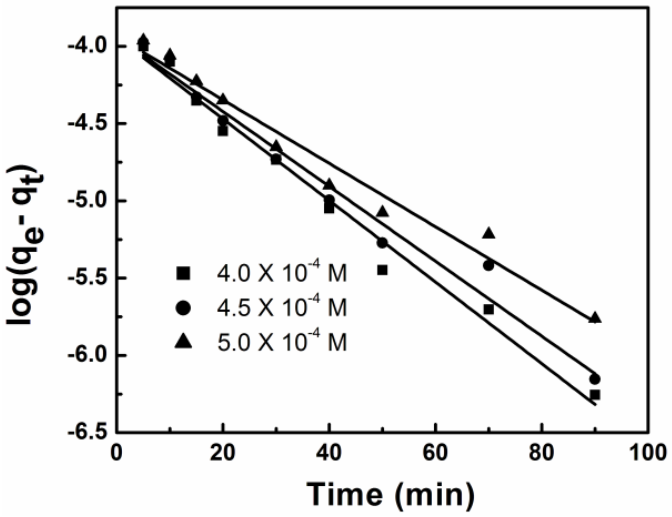

Figure 4.38. Pseudo 1st order adsorption of SO dye onto MDFLG.

The pseudo 2nd order chemisorption kinetic rate equation is expressed as follows [126]:

$$\frac{t}{q_t} = \frac{1}{k_2 q_e^2} + \frac{1}{q_e} t \qquad (11)$$

where k_2 (g/mol/min). The 2nd order parameters q_e and k_2 can be calculated from the slope and intercept, respectively of $\frac{t}{q_t}$ Vs. t plot (Fig. 4.39). Different 2nd order parameters are listed in Table 4.3. The values of equilibrium adsorption capacity and pseudo 2nd order rate constant decreased with increasing initial SO dye concentration. The R^2 values are nearly equal to unity (~0.999) which is a clear indication that the adsorption of SO onto MDFLG is due to chemical adsorption. In addition, the calculated $q_e$values are in good agreement with the experimentally obtained $q_e$values, which confirms that the adsorption of SO dye onto MDFLG surface follows pseudo 2nd order reaction.

SO adsorbed onto MDFLG was desorbed by acetone and ethanol to an extent of ~14.8 and ~73.4%, respectively. The maximum desorption took place with ethanol as the desorbing

medium. This strongly suggests that chemi-desorption is the major mode of dye removal from the adsorbent. Even after 3 cycles of the desorption experiments in ethanol, MDFLG could remove ~94% (Fig. 4.40) of SO dye from the aqueous solution.

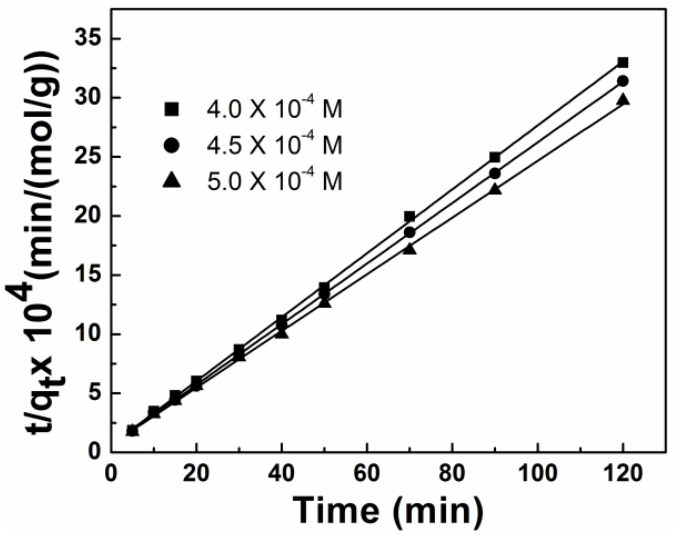

Figure 4.39. Pseudo 2nd order adsorption of SO dye onto MDFLG.

Table 4.3. Adsorption kinetic parameters for the adsorption of SO onto MDFLG.

Adsorbate Conc. (M)	Experimental q_e (mol/g)	Pseudo 1st order			Pseudo 2nd order		
		Calculated q_e (mol/g)	k_1 (/min)	R^2	Calculated q_e (mol/g)	k_2 (g/mol/min)	R^2
4.0×10^{-4}	3.362×10^{-4}	0.94×10^{-4}	0.063	0.978	3.7×10^{-4}	11.57×10^{2}	0.9998
4.5×10^{-4}	3.510×10^{-4}	1.91×10^{-4}	0.054	0.961	3.9×10^{-4}	11.12×10^{2}	0.9998
5.0×10^{-4}	3.586×10^{-4}	2.17×10^{-4}	0.051	0.962	4.17×10^{-4}	8.36×10^{2}	0.9999

A real effluent was collected from a textile industry and experiments are carried out to remove the mixture of dyes from the effluent (50 ml) through adsorption using 0.02, 0.05 and 0.1 g of MDFLG. Figure 4.41 shows the UV-visible absorption spectrum for the textile

effluent before and after treating it with MDFLG. Decrease in the absorbance in the range of 300−450 nm in the cases of 0.05 and 0.1 g of MDFLG clearly indicates effective removal of mixture of dyes from the effluent.

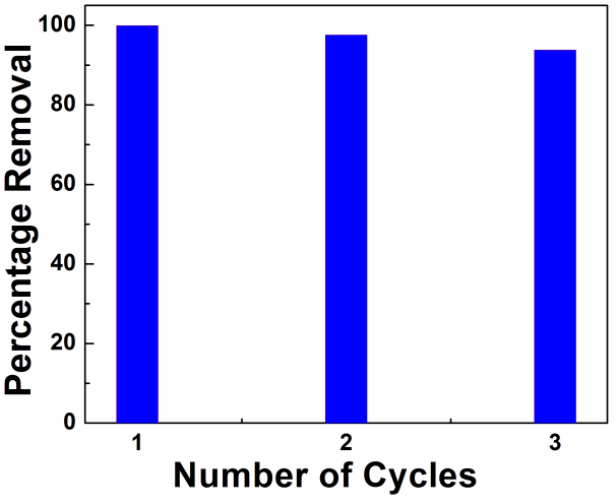

Figure 4.40. Reusability of 0.1 g of MDFLG to remove SO dye from 5 x10^{-4} M aqueous solution.

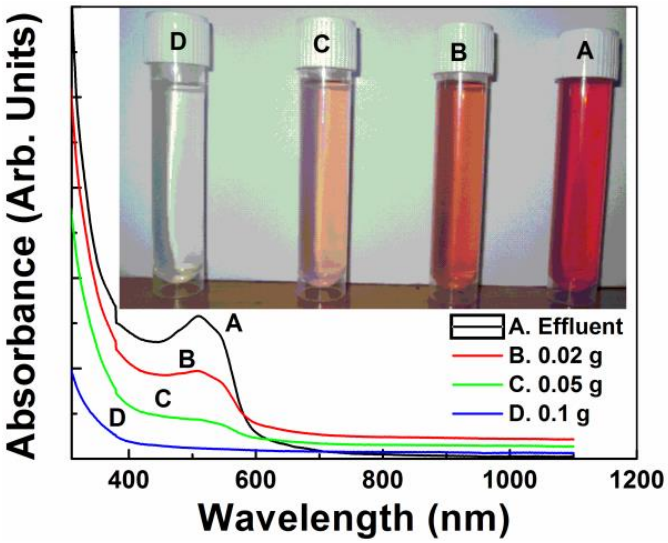

Figure 4.41. UV-visible absorption spectra obtained from different samples. A represents untreated effluent whilst B, C and D represent effluent after treating with 0.02, 0.05 and 0.1 g of MDFLG. Inset shows photograph of untreated and treated effluent samples.

4.6.4 MgO Decorated FLG as an Anode Material in Li Ion Battery

MDFLG synthesized in this thesis work was extensively tested as an anode material in Li ion battery in another work [64] owing to its suitable characteristics as discussed in section 4.1. Careful electrochemical characterization was done to measure anodic response of MDFLG in a typical Li ion battery. MDFLG exhibited a high specific surface area of 393 m^2/g and high mesoporosity (average pore volume 0.9 cm^3/g). It exhibited a high reversible capacity and excellent constant cyclic performance. A reversible capacity of as high as 1052 mAh/g was measured during the first cycle. Even at the end of the 60th cycle, more than 83% of the capacity could be retained. Electrochemical impedance spectroscopic studies confirmed easy lithiation kinetics in the fabricated batteries and an ideal conducting electrode nature of MDFLG. An increase in the capacity has been observed during long-term cycling owing to electrochemical exfoliation of graphene sheets. Owing to its good thermal stability and superior cyclic performance with high reversible capacities, MDFLG is an excellent alternative to graphite as an anode material in Li-ion batteries.

4.6.5 Antibacterial Activity of MgO Decorated FLG

Well diffusion method was used for testing antibacterial activity of MgO dopped graphene against Escherichia coli (E.coli) strain. MDFLG are dispersed in deionized water with three different concentrations for testing its activity: A with 1 mg of MDFLG dispersed in 50 µl of deionized water, B with 1.5 mg and C with 2 mg of MDFLG dispersed in 50 µl of deionized water. E. coli was chosen as the model pathogen for antibacterial activity experiments. E. coli was cultured in Luria-Bertani (LB) nutrient solution at 37 °C for 18 h to get the exponential growth phase. The cells were obtained by centrifugation. The obtained cells were washed in saline solution (0.9% NaCl) to remove unwanted residues. The cells were re-suspended in a saline solution. LB agar is used for well diffusion method. It is prepared by adding 40 g LB agar powder in distilled water or deionized water. The volume considered

was 1000 ml and LB agar was mixed thoroughly. The mixture was gently heated to boiling and then sterilized by autoclaving at 121 °C and 15 psi pressure for 15 min. The sterilized LB agar suspension is poured into sterile petri-plates and allowed to solidify. Plates were allowed to dry before applying the sample. Then E.coli bacterial culture was taken and spread evenly over the entire surface of the plate by using glass rod in three directions. The wells were casted by porer on the test plates. The samples were loaded with equal volume (50 µl) into the wells. The test plates were incubated at 37 °C temperature. The activity of the samples was clearly visible from 19-24 h on the plates. The antibacterial activity of MDFLG was identified by the formation of zone of inhibitions (Fig. 4.42) for each sample after 24 h. The results showed that the zone of inhibition increases with the increase in concentration of MDFLG (Fig. 4.43).

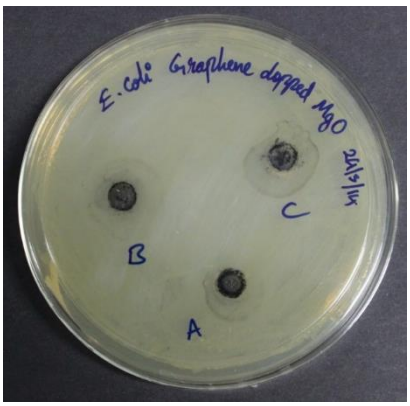

Figure 4.42. Antibacterial activity of MDFLG and zone of inhibitions.

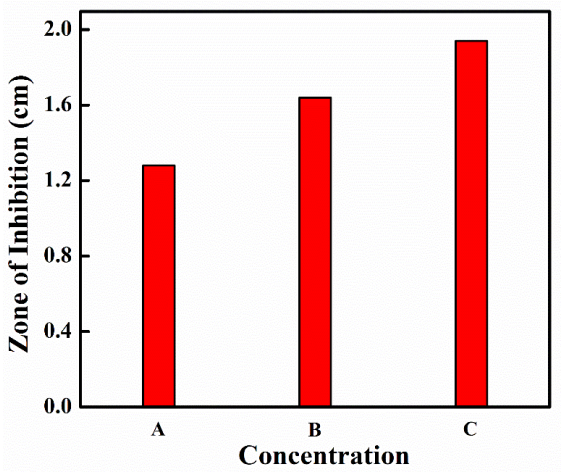

Figure 4.43. Zone of inhibition values with varying MDFLG concentrations.

4.6.6 Hydrogen Adsorption of MgO decorated FLG

Hydrogen adsorption by MDFLG (Fig. 4.44) at different hydrogen pressures has been studied here by using the pressure reduction method in which the hydrogen concentration is calculated from the observed pressure change before and after hydrogen adsorption at a constant calibrated volume and at a constant temperature. For the calculation of hydrogen concentration present in the material, Vander Waals equation of state was used at higher gas pressure while the ideal gas law was used at lower pressure of hydrogen gas. The hydrogen absorption capacity is expressed in terms of wt% defined by

$$\text{Weight Percent (wt. \%)} = \frac{\textbf{Weight of the hydrogen molecule}}{\textbf{Weight of MDFLG}} * 100$$

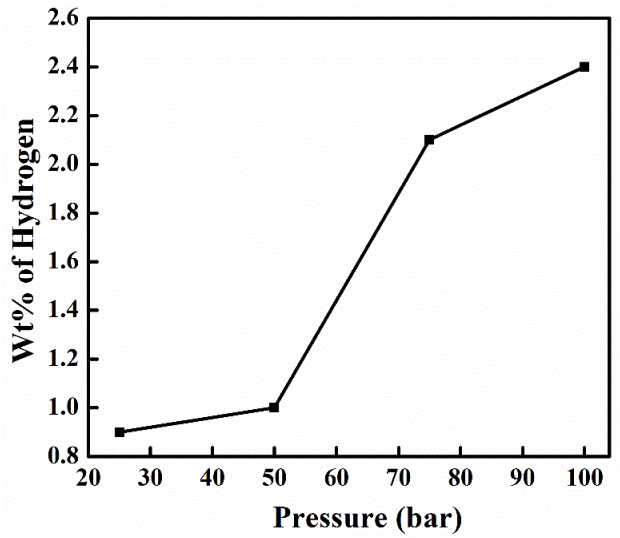

Figure 4.44. Hydrogen adsorption capacity of MgO decorated FLG at different pressures.

For the determination of adsorption levels for MDFLG in the pressure range $1 \leq P\ (atm) \leq 150$ atm, 0.1 g of the sample was taken in the sample tube which was then inserted into the sample cell. The entire section was then evacuated to 10^{-9} mbar using a turbo molecular pump. The sample was first heated to 250 ºC for about 2 h to remove any dissolved gases present in the sample. The furnace was then cooled to 100 ºC and hydrogen gas of initial pressure 25 atm was allowed to react with the sample. The furnace was then slowly cooled to

room temperature and the concentration of hydrogen in the sample was calculated. The sample was then degassed at about 250 ºC and the hydrogen adsorption-desorption cycle was repeated until concordant value of hydrogen concentration was obtained and the sample was activated for hydrogen adsorption. From Fig. 4.44 it is very clear that the hydrogen adsorption capacity of MDFLG is excellent. Moreover, it increased with increasing pressure.

4.6.7 Non-linear Ferromagnetic Short Range Ordering in MgO decorated FLG

An elaborate analysis of high-precision magnetization data pertaining to MgO decorated FLG [129] showed the persistence of a non-collinear FM short-range order in the sample at temperatures as high as 300 K and a concomitant paramagnetic component is present at all the temperatures. The analysis showed that there is an exponential growth of the correlation length for the spins at the zigzag edges of graphene as the temperature falls below the temperature, $T_x \cong 10\,K$ where a crossover from extremely weak to moderately weak magnetic anisotropy occurs. The analysis also showed that a paramagnetic response is induced by the defects in nm-sized MgO crystallites in the sample. The M-H curve of MgO decorated FLG as obtained by using Vibrating Sample Magnetometer is shown in Fig. 4.45.

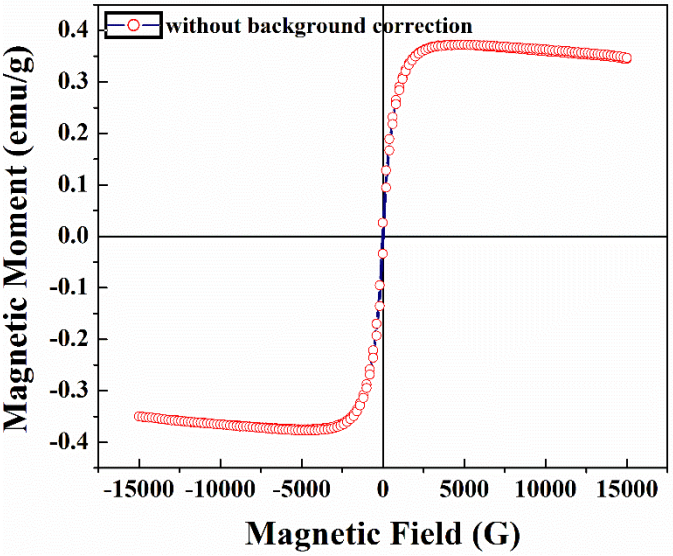

Figure 4.45. Magnetization versus magnetic field of MgO decorated FLG.

4.6.8 Plasmid DNA Isolation Using S, N Doped FLG

S, N doped FLG is experimented for the purification of plasmid DNA from sonicated bacterial lysate [130]. As-synthesized S, N doped FLG powder (i.e., without any pre-preparation and surface modification) was reusable after a simple washing step. Quality and quantity of DNA are found to be good. The quantity of DNA obtained was acceptable as per the commercial standards.

References

[1]. W. S. Hummers and R. E. Offeman, J. Am. Chem. Soc. 80(6), 1339-1339 (1958).

[2]. D. C. Marcano, D. V. Kosynkin, J. M. Berlin, A. Sinitskii, et al., ACS Nano. 4(8), 4806-4814 (2010).

[3]. J. C. Meyer, A. K. Geim, M. I. Katsnelson, K. S. Novoselov, et al., Nature. 446, 60 (2007).

[4]. J. C. Meyer, A. K. Geim, M. I. Katsnelson, K. S. Novoselov, et al., Solid State Commun. 143, 101 (2007).

[5]. A. Lerf, H. He, M. Forster and J. Klinowski, J. Phys. Chem. B. 102, 4477 (1998).

[6]. W. Zhang, J. Cui, C. Tao, Y. Wu, et al., Angew Chem Int Ed. 48(32), 5864-5868 (2009).

[7]. D. Graf, F. Molitor, K. Ensslin, C. Stampfer, et al., Nano Lett. 7(2), 238-242 (2007).

[8]. A. Das, B. Chakraborty and A. K. Sood, Bull. Mater. Sci. 31(3), 579-584 (2008).

[9]. A. C. Ferrari, J. C. Meyer, V. Scardaci, K. S. Novoselov, et al., Phys Rev Lett. 97(18), 187401 (2006).

[10]. V. Sridhar, J.-H. Jeon and I.-K. Oh, Carbon 48(10), 2953-2957 (2010).

[11]. G. Chen, W. Weng, D. Wu, P. Wang, et al., Carbon 42(4), 753-759 (2004).

[12]. T. Szabo, O. Berkesi, P. Forgo, K. Josepovits, Chem. Mater. 18, 2740-2749 (2006).

[13]. C. Nethravathi and M. Rajamathi, Carbon 46, 1994-1998 (2008).

[14]. V. H. Pham, T. V. Cuong, S. E. W. Shin and J. S. Chung, J. Mater. Chem. 21, 3371 (2011).

[15]. K. S. Subrahmanyam, S. R. C Vivekchand, A. Govindaraj and C. N. Rao, J. Mater. Chem. 18(13), 1517-1523 (2008).

[16]. A. C. Ferrari, Solid State Commun. 143(1-2), 47-57 (2007).

[17]. M. S. Dresselhaus, A. Jorio and R. Saito, Annu. Rev. Condens. Matter Phys. 1, 89-108 (2010).

[18]. L. G. Canado, M. A. Pimenta, B. R. A. Neves, M. S. S. Dantas, et al., Phys. Rev. Lett. 93, 247401 (2004).

[19]. S. Cho, K. Kikuchi and A. Kawasaki, Carbon 49, 3865-3872 (2011).

[20]. E. Smidt, P. Lechner, M. Schwanninger, G. Haberhauer et al., Appl. Spectrosc. 56, 1170-1175 (2002).

[21]. N. B. A. Mansor, J.-P. Tessonnier, A. Rinaldi, S. Reiche, et al., Sains Malaysiana. 41(5), 603-609 (2012).

[22]. J. Garai, S. E. Haggerty, S. Rekhi and M. Chance, Astrophys. J. 653, 153-156 (2006).

[23]. M. Lu, T. Ohba, K. Kaneko, H. Kanoh, et al., Materials 6, 535-543 (2013).

[24]. W. S. Jang, S. S. Chae, S. J. Lee, K. M. Song, et al., Carbon 50, 943-951 (2012).

[25]. O.-K. Park, Y.-M. Choi, J. Y. Hwang, B.-C. Ku et al., Nanotechnol. 24, 185604 (2013).

[26]. W. Chen, L. Yan and R. Bangal, Carbon 48, 1146-1152 (2010).

[27]. V. H. Pham, H. D. Pham, T. T. Dang, J. S. Chung, et al., J. Mater. Chem. 22, 10530-10536 (2012).

[28]. R. Jia, J. Chen, J. Zhao, J. Zheng, et al., J. Mater. Chem. 20, 10829-10834 (2010).

[29]. X. Li, H. Wang, J. T. Robinson, H. Dai, et al., J. Am. Chem. Soc. 131, 15939-15944 (2009).

[30]. J. Park, T. Back, W. C. Mitchel, R. Naik, et al., Sci. Rep. 5, 14374 (2015).

[31]. F. Bottger-Hiller, A. Mehner, S. Anders, L. Kroll, et al., Chem. Commun. 48, 10568-10570 (2012).

[32]. D. M. Fernandes, M. Nunes, R. J. Carvalho, P. de Oliveira, et al., Inorganics 3, 178-193 (2015).

[33]. M. Jana, P. Khanra, N. C. Murmu, P. Samanta, et al., Phys. Chem. Chem. Phys. 16, 7618 (2014).

[34]. T. Terse-Thakoor, K. Komori, P. Ramnani, I. Lee, et al., Langmuir 31, 13054-13061 (2015).

[35]. R. Burgess, C. Buono, P. R. Davies, T. Legge, et al., J. Catal. 323, 10-18 (2015).

[36]. N. Díez, A. Śliwak, S. Gryglewicz, B. Grzyb, et al., RSC Adv. 5, 81831 (2015).

[37]. A. Barinov, L. Gregoratti, P. Dudin, S. L Rosa, et al., Adv. Mater. 21, 1916 (2009).

[38]. X.-G. Li, K.-L. Huang, S.-Q. Liu and L.-Q. Chen. Trans. Nonferrous Met. Soc. China. 17, 195-199 (2007).

[39]. D. Mo and D.-Q. Ye, Surf. Coat. Technol. 203, 1154-1160 (2009).

[40]. M. M. Viana, M. C. F. S. Lima, M. S. Wong, V. Caliman, et al, J. Braz. Chem. Soc. 26, 978-984 (2015).

[41]. S. Saxena, T. A. Tyson and E. Negusse, J. Phys. Chem. Lett. 1, 3433-3437 (2010).

[42]. A. Hunt, D. A. Dikin, E. Z. Kurmaev, P. Bazylewski, et al., Adv. Funct. Mater. 22, 3950-3957 (2012).

[43]. J. Long, X. Xie, J. Xu, Q. Gu, et al., ACS Catal. 2, 622-631 (2012).

[44]. Z. Tian, J. Li, G. Zhu, J. Lu, et al., Phys. Chem. Chem. Phys. 18, 1125 (2016).

[45]. H. Gao, L. Song, W. Guo, K. Hackenberg, et al., Carbon. 504, 476-482 (2012).

[46]. K. Zhou, W. Zhou, X. Liu, H. Liu, et al., Nano Energy 12, 510-520 (2015).

[47]. A. M. Puziy, O. I. Poddubnaya, R. P. Socha, J. Gurgul, et al., Carbon 46, 2113-2123 (2008).

[48]. M. Chen, J. Liu, W. Zhou, J. Lin, et al., Sci. Rep.5, 10389 (2015).

[49]. H. Wang, T. Maiyalagan and X. Wang, ACS Catal. 2, 781-794 (2012).

[50]. D. Choudhury, B. Das, D. D. Sarma and C. N. R. Rao, Chem. Phys. Lett. 497, 66-69 (2010).

[51]. R. Voggu, B. Das, C. S. Rout, C. N. R. Rao, J. Phys. Conden. Matter. 20, 472204 (2008).

[52]. S. Van Dommele, A. Romero-Izquirdo, R. Brydson, et al., Carbon 46,138-148 (2008).

[53]. H. L. Poh, P. Simek, Z. Sofer, I. Tomandl, etc., J. Mater. Chem. A, 1, 13146 (2013).

[54]. D. Usachov, O. Vilkov, A Griineis, D. Haberer, et al., Nano Lett. 11, 5401-5407 (2011).

[55]. L. Zhang, H. Huang, H. Yin, Y. Xia, et al., J. Mater. Chem. A 3, 16513 (2015).

[56]. X. Liu, W. Zhou, L. Yang, L. Li, et al., J. Mater. Chem. A 3, 8840 (2015).

[57]. M. M. Nasef, H. Saidi, H. M. Nor and M. A. Yarmo, J. Appl. Polym. Sci. 76, 336–349 (2000).

[58]. J. Xu, J. Shui, J. Wang, et al., ACS Nano 8, 10920-10930 (2014).

[59]. D. Sun, R. Ban, P.-H. Zhang, G.-H. Wu, et al., Carbon 64, 424-434 (2013).

[60]. W. Gu, M. Sevilla, A. Magasinski, A. B. Fuertes, et al., Energy Environ. Sci. 6, 2465 (2013).

[61]. K. Singh, N. A. Travlou, S. Bashkova, E. Rodríguez-Castellón, et al., Carbon 80, 183-192 (2014).

[62]. J. Wu, S. Bai, X. Shen and L. Jiang, Appl. Surf. Sci. 257, 747-751 (2010).

[63]. C. Namasivayam and D. Kavitha, Dyes Pigments 54, 47-58 (2002).

[64]. S. Petnikota, N. K. Rotte, M. V. Reddy, V. V. S. S. Srikanth, et al., ACS Appl. Mater. Interfaces 7, 2301 (2015).

[65]. M. J. Matthews, M. A. Pimenta, G. Dresselhaus, M. S. Dresselhaus et al., Phys. Rev. B 59, R6585(R) (1999).

[66]. L. Bokobza and J. Zhang, eXPRESS Polymer Lett. 6, 601-608 (2012).

[67]. Q. Zhao and H. D. Wagner, Phil. Trans. Royal Soc. Lond. A, V 362, 2407-2424 (2004).

[68]. M. S. Dresselhaus and P. C. Eklund, Adv. Phys. 49, 705-814 (2000).

[69]. F. Tuinstra and J. L. Koenig, J. Phys. Chem. 53, 1126 (1970).

[70]. S. Petnikota, N. K. Rotte, V. V. S. S. Srikanth, B. S. R. Kota, et al., J. Solid State Electrochem. 18(4), 941 (2014).

[71]. J. Clark, M. S. Shohhet, D. Korakas and G. Varvounis, J. Heterocycl. Chem. 30, 1065-1072 (1993).

[72]. K. Eger, E. Klunder and M. Schmidt, J. Med. Chem. 37, 3057 (1994).

[73]. D. B. Longley, D. P. Harkin and P. G. Johnston, Nature Rev. 3, 330-338 (2003).

[74]. O. A. Fathalla, I. F. Zeid, M. E. Haiba, A. M. Soliman, et al., World J. Chem. 4(2), 127-132 (2009).

[75]. Yogesh Pore, Bhanudas Kuchekar, Digest Journal of Nanomaterials and Biostructures. 3(4), 293-298 (2008).

[76]. T. S. Chitre, K. G. Bothara, S. M. Patil, K. D. Asgaonkar, et al., Int.. J. Res. Pharm. Biomed. Sci. 2, 616-623 (2011).

[77]. L. F. Jalander and J. Lonnqvist, Heterocycles. 48, 743-747 (1998).

[78]. J. L. G. Navio, A. Lorente and J. L. Soto, Heterocycles. 19, 305-310 (1982).

[79]. K. Fink, R. B. Henderson, R. M. Fink, J. Biol. Chem., 221, 425 (1956).

[80]. J. Caravica and S. Grisolia, J. Biol. Chem., 231, 357 (1958).

[81]. E. Philippi, F. Hendgen and F. Hernler, Monatsch. 69, 270 (1936).

[82]. G. Aridoss, S. Amirthaganesan and Y. T. Jeong, Bioorg. Med. Chem. Lett. 20, 2242 (2010)

[83]. H. Tsukamoto and Y. Kondo, Angew. Chem. 47, 4851 (2008).

[84]. D. A. Spiegel, F. C. Schroeder, J. R. Duvall andS. L. Schreiber, J. Am. Chem. Soc. 128, 14766 (2006)

[85]. P. V. Ramachandran, T. E. Burghardt and L. Bland-Berry, J. Org. Chem. 70, 7911 (2005).

[86]. X.-F. Zhu, J. Lan and O. Kwon, J. Am. Chem. Soc. 125, 4716 (2003).

[87]. C. Legault and A. B. Charette, J. Am. Chem. Soc. 125, 6360 (2003).

[88]. P. Buonora, J.C. Olsen and T. Oh, Tetrahedron. 57, 6099 (2001).

[89]. Y. Kita, H. Maekawa, Y. Yamasak, I. Nishiguchi, Tetrahedron. 57, 2095 (2001).

[90]. J. F. Caplan, A. Sutherland and J. C. Vederas, J. Chem. Soc., Perkin Trans. 1, 2217 (2001).

[91]. T. J. Harrison and G. R. Dake, J. Org. Chem. 70, 10872 (2005).

[92]. X. Li, L. Song, C. Xing, J. Zhao and S. Zhu, Tetrahedron. 62, 2255 (2006).

[93]. R.-G. Han, Y. Wang, Y. Y. Li and P. F. Xu, Adv. Synth. Catal. 2008, 350, 1474 (2008).

[94]. N. Zanatta, L. S. da Fernandes, F. M. Nachtigall and H. S. Ceolho, Eur. J. Org. Chem. 1435 (2009)

[95]. V. Sridharan, S. Maiti and J. C. Menendez, Chem. Eur. J. 15, 4565 (2009).

[96]. W.-B. Liu, H.-F. Jiang, S.-F. Zhu and W. Wang, Tetrahedron. 65, 7985 (2009).

[97]. C. A. Sperger, P. Mayer and K. T. Wanner, Tetrahedron. 65, 10463 (2009).

[98]. S. Preethi, A. Sivasamy, S. Sivanesan, V. Ramamurthi, et al., Ind. Eng. Chem. Res. 45, 7627-7632 (2006).

[99]. Y. Önal, C. Akmil-Başar, D. Eren, Ç. Sarici-Özdemir, et al., J. Hazard. Mater. 128, 150-157 (2006).

[100]. B. H. Hameed, A. T. M. Din and A. L. Ahmad, J. Hazard. Mater. 141, 819-825 (2007).

[101]. E. N. El Qada, S. J. Allen and G.A. Walker, Chem. Eng. J. 135, 174-184 (2008).

[102]. I. A. W. Tan, A. L. Ahmad and B. H. Hameed, J. Hazard. Mater. 154, 337-346 (2008).

[103]. R. Bradley, Adsorpt. Sci. Technol. 29, 1-28 (2011).

[104]. X. Song, Y. Wang, K. Wang and R. Xu, Ind. Eng. Chem. Res. 51, 13438-13444 (2012).

[105]. A. Czyżewski, J. Karolczyk, A. Usarek and J. Przepiórski, Bull. Mater. Sci. 35, 211-219 (2012).

[106]. S. W. Bain, Z. Ma, Z. M. Cui, L. S. Zhang, et al., J. Phys. Chem. C 112, 11340-11344 (2008).

[107]. J. Hu, Z. Song, L. Chen, H. Yang, et al., J. Chem. Eng. Data 55, 3742-3748 (2010).

[108]. W. Z. Liu, F. Huang, Y. J. Wang, T. Zou, et al., Environ. Sci. Technol. 45, 1955-1961 (2011).

[109]. X. M. Wu, H. Q. Cao, G. Yin, J. F. Yin, et al., Phys. Chem. Chem. Phys. 13, 5047-5052 (2011).

[110]. J. B. Lian, C. H. Zhang, P. Wang and D. H. L. Ng, Chem. Asian J. 7, 2650-2655 (2012).

[111]. C. Y. Cao, J. Qu, F. Wei, H. Liu, et al., ACS Appl. Mater. Interfaces 4, 4283-4287 (2012).

[112]. L. H. Ai, H. T. Yue and J. Jiang, Nanoscale 4, 5401-5408 (2012).

[113]. T. G. Venkatesha, Y. Arthoba Nayaka and B. K. Chethana, Appl. Surf. Sci. 276, 620-627 (2013)

[114]. K. N. Nguyen, T. T. H. Phi, D. L. Tran and Q. H. Tran, J. Colloid Interface Sci. 398, 210-216 (2013).

[115]. P. Tian, X. Han, G. Ning, H. Fang, et al., ACS Appl. Mater. Interfaces 5, 12411-12418 (2013).

[116]. C. Namasivayam and D. Kavitha, Dyes Pigments 54, 47-58 (2002).

[117]. Ö. Gök, A. Safa Özcan and A. Özcan, Appl. Sur. Sci. 256, 5439-5443 (2010).

[118]. E. Bulut, M. Ozacar and I. A. Sengil, J. Hazard. Mater. 154, 613-622 (2008).

[119]. I. D. Mall, V. C. Srivastava, G. V. A. Kumar and I. M. Mishra, Colloids Surf. A. 278, 175-187 (2006).

[120]. G. Crini, H. N. Peindy, F. Gimbert and C. Robert, Sep. Purif. Technol. 53, 97-110 (2007).

[121]. Y. Bulut and H. Aydın, Desalination 194, 259-267 (2006).

[122]. C. Namasivayam and N. Kanchana, Chemosphere. 25, 1691-1706 (1992)

[123]. J. P. Hobson, J. Phys. Chem. 73, 2720-2727 (1969).

[124]. M. M. Dubinin, Chem. Rev. 60, 235-266 (1960).

[125]. A. Dabrowski, Adv. Colloid Interface Sci. 93, 35-224 (2001).

[126]. S. Wang and Z. H. Zhu, J. Hazard. Mater. 136, 946-952 (2006).

[127]. Y. S. Ho and G. Mckay, Process. Saf. Environ. 76, 332-340 (1998).

[128]. P. P. Selvam, S. Preethi, P. Basakaralingam, N. Thinakaran, et al., J. Hazard. Mater. 155, 39-44 (2008).

[129]. K. V. Sreenivasulu, ongoing PhD work, School of Engineering Sciences and Technology, University of Hyderabad. (The work is also unpublished)

[130]. Harish Ohja, ongoing PhD work, School of Engineering Sciences and Technology, University of Hyderabad. (The work is also unpublished)

Chapter 5 Conclusions and Future Scope

5.1 Conclusions

This thesis has presented the research work which was carried out to synthesize and characterize graphene related materials. The idea was to use simple methods to obtain novel graphene related materials. The methods (both related to synthesis and characterization) had to be chosen based on the availability of facilities while not compromising on the general characteristics to be studied. All in all, through this thesis work it was demonstrated that novel materials can be synthesized with minimal sophisticated facilities and moreover they can also be demonstrated as extremely useful in a variety of applications. The innate nature of the synthesis processes used in this work make the processes industrially viable, environmental friendly, inexpensive and time-effective. In this PhD thesis work, i) graphene oxide (GO) was converted into few-layered graphene (FLG) without using any reducing agent, ii) S, N doped FLG and ZnO decorated S, N doped FLG are synthesized using a novel chemical-mechanical process, and iii) MgO decorated FLG and MgO and NiO decorated FLG are synthesized using a simple combustion method. The synthesized materials have thoroughly characterized for morphology, crystallinity and phase. Except for ZnO decorated S, N doped FLG and MgO and NiO decorated FLG, every other of the synthesized materials have been tested in some application or the other.

FLG was synthesized by microwave irradiation (MWI) of GO (in a household microwave oven without using any reducing agents) followed by a simple sonication step. This method does not evolve any unsafe by-product gases which is otherwise the case when reducing agents are used in the reduction of GO to graphene or FLG. The synthesized FLG was tested as an anode material in Li-ion batteries. The test results showed that FLG exhibited an average capacity of 385 $mAhg^{-1}$ at low current rate (0.1 C, over 60 Cycles). At high current

rate (1 C), for initial 30 cycles, FLG exhibited an average capacity of ~270 $mAhg^{-1}$ while it decreased to ~225 $mAhg^{-1}$ over 60 cycles. These results prove that FLG could substitute graphite as an anode material in Li-ion batteries.

S, N doped FLG was synthesized by MWI of acid treated graphite flakes which are obtained by just soaking the graphite flakes in a proper acid mixture. In a similar manner, different ZnO decorated doped FLG composites are synthesized by taking appropriate amounts of Zn containing precursor and by varying the amount of S, N containing graphene worms during the reaction. S, N doped FLG was used as a catalyst for preparation of 6-aryl 5-cyano 2-uracil and and tetrahydropyrimidine, versatile biologically active molecules. With the aid of S, N doped FLG plasmid DNA could also be isolated.

MgO decorated FLG (MDFLG) was synthesized using a rudimentary combustion process involving combusting of Mg in the presence of dry ice. Similarly NiO and MgO decorated FLG was also synthesized by combusting an appropriate amount of ball-milled blend of NiO and Mg turnings. MDFLG was used as an adsorbent to remove Safranin O dye and real textile effluent from water. The same material was also used as an anode material in Li ion batteries. MDFLG exhibited a reversible capacity as high as 1052 mAh/g during the 1^{st} cycle. Even at the end of the 60^{th} cycle, more than 83% of this capacity could be retained. Basic experiment to indicate the hydrogen storage capacity of MDFLG was also carried out. This adsorption experiment at different pressures of hydrogen gas showed that MDFLG is excellent in adsorbing high amount of hydrogen gas. The experiment also showed that the adsorption capacity high at elevated pressures. MDFLG also exhibited an excellent activity against E.coli bacterium. The anti-bacterial activity of MDFLG was high when more amount of it was considered in the experiments. Non-linear ferromagnetic short range ordering at room and high temperatures was also noticed in MDFLG. This study gives a great scope in understanding the feasibility of graphene and related materials in magnetic applications.

5.2 Future Scope

The immediate future scope of this work is listed in the following:

- Scaling up of methods to obtain graphene related materials will be the first and foremost immediate future scope. For example, converting GO (as prepared by Hummers method) and ATGFs into FLG by using microwave irradiation and ultrasonication can be taken up in the initial stages of scaling-up. In doing so, instead of using commercial graphite flakes, industrial graphite waste could also be tried as the starting material.
- FLG can be used as a filler in metal and polymer matrix composites for energy applications like EMI shielding, electrodes in supercapacitors and dye sensitized solar cells and so on.
- Specific studies on elucidating the Li ion storage mechanism with regards to the FLG synthesized in this work would lead to the development of new types of FLG that can enhanced the capacity.
- With regards to temperature related stability of the samples, differential calorimetry and thermogravimetric analysis can be taken up. This is owing to the possibility of usage of the materials synthesized in this work in applications at elevated temperatures.
- S, N doped FLG can be used as a catalyst in a variety of organic and inorganic reactions as well as energy storage applications. S, N doped FLG can be used in proliferation of cancer cells similar to the way r-GO is typical used for the same purpose.
- ZnO decorated S, N doped FLG can be used in opto-electronic and UV emitting diodes. In this context a preliminary work was already carried out but not discussed in the main chapters of this thesis work. UV-Vis absorption spectra of ZnO and different ZnO–S, N doped FLG composites are shown in Fig. 5.a which clearly show excitonic absorption peaks at 369.45, 370.08, 371.99 and 371.35 nm for bare ZnO, ZnO-1wt% S, N doped FLG, ZnO-2wt% S, N doped FLG and ZnO-3wt% S, N doped FLG, respectively. These

values are much below the band gap wavelength of 388 nm of bulk ZnO. This behaviour is typical for many semiconductors due to internal electric fields within the crystal and inelastic scattering of charge carriers by phonons. More studies in this direction have to be carried out for further understanding. In this regard, photoluminescence (Fig. 5.2) from the samples was recorded.

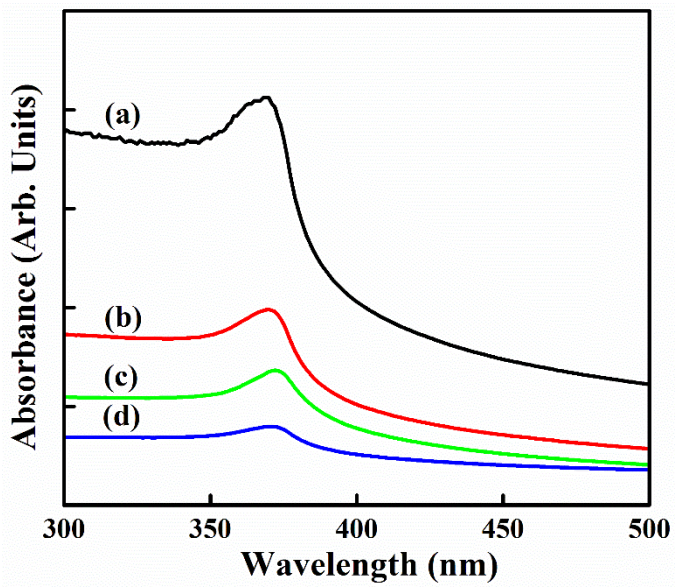

Figure 5.1. UV-visible spectra of (a) Bare ZnO, (b) ZnO-1wt% S, N doped FLG (c) ZnO-2wt% S, N doped FLG and (d) ZnO-3wt% S, N doped FLG.

Strong photoluminescence from ZnO and weak photoluminescence from ZnO decorated S, N doped FLG have been observed under the excitation by 355 nm (~3.5 eV) laser light. Emission across the visible spectral range, 370-650 nm (~3.35-1.9 eV) was mainly observed. A strong peak is observed at 388.7 nm (~3.18eV) in the violet region of the light spectrum. This could be due to exciton recombination corresponding to the near band edge emission of ZnO. A low intensity blue emission peak at 492.8 nm (2.51 eV) is also observed. A Cyan emission peak appeared at 513.8 nm (~2.41eV) is also observed. The broader Blue, Cyan emission peaks could be due to oxygen vacancies and interstitial atomic defects in ZnO.

Apart from these peaks in all the samples, two additional peaks (397.5 nm (3.11eV) and 408.9 nm (~3.03eV) are observed in the violet region in case of ZnO-2wt% S,N doped FLG.

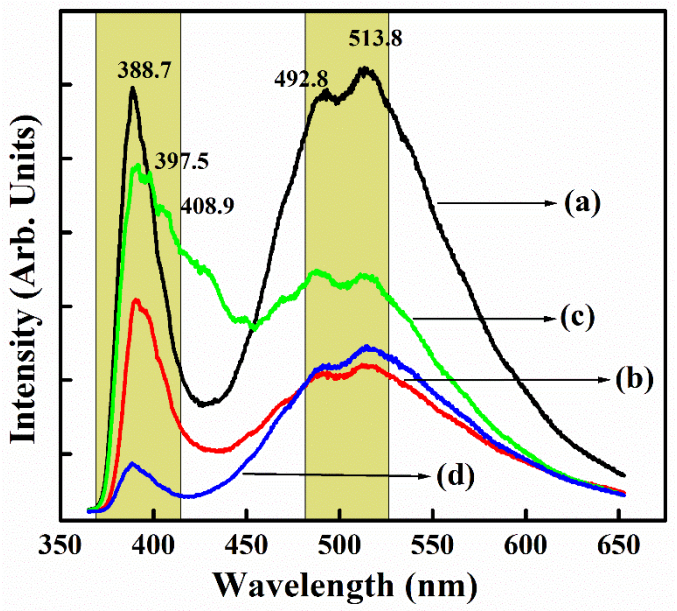

Figure 5.2. Photoluminescence spectra of (a) Bare ZnO, (b) ZnO-1wt% S, N doped FLG (c) ZnO-2wt% S, N doped FLG and (d) ZnO-3wt% S, N doped FLG.

The photoluminescence results clearly show that the materials in discussion have a great potential for unique emission and therefore present a great future scope.

- Metal oxides exhibit large Li ion storage capacities and positive Li ion intercalation voltages and therefore they are used as anode materials in Li ion batteries (LIBs). Nanosized transition metal oxides (TMOs) are also used as anode materials in LIBs. However, TMOs are not considered to be industrially viable owing to their poor electrical conductivity, large volume changes during cycling and tendency for easy agglomeration. To mitigate these problems, binary composites constituted by graphene and TMOs are developed. In this regard, MgO decorated FLG composite was shown as an excellent anode material in LIBs. Similarly materials constituted by NiO and graphene have also been tried as anode materials in LIBs. These composites are synthesized mainly by easy hydrothermal processes or chemical routes. Similar to the above mentioned binary

composites, researchers have tried ternary composites as anode materials in LIBs. In this context, MgO and NiO decorated FLG can be tested as an anode in LIBs.

- In the case of FLG synthesized in this work, initial irreversible capacity (ICL) with regards to Li ion storage was found to be high. For practical applications reduction of is needed. This could be an interesting scope of research with regards to both science and technology.
- It is well known that Surface Enhanced Raman Scattering (SERS) is through either charge transfer mechanism or electromagnetic enhancement. In this context, graphene enhanced Raman scattering which is basically through charge transfer mechanism is under study. Here subsists the motivation of the future scope which can involve study of SERS activity of various graphene related materials (namely graphene oxide, reduced-graphene oxide, FLG, and metal or metal oxides or metal nitrides decorated FLG) synthesized in this thesis work. The aromatic nature of graphene allows for stacking with biomolecules making it a strong binding site for biomolecules, making it a good choice for bio-sensing systems. In this regard, the realization of certain biological applications has been discussed in this thesis. In the immediate future the capability of the above mentioned materials' ability to sense bio-molecules through SERS can be taken up. In this context, the synthesis conditions can be optimized to obtain high sensing of plasmonic signal, detection limits and increase in efficiency of the materials. Complementary to this, analysis of the optical reflectance spectra of the materials can be considered to obtain the optical constants and dielectric functions, which give information the presence of Surface plasmon resonance in the materials. Further, changes in Band gap and Urbach energy can be correlated with adsorption of bio-analytes on the materials' surface. The materials can also be further characterized for electrochemical changes by using cyclic voltammetry with and without the presence of analytes.